Politecnico di Torino

Master of Science in Mechanical Engineering
Department of Mechanical and Aerospace Engineering

2023/2024

The role of post surface finishing on the surface quality and fatigue behavior of Ti-6Al-4V alloy produced via Laser Powder Bed Fusion Additive Manufacturing process

Supervisors:

Politecnico di Torino
Prof. Abdollah Saboori

Politecnico di Milano
Prof. Sara Bagherifard

Candidate:

Mohammad Yousefi

Abstract

Metal Additive Manufacturing (AM) is an impressive approach revolutionizing industrial production. Originating with a virtual model, this method employs a layer-by-layer process in three-dimensional space, using metallic materials to create intricate components. Its key advantages include unparalleled design freedom, catering to the demands of high-precision sectors like biomedical, automotive, etc. Moreover, metal AM significantly contributes to sustainability by minimizing material waste, a stark departure from traditional manufacturing processes. Despite these advantages, challenges persist, notably in surface quality and mechanical performance in the as-built condition, requiring careful consideration of manufacturing parameters and strategic post-processing. In conclusion, while metal AM presents transformative possibilities, addressing challenges through strategic post-processing is crucial. This thesis constitutes a focused exploration into a specific aspect of post-processing: the impact of Tumble Finishing on the physical, microstructural, and mechanical properties of Titanium-6Aluminium-4Vanadium alloy fabricated through Laser Powder Bed Fusion (L-PBF). The ensuing experimental findings reveal the remarkable efficiency of Tumble Finishing in enhancing the surface quality, and therefore improving fatigue performance of specimens.

Keywords: *Additive Manufacturing, L-PBF, Surface Treatment, Fatigue Behavior*

Acknowledgments

Before delving into the details of my work, I feel compelled to express my sincere appreciation to the individuals who have played significant roles in my academic journey over the past few months. Foremost, my heartfelt gratitude goes to my supervisor, **Professor Abdollah Saboori**, whose great support and guidance have been vital in shaping my experience throughout this endeavor. Professor Saboori not only provided me with the invaluable opportunity to contribute to a stimulating project but also imparted essential lessons on the significance of meticulous planning, attention to detail, and the ability to approach challenges with a critical mindset. His mentorship has been a source of inspiration and has significantly contributed to my growth as a researcher. Equally deserving of acknowledgment is my co-supervisor at Politecnico di Milano, **Professor Sara Bagherifard**. Professor Bagherifard has been a constant pillar of support, offering valuable insights, corrections, and encouragement at every stage of the project. Her guidance has fueled my curiosity and motivation, enriching my academic experience. I am particularly grateful for her assistance in the preparation and execution of experiments, which have been integral to the success of my thesis. A debt of gratitude is also owed to **Erika Lannunziata**, and the dedicated researchers whose collaborative efforts were indispensable in preparing the experimental setups. Their expertise and assistance have significantly enhanced the quality and validity of the experiments conducted. Last but certainly not least, I extend my deepest thanks to my family, whose unwavering support has been a constant source of strength throughout my academic career. Their encouragement and understanding during every moment of my journey have been invaluable, providing me with the foundation to pursue and achieve my academic goals.

Contents

List of Figures

List of Tables

Acronyms

- AM Additive Manufacturing;
- CE Chemical Etching;
- DMLS Direct Metal Laser Sintering;
- DED Direct Energy Deposition;
- DfAM Design for Additive Manufacturing;
- EBSD Electron Back Scatter Diffraction;
- EBM Electron Beam Melting;
- EB-PBF Electron Beam-Powder Bed Fusion;
- FEM Finite Element Method;
- GOS Grain Orientation Spread;
- HFMI High-Frequency Mechanical Impact;
- HIP Hot Isostatic Pressing;
- LoF Lack-of-fusion;
- L-PBF Laser-Powder Bed Fusion;
- µCT Micro Computed Tomography;
- Nd: YAG Neodinium Ytterbium Aluminium Garnet;
- OM Optical Microscope;
- PBF Powder Bed Fusion;
- SEM Scanning Electron Microscope;
- SLM Selective Laser Melting;

Chapter 1 : Introduction

This study delves into the field of Additive Manufacturing (AM), specifically emphasizing the use of metallic materials (metal AM). This domain, marked by innovation, unfolds with vast dimensions, offering numerous opportunities for in-depth exploration, process refinement, and optimization. Positioned as one of the primary emerging technologies in manufacturing, the interest in AM grows steadily each year. AM technology, recognized as an additive technique, facilitates design freedom unattainable by traditional subtractive manufacturing methods, simultaneously addressing concerns about material waste. AM lies in its capacity to materialize complex shapes, utilizing various technologies and materials that attract industries. However, metal AM is not without its challenges. Surface quality and the mechanical performance of as-built parts often fall short of expectations for their final use. Consequently, manufacturing parameters and post-processing techniques become pivotal aspects, as evidenced by the multitude of studies focused on them. The extensive list of parameters influencing the outcome of metal AM, coupled with the post-processing possibilities, poses a challenge to achieving an understanding of the correlations within the field. While the landscape is vibrant with scientific research, experimental activities, and publications, a comprehensive comprehension of all factors and a definitive "best route" for producers remain elusive.

Guiding this exploration are esteemed experts, Professor Abdollah Saboori from PoliTo and Professor Sara Bagherifard from PoliMi, whose research concentrates on metal AM manufacturing and post-processing. On the industrial aspect, collaboration with companies such as PrimaAdditive, InTrauma, and IRIS adds practical insights. While not directly involved in the activities, these institutions play a crucial role in identifying industrial requirements and emphasizing the relevance of the research. PrimaAdditive, a manufacturer of metal AM machinery, offers valuable customer service and collaborates with universities and research entities. InTrauma, a biomedical company specializing in bone internal fixators, emerges as a potential end-user of AM technologies. IRIS, a small-medium enterprise focusing on innovation, particularly with laser and plasma technologies. These industrial actors represent different aspects of the metal AM field. Innovative manufacturing companies, like IRIS, focus on the technology's applications, catering to specific product requests, even on a small or custom-made scale. The biomedical field, often associated with AM, benefits significantly from the design freedom provided by such technologies, especially in the production of custom-made medical devices. InTrauma stands out as a potential final user of this technology, with the chance to tailor the surface quality of AM parts for improved cell-material interaction and osteointegration of prostheses. However, the appeal of AM extends beyond the biomedical field, reaching into the automotive, design, and jewelry sectors. Surface quality remains a significant challenge in metal AM, and these sectors

find themselves among the customers of PrimaAdditive, which not only produces and sells AM machines but also supports clients in design, software use, and knowledge transfer. PrimaAdditive specializes in Laser-Powder Bed Fusion (L-PBF) and Direct Energy Deposition (DED) machinery. The decision to focus on L-PBF, one of the most relevant technologies for metal AM, underscores its practical application. All specimens were printed directly using an L-PBF machine produced by PrimaAdditive.

The analysis of industrial requirements emphasizes that metal AM is a multidisciplinary field where every step of the process, including the selection of the starting raw material (metallic powder), plays a crucial role. Anticipating the printing outcome necessitates a keen understanding of the quality and properties of the raw material, which are as relevant as subsequent printing parameters and post-processing. The goal of this work is to contribute to research on metal AM from an experimental standpoint, conducting a comprehensive study from raw material characterization to post-processing. Given the vast range of possibilities within the field, a specific context was needed to design the experimental study. L-PBF and Electron Beam-Powder Bed Fusion (EB-PBF) emerged as the two most relevant metal AM technologies. Based on the availability of PrimaAdditive machinery, L-PBF was chosen as the technology of interest for the project. The chosen material for scrutiny is the Titanium – 6 Aluminum - 4 Vanadium (Ti6Al4V) alloy, renowned for its high-quality attributes and widespread applications in biomedical, automotive, etc. The design of experiments was collaboratively discussed and developed throughout the thesis between the student and the supervisors. The research journey began with the characterization of raw powder to ensure a comprehensive study. Highlighting the crucial role of post-processing in metal AM, the research delves into the investigation of a specific post-treatment: The Tumble Finishing based on mechanical treatment. The impact of this treatment on multiple properties is investigated through a series of characterizations on the printed specimens, with a specific focus on fatigue performance—a parameter particularly relevant in complex and long-term applications. Following the abstract and the introduction, the State of the Art chapter introduces the AM field, and also providing a detailed description of available post-treatments. The Solution chapter intricately describes the experimental study, covering specifications, motivated design of specimens, design of experiments, and the equipment and methodologies employed for manufacturing, post-processing, and characterizations. The results of the tests are presented with pictures and graphs, followed by critical discussions that provide insights into the findings. Future perspectives for further research in this field follow, providing a roadmap for future endeavors. Finally, the Conclusion chapter sums up the storyline of the thesis, focusing on the goals and the main findings, highlighting their relevance for the field and suggesting possible future developments. In conclusion, this detailed exploration seeks to illuminate the intricate world of metal AM, from industrial applications to experimental intricacies, contributing valuable insights to the ongoing discourse.

Chapter 2 : State of the Art

The analysis of the State of the Art is an important part within the thesis, serving two primary purposes. Firstly, it provided me with a strong foundational knowledge of the wide and multidisciplinary topic of metal AM. Secondly, it was of paramount importance for a research project to have a profound understanding of current existing solutions. Prior to starting on any experimental research, a thorough comprehension of cutting-edge knowledge is vital. Familiarity with existing research, previous experimental results and the current challenges of the field is essential for designing a study that is both feasible and capable of producing relevant results. The aim of the thesis was to enrich and expand the current State of the Art in the metal AM sector. This objective was approached through undertaking of an experimental study. The experimental research focused on the effects of post-treatment in metal AM, an area that emerged as a key aspect in the literature. Multiple post-treatments are available, and there are vast opportunities to study their effects on the performance of printed parts. The present chapter will provide a necessary introduction to the AM field, followed by knowledge on the relevant properties of metal AM parts and post-treatments.

2.1 Additive Manufacturing Process

AM technologies represent an innovative approach to manufacturing that involves starting from a virtual model of a desired part (CAD model). This model is then converted to Stl. File and transformed into a physical object through a layer-by-layer process that takes place in three-dimensional space (Fig. 1 [1,2]. The benefits of this technique are numerous, including unparalleled design flexibility that was once impossible with traditional manufacturing methods. Unsurprisingly, it has become an increasingly popular method in industries such as biomedical, automotive engineering, etc. [3].

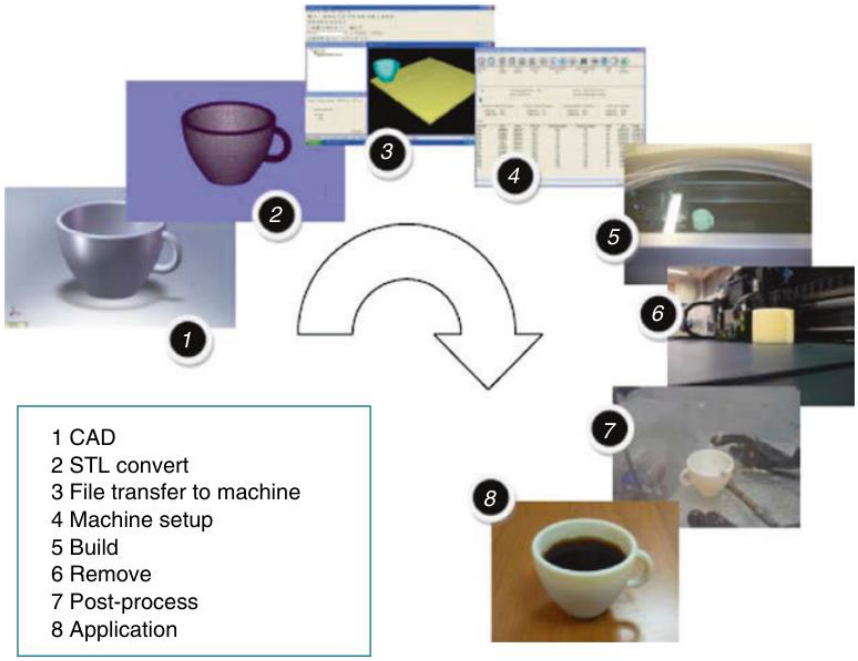

Fig. 1: overall route of AM process starting from CAD model to the final part [1].

There have been many methods to classify the AM process, and each of them has its own advantages and disadvantages. One of those ways is ASTM standards in which AM are classified accurate way. Below the classification made be ASTM is elaborated [4]:

Material Extrusion:

- Fused Deposition Modelling (FDM)
- Contour Crafting

Power Bed Fusion:

- Selective Laser Sintering (SLS)
- Direct Metal Laser Sintering (DMLS)
- Selective Laser Melting (SLM)
- Electron Beam Melting (EBM)

Vat Photopolymerization:

- Stereolithography (SLA)

Material Jetting:

- Polyjet/Inkjet Printing

Binder Jetting:

- Indirect Inkjet Printing (Binder 3DP)

Sheet Lamination:

- Laminated Object Manufacturing (LOM)

DED:

- Laser Engineered Net Shaping (LENS)
- Electron Beam Welding (EBW)

The above mentioned technologies suggest a specific way of production strategies and material properties, which therefore, affects the time of the production, quality of the parts, and the costs involved.

2.1.1 AM Pros and Cons

Pros

The main advantages of AM method according to [5, 6, 7, 8] can be grouped below:

- Design Flexibility: since in AM there is a reduction in manufacturing constraints, we have flexibility on the component design with respect to shape and geometries.
- Material Customization: if a material property that is suitable for our needs is not available, we can customize the material in many ways. For instance, mixing powders, using fibers in filaments, and utilizing bio-compatible materials.
- Reduced Internal Process Logistic: because AM involves less operations, there are a reduced internal process logistics, which leads to a reduction of the time needed for the design to manufacturing. Moreover, in many companies, 3D printing can be used to produce prototypes before the production, which results in saving time and money.
- Topology optimization: It is a numerical based process that changes the shape of part automatically (Fig. 2). This procedure is impossible to be performed via traditional manufacturing. The use of AM combined with topology optimization can lead to reduction in weight, time and waste materials.

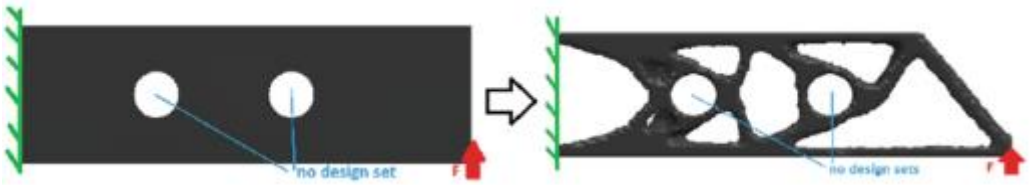

Fig. 2: Topology optimized of a cantilever beam [5].

- Assembly Connection Minimization: we can produce complex geometries in one operation rather than creating different parts and then make an assembly of them. Therefore, the time needed for bolting connection or welding is reduced. Additionally, one-piece parts are much safer with respect to an assembly one. Specifically, assembly connections are critical in a vibrational environment that impose fatigue stress on the components, and thereby the maintenance expenses are high.
- Manufacturing decentralization: by using AM, we can do the manufacturing process and deliver the components remotely.
- Reduction of repairing times: it is possible to repair damaged parts by adding new layers. Therefore, it is not necessary to replace the part with a new one, which reduces the time and the costs.
- Multi-Material Capability: by using AM, we can use numerous materials in a single part (Fig. 3). This capability of AM makes it more advantageous over the traditional manufacturing process.

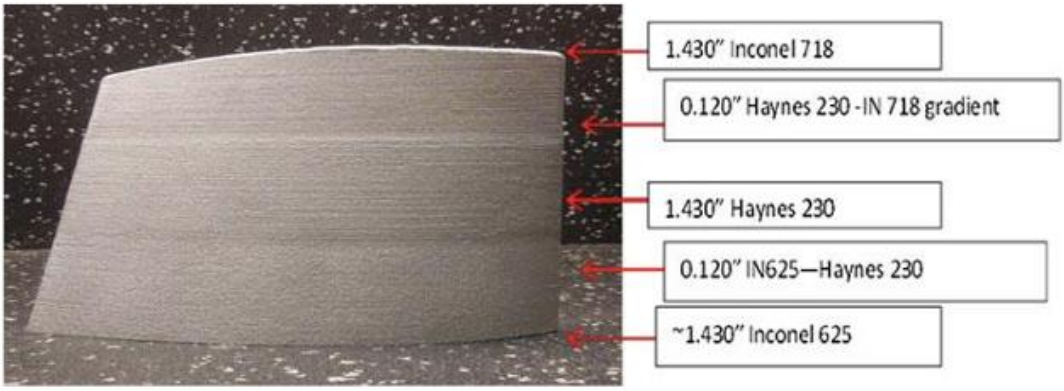

Fig. 3: Utilizing different alloys in an airfoil [8].

Cons

According to the studies done by Attaran [7] and Bacciaglia et al. [5] the disadvantages of AM can be grouped below:

- Surface roughness: a typical negative aspect of AM process is the rough surface, which makes it essential to do post-processing.
- Limited material portfolio and limited building size: compared to the traditional manufacturing methods, AM involves a limited amount of materials. Additionally, there is a limited size for producing parts. The largest machine is able to manufacture only at a volume of 1 m^3, and this is a great limiting parameter for the applications that involve larger dimensions.
- Anisotropic material: the process of AM includes a high anisotropic behavior which makes it problematic in various applications.
- Hight cost: generally, AM machines are much more expensive than traditional milling and turning machines. For example, for a SLM AM machine, the cost is 800 k€. However, for a traditional CNC is 200 k€. Moreover, the material used in AM, inserting atmosphere, or keeping a vacuum regime inside the chamber are quite expensive.
- Slow certification process: Since AM is a new technology, there is less information in order to understand the material behavior during the operation, specially to see the fatigue behavior.
- Inspection and Maintenance: as mentioned earlier, producing a complex assembly in a single part is advantageous. However, in some cases, it creates problems regarding maintenance and repair. Specifically, sometimes the whole component is replaced with a new one.

2.2 Metal AM categories

Due to the combination of the freedom in manufacturing and thermo-physical features, Metal AM is the most favorable among all the AM classifications. Having these properties, Metal AM with complex shapes is able to withstand in sever conditions of stress while securing their functionalities. Moreover, Metal AM is capable of producing parts with various complex features which eliminate the need for producing multiple parts to be assembled later on. Therefore, the cost related to the production of different parts will be decreased, and the component will be lighter [9]. As a result of these advantages, Metal AM is widely used in many sections such as automotive, biomedical, etc.

In general, the manufacturing of the part first starts from a feedstock material in powder or wire form. Secondly, it is melted by a laser or an electron beam melting source, and finally it is solidified into overlapped layers.

The two comment Metal AM technologies are DED and PBF, which their sub-technology is elaborated below.

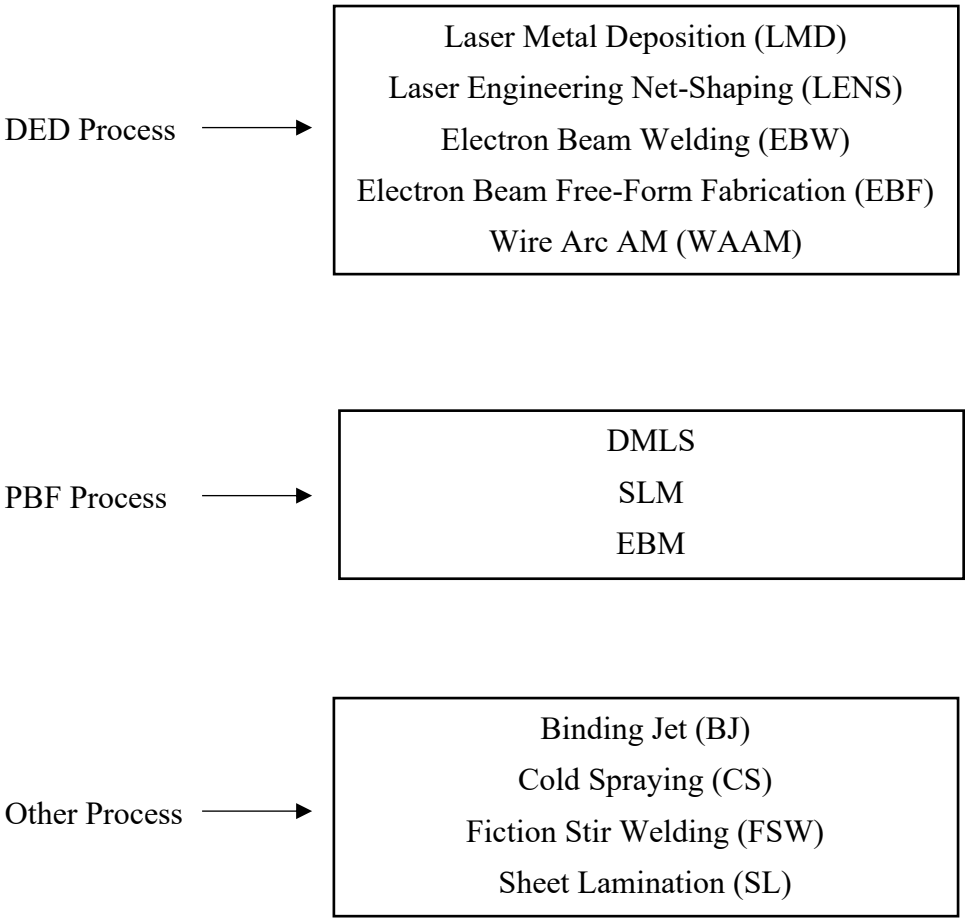

2.2.1 DED Technology

In this process, the material is fed and melted on a platform at the same time. Generally, the feedstock is a powder or a wire, and by using an energy resource is melted [10]. This technology can be performed in a multiaxial machine in which a 3D positioning implemented; as a result, it is feasible to build intricate parts without the need for using support structures [11]. This technology is ideal for producing component repair of Turbine blades, engine combustion chambers, and compressors. Additionally, the material that is usually used in this technology is Ni-based alloys. In Fig. 4: A schematic of DED system with (a) powder feedstock (b) wire feedstock [10]. is shown.

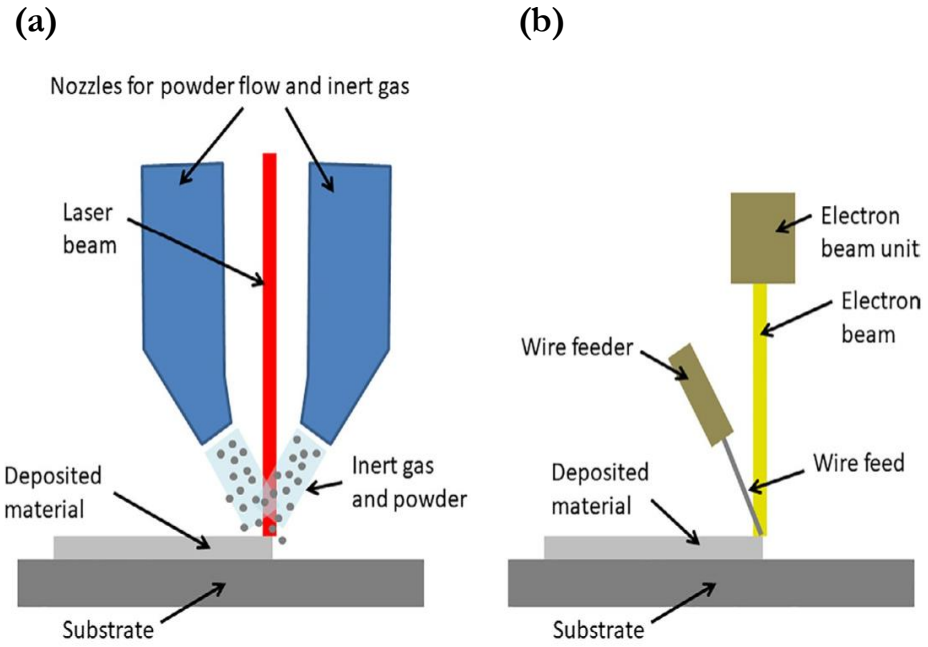

Fig. 4: A schematic of DED system with (a) powder feedstock (b) wire feedstock [10].

As it was mentioned earlier, the DED technology can be divided into two processes according to their feedstock, which are wire DED system and blown powder DED system. These two techniques are elaborated in the next sections.

DED-Wire Feeding

This process can be done both in open air utilizing a shielding gas or in an enclosed chamber using a regulated atmosphere. In the both cases, owing to the robotic arm, there is a high freedom in the sense of building. Additionally, there are sophisticated sensors and transductors that manage and control the performance of the process [12]. A schematic of this process is shown in Fig. 5.

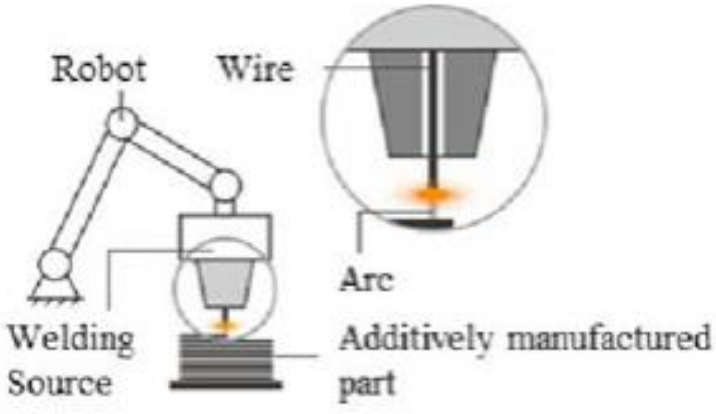

Fig. 5: General process of Wire Arc Additive Manufacturing (WAAM) [185].

The deposition initiates when a laser or an electron beam melts the wire onto the substrate, creating the initial layer. This technology uses almost 100% of the material with no porosity inside. On the other side, the dimensional accuracy and surface roughness is quite high, and a post-process work is essential

before the actual use of the component, as a result, this technique is used for structural and functional parts [13] .

DED-Powder Feeding

In this method, a nozzle is fixed onto a two or three axis mechanical system arm, housing the main energy resource that typically is Nd-YAG or CO2 laser, or an electron beam. Moreover, the building plate is connected to a distinct mechanical system with two or three degrees of freedom. In total, the combination of the main mechanical arm and building plate give us a nine degree of freedom [14]. The deposition head contains a feeding mechanism embedding of one or several channels, which blend metal powder and carrier gas along with shielding gas. The shielding gas is a crucial element that prevents impurities and material oxidation. As the substrate melts, it generates a melt pool because of the interaction between the laser source and the plate and the fluxing particles get trapped within it [13].

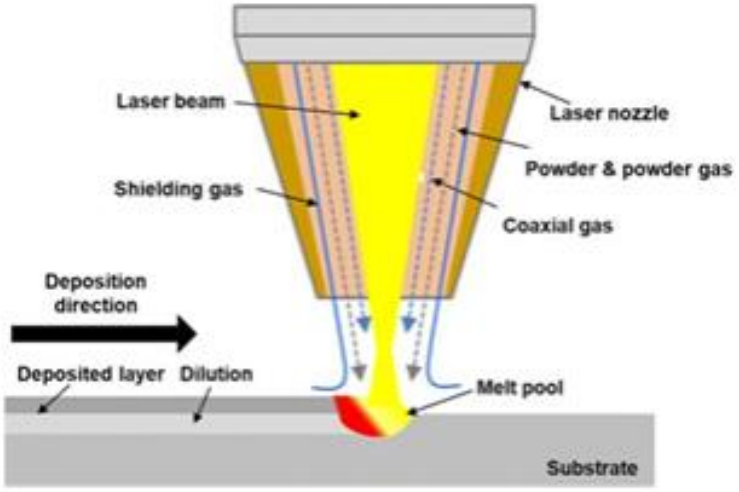

Fig. 6: General schematic for Laser Beam Metal Deposition (LBMD) process [186].

Process parameters in this technique highly affect the mechanical properties and microstructure of the produced part [6, 15] which are listed below:

- Transverse Speed (1-20 mm/s): this parameter influences the shape, width, and the rate of the cooling of the tracks. The higher the transverse speed the faster the cooling rate, which results in finer and columnar grains. On the other side, lower transverse speed values induce slower cooling rates leading to a coarser microstructure.
- Laser Power (100-5000 W): has a direct impact on both cooling rates and microstructure. Unlike the pervious parameter, higher laser power level fosters coarse microstructure, whereas lower laser power results in the formation of fine, columnar microstructure. Nonetheless, for a more accurate analysis, it is essential to consider the actual energy absorbed by the material, not considering the reflected radiation.
- Powder Flow Rate: affects the uniformity and adherence of the deposit. Evaluating this parameter is difficult because of the complexity of prediction. Usually, this parameter is considered as a constant variable.

- Laser Beam and Powder Stream: have a direct influence on the heights of the layers and their boundaries. It considers the dynamic interaction between the powder stream and the laser beam (Fig. 7).

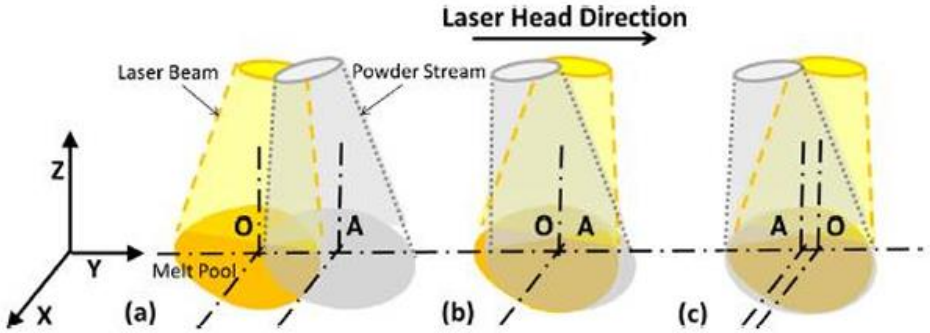

Fig. 7: Laser and power beam dynamic internation [42].

- Hatching Strategy: it examines the path followed by the deposition head within a two-dimensional space (Fig. 8). This variable significantly affects the residual stress, any potential deformation of the part and the thermal distortion.

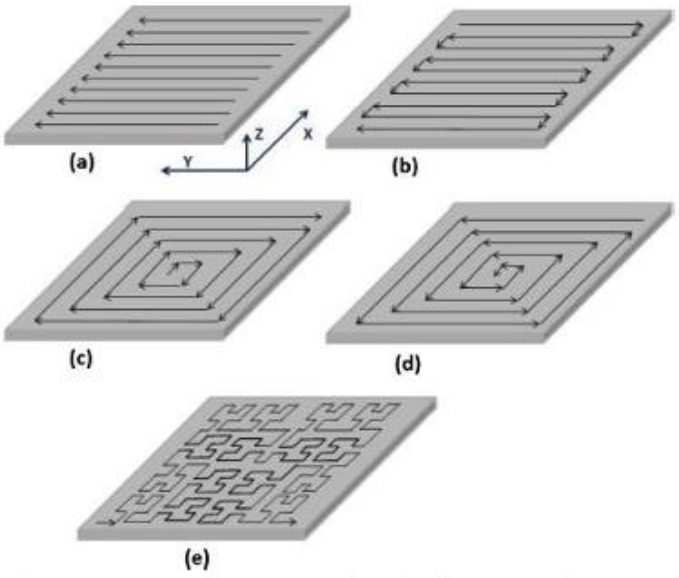

Fig. 8: Scaning strategies [6].

2.2.2 Powder Bed Fusion (PBF) Processes

PBF technologies, by adopting a focused energy source, melt the powder. Specifically, A leveling roller distributes a thin layer of powder over the platform, and a moving energy source melts the powder into successive cross-sections as specified by the CAD file. The initial layer adheres to the build plate, which may be pre-heated and is usually made of the same material as the part being constructed. After completing each layer, the platform lowers by a distance equal to the layer's thickness. A leveling roller then spreads a new layer of powder over the solidified one, and the building process is repeated. This cycle continues iteratively until the final part is completed [16].

These technologies dominate the metal AM market due to their extensive use in various fields. The primary difference among PBF technologies lies in the energy source used to melt the powder. Based on this distinction, they are categorized into L-PBF or SLM and EB-PBF or EBM processes [20,21].

EBM Process

EBM developed and patented by the Swedish company Arcam AB [19], uses electron beam energy to melt a metal powder bed. The hardware system (Fig. 9) includes an electron beam generated by a 60 kV electron gun located at the top of the machine, which is focused on the powder bed using an electromagnetic lens system. Initially, the electron beam preheats the powder bed to 80% of its melting temperature using high scan rates (~10^4 mm/s) and a high beam current (~30 mA). Following this, the scan rate and current are reduced to 10^2 mm/s and 5-10 mA, respectively, to fully melt the metal powders based on the CAD model of the component. After each scan, the build platform lowers by one layer thickness, which typically ranges from 50 to 200 µm, depending on the material. Two hoppers supply the metal powder, which is spread onto the building platform by a rake. Once the deposition is complete, the process restarts. The powder typically consists of spherical particles, averaging 45 to 105 µm in size, produced through gas atomization. This process operates under vacuum conditions (around 1×10^{-5} mbar). Additionally, during the electron scanning of the powder bed, a partial pressure of helium (2×10^{-3} mbar) is maintained in the process chamber to prevent chemical contamination of the material. These conditions make this technology suitable for processing materials with a high affinity for oxygen, such as titanium alloys.

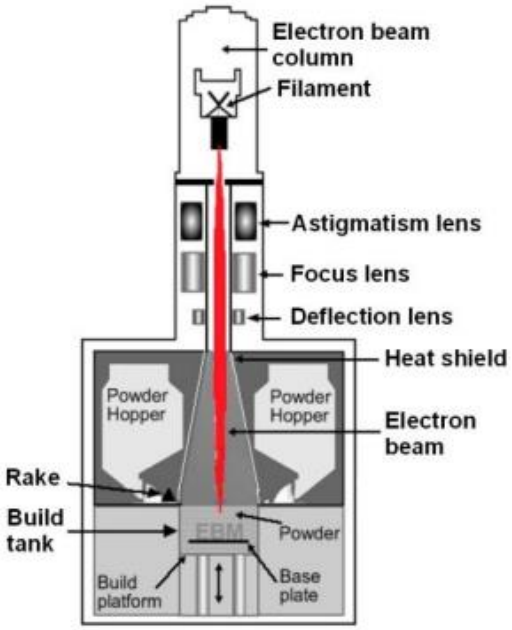

Fig. 9: Diagram illustrating the EB-PBF process [70]

Unlike other metal AM processes, EBM preheats the powder bed to high temperatures (e.g. ~750 °C for titanium alloys [20] or 400 °C for pure copper [21]) to partially sinter the metal powders and enhance the electrical conductivity of the powder bed, thereby preventing process instabilities [22]. This preheating reduces residual stresses in the manufactured parts and alters their microstructures. In EBM parts, the amount of residual stress is significantly lower, and the final microstructures are coarser compared to L-PBF or DED parts. This difference results from the lower thermal gradients and cooling rates characteristic of the EBM process. These factors help minimize part distortions and eliminate the need for post-processing annealing treatments [23].

The process parameters in EBM, such as beam power, scanning velocity, line spacing, scanning strategy, and focus offset, determine the energy delivered and the melting approach used for the powder bed. In this technology, melting occurs through the absorption of the electron beam by the powder bed, where the kinetic energy of the electrons is transferred to the powder particles, which converts into heat and forms a melt pool [24]. When powders absorb the kinetic energy of electrons, they also acquire

a negative charge, which can lead to issues such as 'smoke' and beam diffusion [25]. To prevent a high concentration of negative charges in the powder bed, scan strategies need to be properly adjusted. Additionally, only conductive powders, such as metals, can be used with EBM. This limitation is a significant drawback of electron beam melting compared to laser-based technologies [25].

EBM is characterized by high scanning speeds (up to 8000 m/s [26]) and thick layers, which result in higher productivity rates compared to L-PBF processes. Additionally, operating in a vacuum reduces chemical contamination, unlike the low oxygen content atmosphere used in L-PBF. Combined with lower residual stresses, these benefits make EBM highly competitive in the AM market. However, the surface quality of EBM parts is inferior to that of L-PBF parts. This is due to the thicker layers and larger particle sizes used in EBM, resulting in a final roughness of 25 to 35 μm, nearly three times that of L-PBF (~11 μm) [22]. Higher roughness values can decrease the fatigue resistance of components, limiting their industrial applications and potentially necessitating post-processing surface modifications. However, studies on the interactions between the human body and prostheses made by EBM have shown that cell adhesion on these rough surfaces is greatly enhanced [28, 29, 30]. As a result, EBM has been widely adopted in the biomedical field, particularly in the orthopedic market [30]. Components such as acetabular cups, knee and maxillofacial plates, and hip and jaw replacements produced by EBM have been certified since 2007 and approved for in-body applications by the United States Food and Drug Administration since 2010 [31]. Since 2014, over 40,000 acetabular cups have been produced and implanted in patients [32], thanks to EBM ability to create cellular structures with precise control over pore size, strut diameter, and cell geometry, as illustrated in Fig. 10.

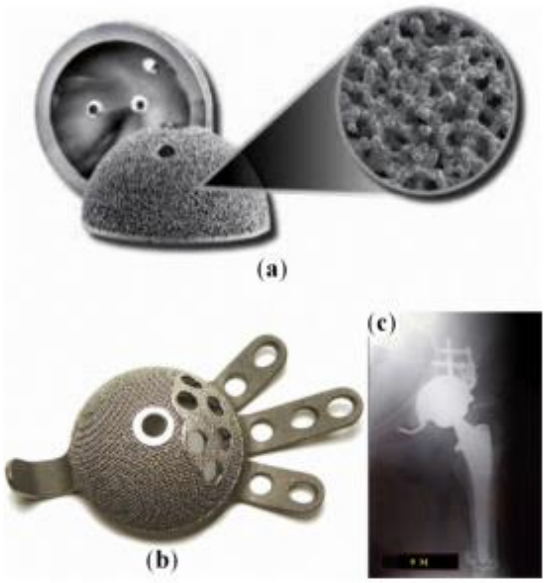

Fig. 10: Examples of acetabular cups produced using the EBM process include: (a) a Ti-6Al-4V implant produced via EBM method [187]. In orthopedic applications of Trabecular Titanium™: (b) an external trabecular structure with optimized surface cell structures, and (c) a radiological outcome of the acetabular cup post-implantation [27].

In addition to biomedical applications, EBM parts have been particularly valuable in the aerospace field due to their reduced costs related to the 'buy-to-fly' ratio (the amount of material purchased to produce 1 kg of the final part) [33] and the ability to fabricate parts in gamma-TiAl alloys [37, 38, 39, 40,41]. In a case study, Dehoff et al. [33] demonstrated that using the EBM process reduced the processing cost of a Ti-6Al-4V BALD bracket by about 50% compared to traditional manufacturing. The EBM process achieved this by lowering the buy-to-fly ratio from 33:1 to 1:1, thanks to its nearly 100% material efficiency.

L-PBF Process

L-PBF, also known as Melting SLM or DMLS, uses a focused laser beam to selectively melt layers of metal powder, creating three-dimensional parts. Typically, the laser system is an Yb fiber laser with power levels up to 1 kW. The L-PBF process starts with a powder spreading system, commonly referred to as a recoater blade, depositing a layer of powder on the building platform. This system can control layer thickness, ranging from 20 to 60 μm. Once the powder is spread, the laser directs its focused beam onto the powder bed, selectively melting the material according to the CAD model of the part [39].

After processing each layer, the building platform lowers by the thickness of one layer, and the deposition step begins again. This layer-by-layer fabrication continues until the part is complete and ready for post-processing operations, which typically include removing support structures and heat treating the parts [39]. A schematic representation of the L-PBF process is shown in Fig. 11 [39].

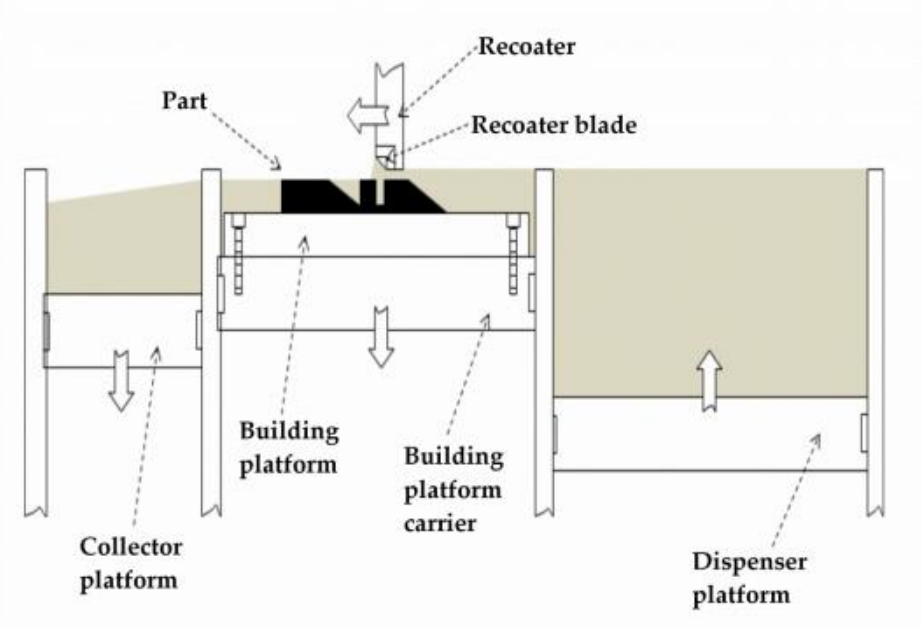

Fig. 11: Diagram illustrating the L-PBF process [40].

L-PBF involves numerous factors and variables that can affect the properties of the final parts. These factors can be categorized into two main groups: powder properties and process parameters, as shown below [40].

Powder Properties

Generally, PBF processes are classified as powder metallurgy processes similar to sintering, Hot Isostatic Pressing (HIP), or Metal Injection Molding. Therefore, the final properties of the fabricated parts—such as density, surface roughness, and chemical composition—are highly dependent on the quality of the powder used [39]. Assessing the properties of the feedstock is essential, as improved confidence in powder selection enables the production of reproducible components with known and predictable properties, as outlined in the ASTM standard F3049-14 [41].

Powder Properties [40] →

- Particle shape
- Particle size and distribution
- Chemical composition
- Thermal conductivity
- Melting temperature
- Absorptivity/reflectivity

Process Parameters

In simple terms, the L-PBF process involves the absorption of laser beam energy by metal powder, resulting in the melting of the material. L-PBF machines have several parameters related to the laser source and the building chamber, which individually and collectively influence the melting behavior and the final quality of the fabricated part [39].

Process Parameters [40] →

- Laser power
- Layer thickness
- Scanning speed
- Scanning strategy
- Hatching distance
- Building orientation
- Protective atmosphere
- Gas flow
- Laser beam diameter
- Bed temperature
- Laser type

2.3 DED and PBF comparison

The following comparison outlines the primary categories of metal AM, highlighting the general differences in process parameters and equipment capabilities [42].

Table 1: Comparison of LMD, SLM, and EBM [42].

LMD	SLM	EBM
Nd-YAG or CO2 laser (100 – 5000W)	One or more fibre laser (200-1000W)	High power electron beam source (up to 3000W)
Ar/He shielding gas	Ar/N2 atmosphere	Vacuum/He atmosphere
Powder preheating not necessary	Powder preheating at 100-200ºC	Powder pre-sintering at 700-900ºC
Base plate preheating	Base plate preheating	Base plate preheating

No build size limitations	Build size limited by the chamber volume (ex. 500x350x300 mm3	Build size limited by the chamber volume
Melt Pool size width 0,25-1mm	Melt Pool size width 0,10,5	Melt Pool size width 0,21,2
Layer thickness 100-200µm	Layer thickness 20-100µm	Layer thickness 50200µm
Surface finish > 25µm	Surface finish 4-11 µm	Surface finish 25-35 µm
Geometric tolerance ± 25 mm	Geometric tolerance ± 005-0,1 mm	Geometric tolerance ± 0,2 mm
Building rate ~ 0,5Kg/h	Building rate ~ 0,5Kg/h	Building rate ~ 80 cm3/h
Repairing	No repairing	No repairing
Generally lower mechanical properties than SLM and EBM (coarser microstructure)	-	-

2.4 Applications of Metal AM

As discussed in previous sections, metal AM is ideal for sectors that require small production runs, high customization, and low-cost prototypes. Therefore, it is particularly well-suited for the automotive, aerospace, and biomedical industries [43].

2.4.1 Automotive applications

One of the earliest adopters of 3D printing was the automotive industry. General Motors has utilized AM for over 20 years to create prototypes, speeding up time to market and reducing product development costs [7]. Beyond prototyping, AM has other applications in the automotive sector. In 2013, Kor Ecologic introduced the Urbee, the first electric car with fully 3D-printed interior and exterior parts [43]. This approach eliminates excess components that increase drag and weight. Although the Urbee is currently a prototype, the company is developing the Urbee 2 for consumer use [43].

Here are some examples of AM applications [43]:

- **Volkswagen**: The German automaker redesigned a front window support, reducing its weight by 74% compared to the original part.
- **Audi**: In 2017, Audi opened a 3D printing center in Ingolstadt, Germany, collaborating with SLM Solutions Group AG, a specialist in metal AM, to produce prototypes and spare parts.
- **Rolls Royce**: The British automaker uses 3D printing to manufacture components for their flagship model, the Phantom, having printed over 10,000 parts.

- **Porsche**: Porsche utilizes 3D printing to create spare parts for its vehicles, using SLM technology for metal parts and SLS for plastic parts and equipment.

- **Formula 1**: In the racing industry, AM technologies are widely used. The ability to rapidly produce innovative geometries is essential for research and testing in wind tunnels. Both 3D SLA and SLS printing systems are used to create wings/ailerons, brake system components, suspension and engine covers, internal pipelines, and deflectors. In the figure below, the front brake duct inlet for wind tunnel testing, produced by the Alfa Romeo Sauber F1 Team using 3D Systems SLS 3D printers [44].

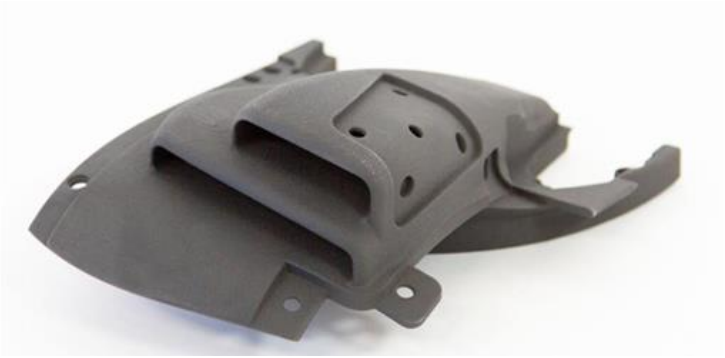

Fig. 12: Brake air inlet designed by SLS method [44].

2.4.2 Aerospace applications

In the aerospace industry, metal AM processes have been employed to produce structural components, turbine blades, and fuel injection nozzles [48, 49, 50, 51], representing 12.3% of all global AM applications [49]. The use of AM in aircraft leads to significant energy cost reductions due to the decreased need for costly materials and the fuel savings from lighter components. Additionally, AM enables the production of high-performance materials, such as Ti-6Al-4V and nickel superalloys, while overcoming challenges associated with machining or tooling these alloys [52, 53]. For instance, in Fig. 13, the bionic partition made for Airbus A320 aircraft using DMLS technology is illustrated. This cutting-edge structure is not only more robust but also 25 kg lighter compared to earlier versions [46]. Another highly publicized aerospace component created through AM is the LEAP engine fuel nozzle by GE Aviation (see Fig. 14). This part features a complex new design with internal cooling channels and has achieved a weight reduction of over 25% [39]. In this instance, rather than manufacturing and then assembling 18 separate components as done in traditional methods, the AM part was produced in a single operation [49, 51].

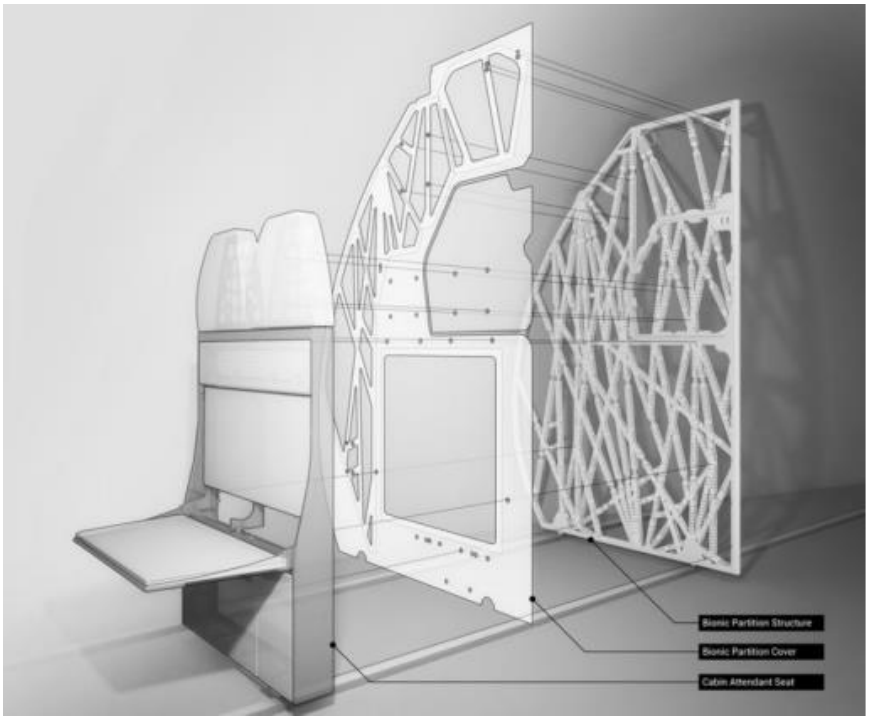

Fig. 13: Bionic partition for the Airbus A320 manufactured using DMLS technology [46].

Fig. 14: LEAP engine fuel nozzle manufactured by GE Aviation [39].

2.4.3 Medical applications

The medical field is undoubtedly a significantly advanced and lucrative market for AM applications. The freedom of design, new lattice structures enhancing mechanical properties [55 – 67], improved prosthesis biocompatibility [68 – 71], and especially the customization of prostheses for individual patients have all driven the swift and substantial growth of AM technologies in the biomedical sector

[72, 73]. The ability of AM to create highly precise, patient-specific implants, including tissues, organs, and bones, is revolutionizing various medical fields such as dentistry and surgery (Fig. 15) [39]. AM can accurately replicate the internal structures of bones, muscles, nerves, and blood vessels using compatible materials. This approach accelerates body healing, makes surgical procedures less invasive and risky, and significantly lowers the chances of implant rejection [39].

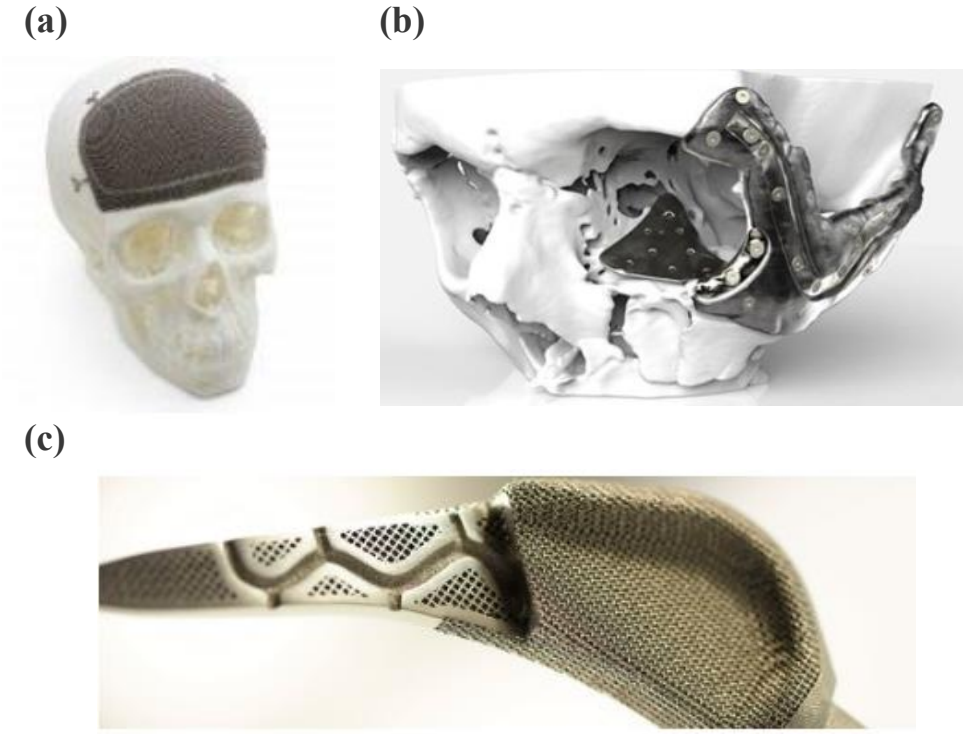

Fig. 15: example of biomedical devices produced via AM. (a): Cranial Implement [188]. (b): Skull implant [189]. (c): Orthopaedic implant [190].

Similar to the aerospace industry, the reduction in tooling operations and material waste are two significant advantages that have greatly contributed to the adoption of AM in the medical device industry, leading to cheaper and faster production [71]. For instance, fabricating a hip stem prosthesis using EBM was 35% less expensive than traditional manufacturing methods [72]. By 2015, over 100,000 acetabular implants had been produced using AM processes, with more than half of them successfully implanted in patients [69].

In addition to the aerospace, automotive, and medical sectors, several other industries have begun adopting AM processes, including armaments, furniture, jewelry, sports, toys, textiles, and the food industry [73]. Tool and mold manufacturers are also integrating AM technologies into their production methods. Looking ahead, the future of AM is increasingly seen as complementary to traditional manufacturing, combining the benefits of both approaches. The AM industry saw revenue growth of 17.4% in 2016, and an even higher 25.9% in 2015, reaching a total market value of $6.063 billion [74].

2.5 Build Orientation in AM

A metal AM part's characteristics depend on a multitude of factors, ranging from powder properties and slicing technique to process parameters and post-treatment methods. The part orientation is a crucial aspect of the build preparation process; it involves aligning the part with the build direction, which is perpendicular to the build plate and determines the direction in which the object is built up layer by layer. The diagram in Fig. 16 provides a visual explanation of the concept of build orientation. Eleven distinct inclinations relative to the build plate have been utilized in the production of titanium alloy specimens [75].

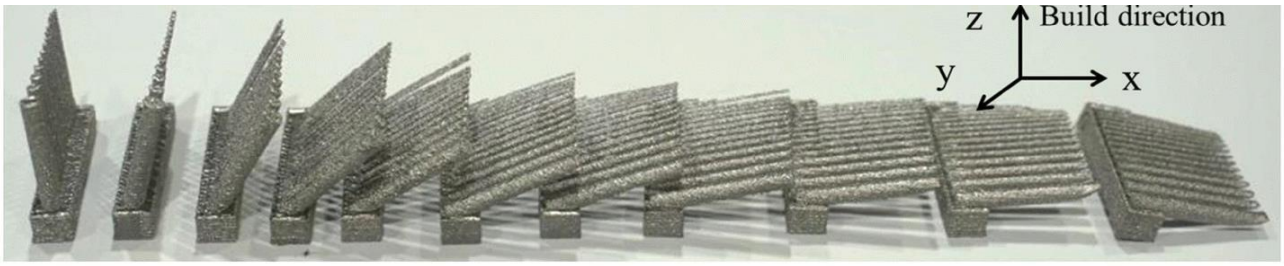

Fig. 16: Visual explanation of build orientation concepts: Ti6Al4V specimens manufactured through EB-PBF in 11 different orientations. Adapted from [75].

This attribute primarily impacts the manufacturability of metal AM components [76]. As a general rule, it's advisable to optimize the orientation of the part to reduce overhanging features within it. This is important because, especially in L-PBF, we often need extra structures to support parts that are at a steep angle. Unfortunately, these extra supports can slow down the manufacturing process, create more waste, and, after printing, they need to be removed, which could affect the smoothness of the surface. Furthermore, we need to recognize that metal AM is a process that uses heat with both powder and melted material, and these have different heat properties. The way we position the part affects how much of the current layer is supported by the powder or melted material. This can affect the quality of the part in many ways and has recently become a focus of attention for researchers. By studying how the orientation of the build affects the properties of metallic AM parts, we can gain better control over the process and make it more reproducible.

Reviewing existing studies in the literature, I find that researchers have used experimental (and sometimes numerical) methods, mostly looking at L-PBF and EB-PBF techniques. They usually use standard specimens, like either tensile or fatigue, or single struts considered as basic components of lattice structures [77]. Regarding the materials, Titanium alloys (mainly Ti6Al4V) are among the most studied, together with Aluminum alloys, Nickel alloys and Stainless Steel. The literature overview indicates that the build orientation has an impact on many features such as surface roughness, porosity, and microstructure, as well as on mechanical properties like fatigue. Furthermore, researchers have studied how the build orientation interacts with post-treatment processes. However, it is noteworthy that these studies include diverse technologies, materials, geometries, and process parameters. The interplay between build orientation and other contributing factors cannot be overlooked. This complexity causes the current absence of comprehensive design and evaluation guidelines related to build orientation within the topic of Design for Additive Manufacturing (DfAM). The absence of such guidelines poses a challenge, as it restricts the ability to make well-informed decisions in optimizing metal AM. Building these guidelines would offer a framework for making better choices during the metal AM optimization process. A systematic review of experimental results available stands out as an essential initial step toward the formulation and development of these guidelines. This systematic review would enable a thorough examination of the existing knowledge base, paving the way for a more cohesive and standardized approach to understanding the relationship between build orientation and the various factors influencing the final product's properties. To sum up, the creation of design and evaluation guidelines holds the potential

to enhance the effectiveness and efficiency of metal AM processes, fostering a more streamlined and informed approach to AM.

2.5.1 Effect of Build Orientation on Surface Roughness and Morphology

One another important feature to be considered is Surface Roughness. Roughness affects how products look and how strong they are against fatigue. That's why a lot of effort has gone into studying how the way we consider build orientation during the building process connects to the roughness of the final product. Roughness matters because it's linked to how ultimate outcome looks. Smoother surfaces usually look better and nicer. But it's not just about visual characteristics – it also affects how strong the material is against getting worn out over time. Scientists and researchers have been paying attention to the relation between build orientation and roughness. This is because understanding this connection is crucial for manufacturing that not only look good but also last longer and work better. It's trying to figure out the best way to construct objects, so they turn out well and stay strong against fatigue.

Weißmann et al. [78] compared the surface roughness of L-PBF and E-PBF which were built in different orientations. They used Ti6Al4V specimen with a costume shape composed of two cylindrical and parallel plates which were connected through four perpendicular struts. Considering L-PBF technology, the vertical struts had lower roughness when compared to 45° ones. On the other side, there was an opposite trend in EB-PBF. In L-PBF method, because of the energy flow, the powder sticked to the underside causing deviations from the designed geometry. This leads to having higher roughness in 45°. While, in EB-PBF, the same situation leads to have a lower roughness because it helped to fill of some surface defects. Nguyen H. and others [79] found that titanium alloy parts made with L-PBF had smoother surfaces than those made with EB-PBF. They explained this by saying that the electron beam in EB-PBF creates more heat, which makes the powder stick more to the surface. In a study by Hoving [80], the surface quality of parts made using different 3D printing conditions was investigated. They examined various build orientations ranging from 0° to 135° for L-PBF maraging steel grade 300. In Fig. 17a, the effects of these orientations on surface texture are shown. Fig. 17b illustrates that surface roughness remains relatively constant between 0° and 90° but increases significantly beyond 90°. This could be because surfaces shift from being upward-facing (up-skin) to downward-facing (down-skin) at angles greater than 90°. Notably, parts built at 60° and 75° angles exhibited the lowest surface roughness.
For build orientations between 0° and 90°, surface roughness values of approximately 10-15 μm (Ra) were observed. However, higher roughness values of about 20 μm, 28 μm, and 73 μm were recorded for orientations of 105°, 120°, and 135°, respectively. This trend was also observed for Rz values. Additionally, Fig. 17c and d depict the influence of build orientation on surface morphology, with parts fabricated at angles over 90° showing poor surface quality.

Moreover, previous studies [81, 82, 83] consistently reported that up-skin surfaces tend to have lower surface roughness compared to down-skin surfaces.

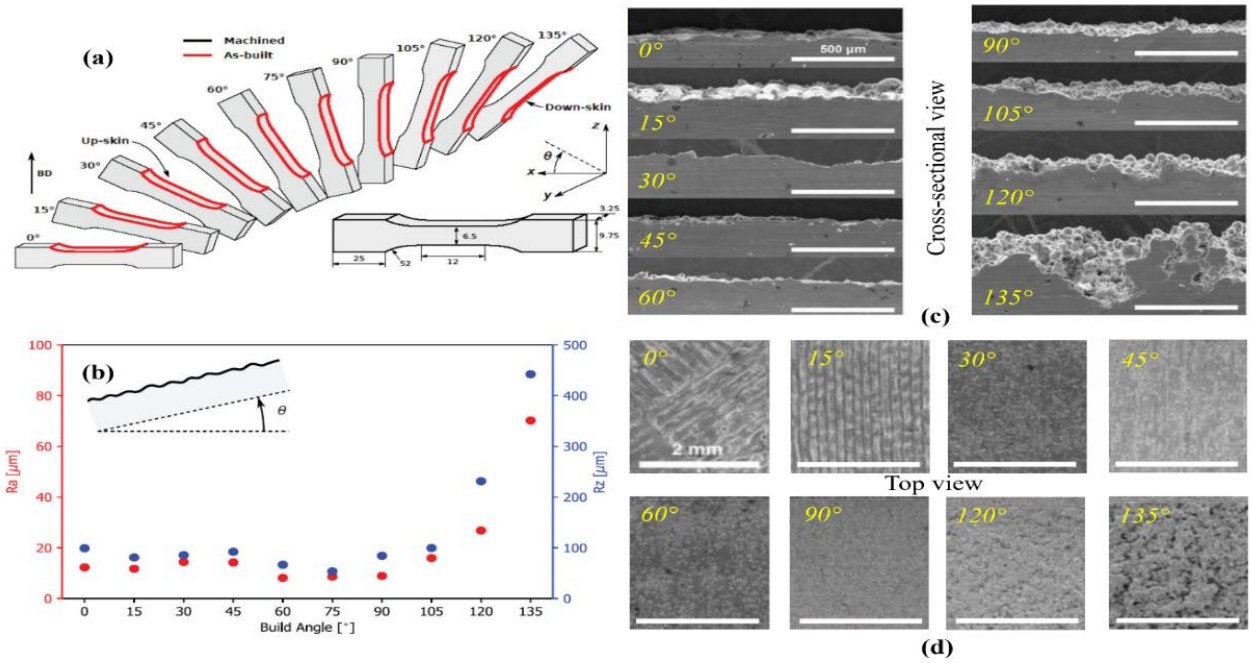

Fig. 17: (a) Specimen orientations ranging from 0° to 135° and the dimensions of L-PBF 18Ni300 specimens, with BD indicating the build direction. (b) Surface roughness (Ra and Rz) plotted against build orientation for L-PBF 18Ni300. Surface morphology of parts fabricated at different build orientations in (c) cross-sectional and (d) top view, highlighting the subpar surface quality of parts produced with a build orientation exceeding 90° [80].

Zhang and colleagues [82] studied L-PBF AlSi10Mg parts. They discovered that the surface roughness on the up skin area was similar for all parts tilted between 10° and 45°. However, as the tilt angle increased (closer to vertical), the roughness on the down skin area decreased. This happened because fewer powder particles clumped together and stuck to the surface as the tilt angle increased. Murchio et. al.[84] thoroughly examined the differences in roughness between the upper and lower surfaces of a material at various inclinations: 90°, 45°, 15°, and 0°. They focused on Ti6Al4V printed with L-PBF, as shown in Fig. 18a. In Fig. 18b, they presented the roughness values across different orientations of the built struts. The struts built vertically (at 90°) exhibited the smoothest surface with approximately 17 μm Ra (roughness average), followed by those at 45°, 15°, and 0° with Ra values of roughly 23, 34, and 73 μm, respectively. The orientation of the build significantly influenced the surface appearance, showing a non-linear trend from steeper to shallower angles. Fig. 18c illustrates how increasing the inclination heightened surface roughness, consistently showing the upper surface smoother than the lower one. Fig. 18d and 6e depict the surface characteristics of the upper and lower faces, respectively, at different build orientations. More surface irregularities were observed on the lower face compared to the upper face of the specimen.

Suard et al.[85] investigated how the roughness varied around the circumference of cylindrical Ti6Al4V specimens produced via EB-PBF at different orientations. They found that in vertically positioned single struts, there were no significant variations in surface roughness around the circumference. However, on inclined or horizontal struts, the roughness on the down-skin was higher. This was attributed to over-melting and a higher density of partially melted particles adhering to the surface. This difference in roughness, especially noticeable at lower angles, is important to consider as it affects the mechanical strength of the specimens, as explained in the following sections.

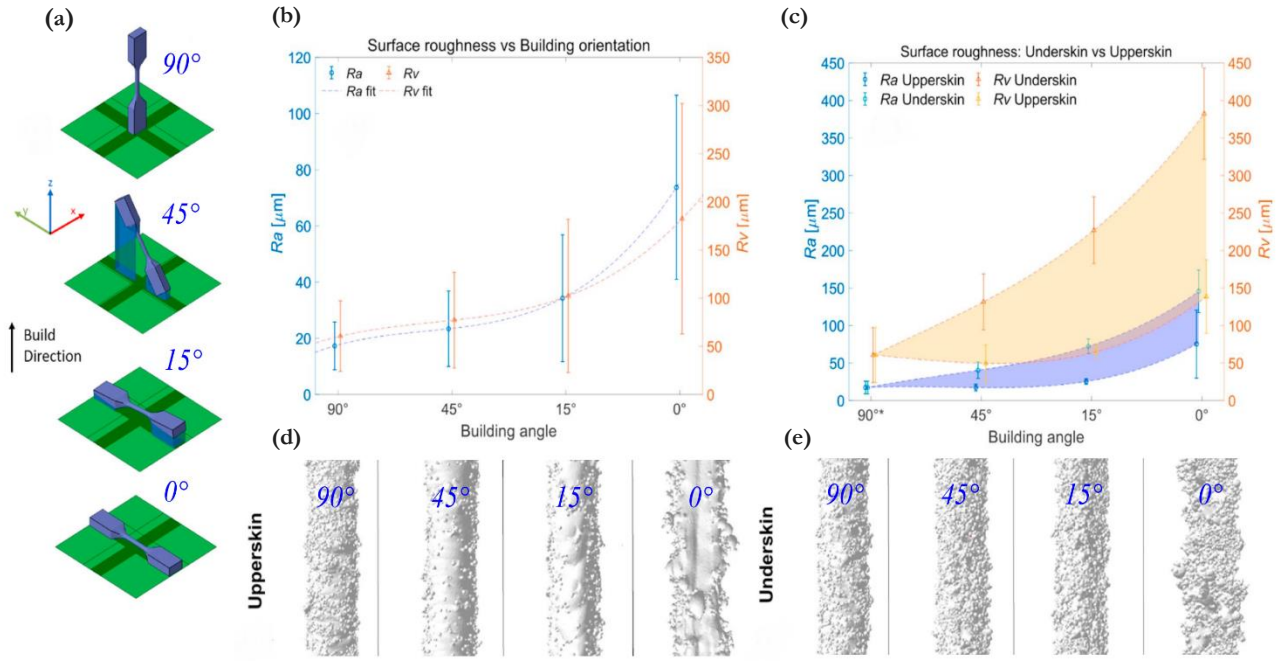

Fig. 18: (a) Build orientations of 90°, 45°, 15° and 0° for L-PBF Ti6Al4V specimens. (b) Surface roughness in terms of R_a and R_v over the considered strut build orientations demonstrating that fabricated strut with build orientation of 90° had the lowest surface roughness, followed by those produced at 45°, 15°, and 0°, respectively. (c) Surface texture variations at different inclinations for up and down-skin were obtained with L-PBF for Ti6Al4V struts. Surface morphology of the (d) up-skin and (e) down-skin faces at different build orientations showing more surface anomalies on the down-skin faces [84].

Another intriguing yet less explored aspect involves examining the contrast in surface roughness between inner and outer surfaces. In their study, Maculotti and colleagues [86] investigated EB-PBF Ti6Al4V shapes consisting of plates set at various inclinations. They compared the results across different orientations (30°-50°-70°-90°) and specifically analyzed the inner and outer surfaces at each inclination. The findings underscored that the outer surfaces exhibited lower surface quality compared to the inner surfaces across all build orientations.

2.5.2 Effect of Build Orientation on Porosity

Many studies have shown that build orientation can really affect how much empty space, or "porosity," it has [75, 82, 87, 88]. If there's too much of this empty space, the part won't be as dense, meaning it won't be as strong [89]. This is especially important for structures made of cellular structures (they are characterized by their porous microstructure that is comprised of solid and void networks) because any unwanted empty spaces within the supports can make the whole structure less dense [90]. The holes inside parts made with AM can come from different things, like how the machine is set up, the way the part is positioned, and even the properties of the powder being used [91, 92].

When working with metal AM, the first thing we need to do is figure out the best settings for the process. This helps make sure the parts we make are completely solid [93]. Research has found that by process parameter optimization for PBF technology, we can create components with hardly any flaws inside them, less than 1% [75, 94, 95]. Fritsch et al., [88] looked into how built orientation affects the number of tiny holes and the quality of the surface in Inconel 625 parts made with L-PBF. They tested different angles for building the parts, from 30° to 90° in 10° increments. According to Fig. 19a, they found that while the number of holes on the up skin didn't follow a clear pattern, there was a decrease in the number of holes on the down skin as the angle changed from 30° to 90° compared to the build plate. This suggested that parts built vertically had fewer overall holes. The decrease seemed to be because there were a smaller number of tiny holes, while larger holes didn't change much (Fig. 19b).

Also, they noticed that there were more holes near the down skin compared to the up skin, regardless of the angle. For instance, Fig. 19c represents the locations of pores along the height of the strut with a build orientation of 30°, where the pores are color-coded based on their size: small (≤30 µm, green) and large (>30 µm, red) pores.

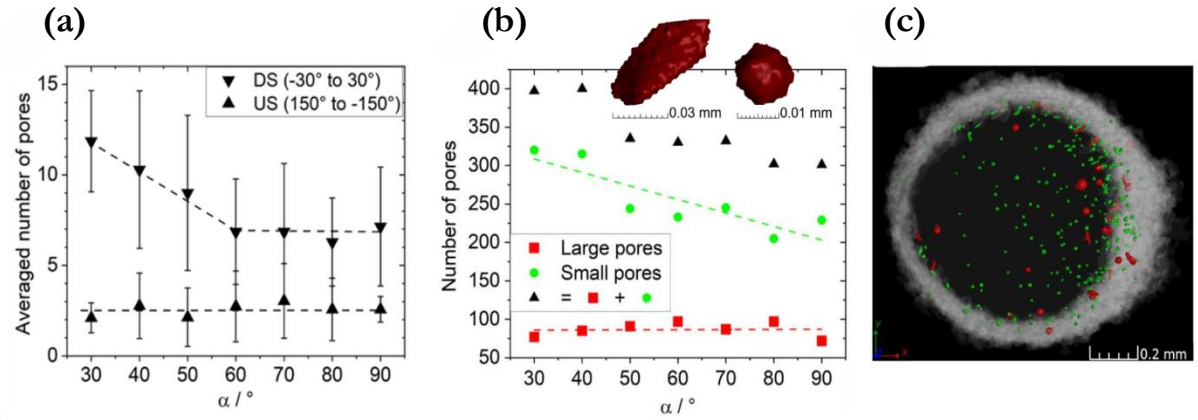

Fig. 19: The porosity analysis results for L-PBF Inconel 625 specimens with build orientations ranging between 30° and 90° with a 10° step in terms of (a) variation in the number of pores on the up-skin (US)/down-skin (DS) of the strut with respect to the build orientation. (b) Distribution of small (green) and large (red) pores on the strut cross-section as a function of build orientation. (c) Locations of pores along the height of the strut having a build orientation of 30° with the solid material being presented with a transparency of 90% (black, in the centre) and the pores color-coded based on the size of small (≤30 µm, green) and large (>30 µm, red) pores [88].

Research has shown that inclined parts tend to have more holes in the down skin area [82, 88, 90, 95]. For example, in Fig. 20a, they show the results for parts made of L-PBF Ti6Al4V at angles of 35.5°, 45°, 60°, and 90°. It shows that there are more holes in the down skin area for all those angles, but when the parts are built vertically, the holes are evenly spread across the whole surface. They provide close-up pictures of the holes in the up skin and down skin surfaces in Fig. 20b [90]. These findings are approved by a study carried out by Delroisse and colleagues [87] on L-PBF AlSi10Mg parts. They found that the number of holes in vertical struts was similar to that of the up skin of inclined parts (0.4%-0.1%), but significantly higher in the down skin (4%). This difference is usually explained by how the part is heated during the building process. When the part is built at low angles, more of it is supported by powder, which has a lower thermal conductivity [82]. As a result, the lower surface of inclined parts stays hotter for longer, causing excessive heating and leading to larger [96] and more pores [82], characterized by instabilities and the formation of gas pores [87]. Delroisse et al. [87] suggest that most of these holes are filled with hydrogen, as the solubility and movement of hydrogen in the cavities increase with temperature.

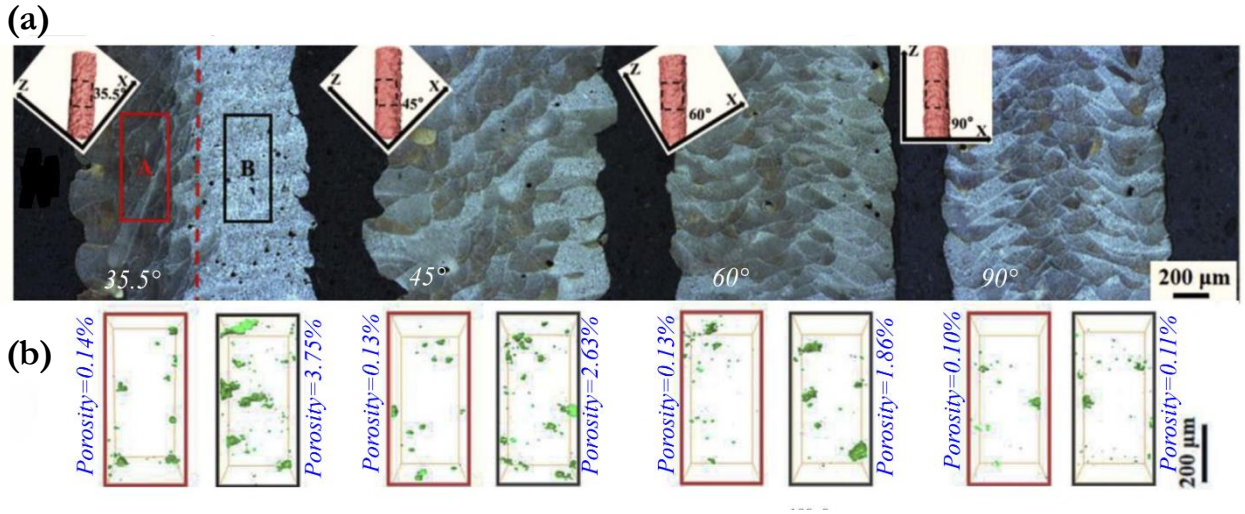

Fig. 20: (a) Distribution of pores between up-skin and down-skin zones in L-PBF Ti6Al4V struts made different inclinations of 35.5°, 45°, 60° and 90°. (b) Detailed micrographs of porosities in the considered scan areas on up-skin and down-skin in the strut built with orientations of 35.5°-90° [90].

Beyond the overall porosity, some researchers examined the relationship between build orientation and other porosity characteristics in more detail. However, the literature results are not always consistent. Suard et al. [94] reported that build orientation in L-PBF Inconel 718 specimens did not affect the mean diameter and the sphericity of pores. Moreover, as shown in Fig. 21a and Fig. 21b (for fabricated specimens with 90° and 35.3° build orientations), pore distribution along the width and length of the part was not affected by build orientation and was described as uniform. The authors considered two single struts of 1 mm diameter with different build orientations to estimate the porosity distributions in BCCZ lattice structures.

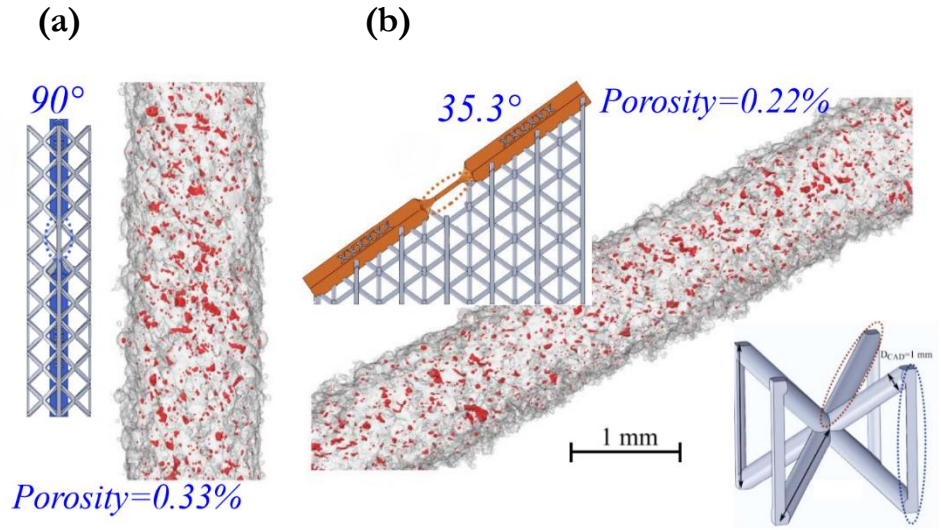

Fig. 21: Uniform distribution of pores along the strut length and width for L-PBF Inconel 718 specimens fabricated with build orientations of (a) 90° and (b) 35.3° [94].

Although the link between build orientation, thermal history, and porosity is highly relevant, its interplay with other process parameters should be further investigated. One example of such analysis is reported by Zhang et al. [82] who studied the relative density of L-PBF AlSi10Mg specimens changing both the scanning speed and the build orientation. As shown in Fig. 22a, lower scanning speed induced more pores (lower relative density (%)) for highly inclined (<20°) parts. On the contrary, at lower inclinations (>20°), the influence of scanning speed was negligible due to the wider inter layer

offset region. Fig. 22b reveals the obtained results of porosity analyses considering same scanning speed of 2200 mm/s with different build orientations of 10°, 15°, 20°, 25°, 30° and 40° demonstrating similar sphericity of pores as well. In contrast to these results, other studies found that pores can be more irregular (sphericity<0.5) and elongated at low angles [75], [81] reporting different distributions for superficial pores [81] with small pores increasing at lower angles [88].

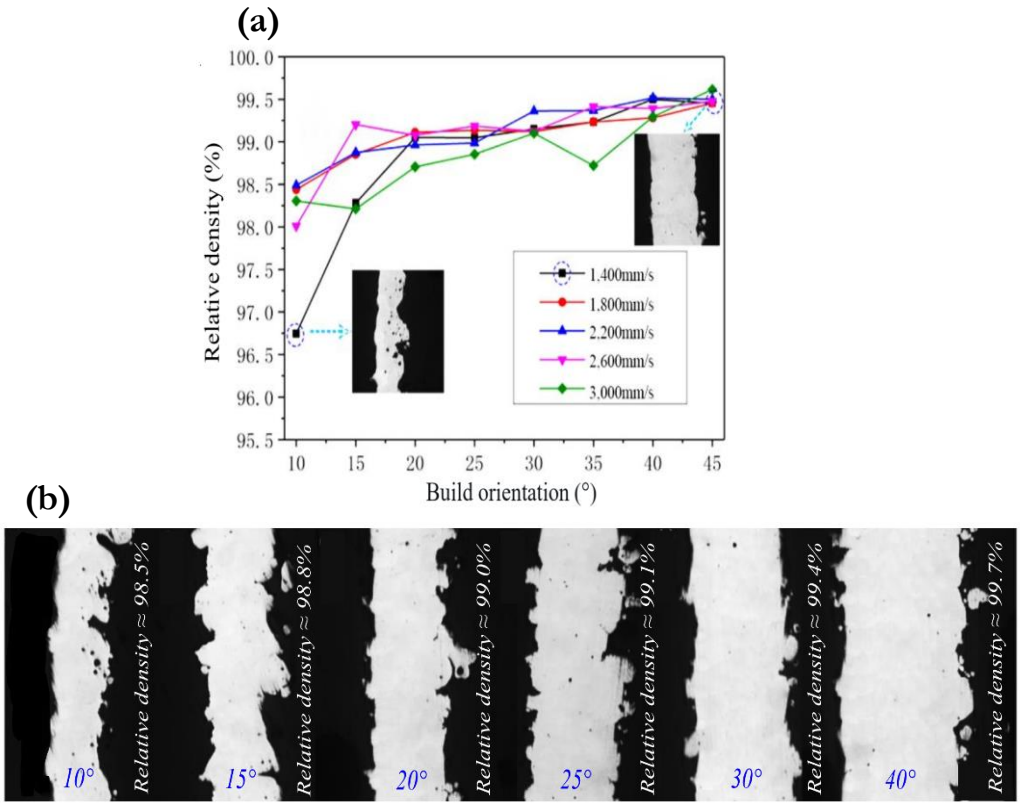

Fig. 22: (a) The influence of scanning speed on the density of the L-PBF AlSi10Mg strut for different build orientations of 10°, 15°, 20°, 25°, 30°, 35°, 40° and 45°. (b) The results of porosity analysis considering the same scanning speed of 2200 mm/s with different build orientations of 10°, 15°, 20°, 25°, 30° and 40° [82].

Considering porosity, however, some studies show a different pattern. They find that there's actually fewer holes when the parts are built at low angles [81, 89, 94, 96, 97]. For example, in Fig. 23a Murchio and colleagues [81] studied L-PBF Ti6Al4V parts and found that the number of holes decreased as the angle of building decreased. They found that the average number of holes was 0.19%, 0.09%, 0.08%, and 0.05% for parts built vertically, at a 45° angle, at a 15° angle, and horizontally, respectively. This was also seen in research by Sombatmai et al. [96] on the same technology and material. Similar trends were found in L-PBF AlSi10Mg parts built at different angles ranging from 0° to 90°, as shown in Fig. 23b [98]. The average hole sizes were 0.01%, 0.06%, and 0.08% for solid cubic pieces built at 0°,45°, and 90°, respectively. Additionally, in Fig. 23c, there's a representation of the normalized density and size of holes. It was noticed that there were more holes in the pieces built at 45° and 90°, with a peak at 1.2 mm−3 (45°) and 1.6 mm−3 (90°) for holes with diameters ranging from 60 µm to less than 70 µm.

This trend is also seen in L-PBF for 316L stainless steel [89]. These findings indicate that parts made with a 45° angle had a higher density compared to vertically built ones. Specifically, relative densities of approximately 99.71%, 99.83%, 99.91%, and 99.96% were reported for parts built vertically, at 75°, 60°, and 45° angles, respectively. Interestingly, researchers explained this trend by thermal history of the parts during production. They suggested that in inclined parts, where there are larger pools of melted material and more heat accumulates on the lower surface, there's less chance of inadequate overlap between the melted sections, which could lead to higher porosity. Thus, different studies point

to the same phenomenon as the reason for opposite trends. However, there are also studies, like the one by Hossain et al. [99] on L-PBF Ti6Al4V and 316L stainless steel parts, that didn't find a clear link between hole formation and build angle. These inconsistencies underscore the need for more thorough and systematic research to understand the extent and nature of this influence.

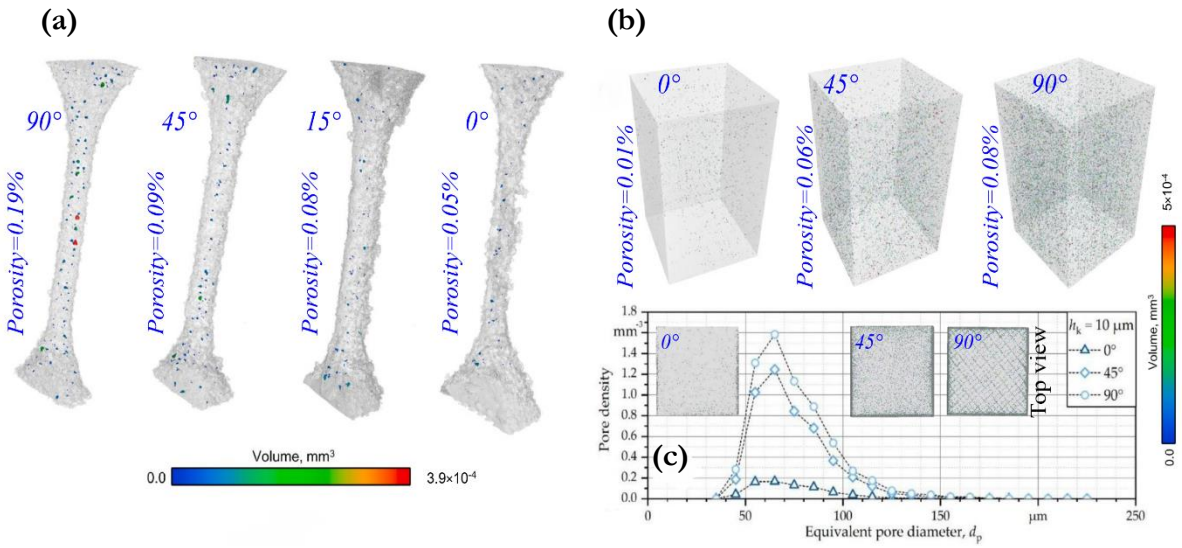

Fig. 23: (a) CT images of porosity distribution within the L-PBF Ti6Al4V struts built at different orientations (90°, 45°, 15°, 0°) in a volumetric scale [81]. (b) Analysis of porosity in L-PBF AlSi10Mg produced with various build orientations ranging from 0° to 90°. (c) Comparison of defect density across different build orientations: 0°, 45°, and 90° [98].

2.5.3 Effect of Build Orientation on Microstructural Properties

The microstructure of metallic AM parts, which is a fundamental characteristic, is influenced by various factors. Specifically, the thermal history plays a crucial role in shaping the microstructure of these parts. In PBF technologies, parameters such as the energy source, scanning speed, distance between hatch lines, layer thickness, and build orientation are known to impact the microstructure of the final part [100, 101, 102, 103]. Due to the rapid scanning process, PBF often leads to the formation of extremely small melted areas, characterized by rapid solidification and cooling rates, resulting in high thermal gradients. As a result, these materials typically exhibit highly refined cellular-like microstructures. This means that the grains or crystal structures within the material are very small and uniform [104].

Because of the rapid cooling rates involved in the manufacturing process of certain alloys like steel or titanium, there's a tendency for metastable phases, particularly martensite, to form. These phases are typically hard and brittle [105], which may not be ideal for the intended use of the parts. Therefore, additional heat treatments are often necessary after the initial manufacturing process to achieve a more suitable microstructure that can withstand real-world conditions [106]. In general, the high thermal gradients during the manufacturing process promote the growth of columnar grains in a directional manner, a phenomenon known as epitaxial growth. This results in the formation of a crystallographic texture with preferred orientations or directions. This texture contributes to the anisotropic behavior of AM parts [107, 108], meaning their properties and performance can vary depending on the direction in which they're tested or used. The thermal variations in PBF technologies, which play a significant role in determining the microstructure, are greatly affected by the build orientation [109]. Essentially, the build orientation dictates the extent of the overlapping area, where a part of the new layer is supported by previously melted material, while the remainder is supported by powder with lower

thermal conductivity compared to the melted material [110]. Additionally, orientations of parts different from vertical result in the formation of up-skin and down-skin regions within the part, which undergo distinct thermal histories during the manufacturing process, as discussed earlier. Therefore, it is essential to examine how the build orientation influences the microstructure of metal parts as they are manufactured.

Dong and colleagues [111] conducted a study where they used L-PBF to create specimens of AlSi10Mg. Their aim was to analyze how the orientation during the build process affected the microstructure of the parts. They examined the microstructure of specimens built at angles of 35.5°, 45°, 60°, and 90° and found a cellular-dendritic microstructure. This microstructure appeared finer on the upper surface and coarser on the lower surface, which was highlighted in areas A and B for the 35.5° orientation in Fig. 24. This difference was more noticeable in struts with greater inclinations, as observed through Scanning Electron Microscope (SEM), particularly in area B for all four orientations in the lower surface zone shown in Fig. 24. The largest grains were observed in the specimen built at an angle of 35.5°. Additionally, specimens at 35.5° and 45° displayed larger and elongated grains (known as columnar grains) compared to those at 60° and in the vertical position, which had smaller, evenly shaped grains (referred to as equiaxed grains). Furthermore, the average grain size decreased as the orientation approached the vertical direction: from 3 µm in the 35.5° specimens to 2 µm at 45°, then to 1.5 µm at 60°, and finally to 1 µm in the vertical specimens.

The authors also studied the heating and cooling patterns of the inclined specimens using Finite Element Method simulation. They discovered a consistent cooling rate on the up-skin, but this rate increased by 51.5% on the down-skin between the 35.5° and vertical specimens. The findings supported the idea that inclined specimens develop larger grain sizes, especially on the lower surface, due to the slower cooling rate, which allows for grain growth. These findings were further confirmed through an examination of microstructural differences in lattice specimens of L-PBF AlSi10Mg. These specimens featured struts with a body-centred cubic unit cell, including both vertical and inclined struts at a 35.5° angle [87]. The analysis revealed that the microstructure on the up-skin of the 35.5° struts was 2.5 to 3 times finer compared to the down-skin. This difference was attributed to the thermal conditions experienced during the manufacturing process. The down-skin of the strut, partially supported by insulating powder, retains heat for a longer duration, resulting in the growth of coarser grains. Conversely, the up-skin, supported by melted material, experiences conditions similar to those of vertically built struts, leading to a higher cooling rate and the formation of finer grains.

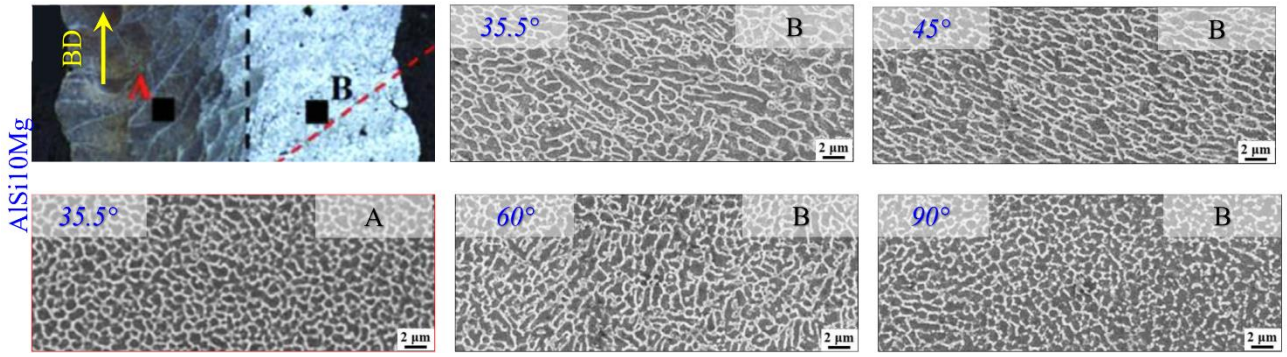

Fig. 24: (a) Microstructural analysis in L-PBF AlSi10Mg specimens with different orientations of 35.5°, 45°, 60°, 90° exhibiting cellular-dendritic microstructure on the up-skin and coarser on the down-skin shown in area A and B [111].

Nezhadfar et al. [112] noted that the typical grain arrangement formed in AM process consisted of columnar grains, surrounded by equiaxed grains, especially near the molten pool. They investigated how the microstructure varied based on the orientation of the build, either horizontal or vertical, for five different aluminum alloys. All specimens were produced using L-PBF with build orientations set vertically and horizontally. Fig. 25a-d display the Inverse Pole Figure maps generated through Electron Back Scatter Diffraction (EBSD) for specimens built at 90° and 0° angles using various aluminum alloys, including AlSi10Mg, Scalmalloy, QuesTek Al, and AlF357, respectively. Isaac et al. [113] also

investigated how different build orientations, specifically 0°, 45°, and 90°, impact the microstructure of L-PBF AlSi10Mg. They found that the mean grain sizes were 8.9 µm for 0°, 8.1 µm for 45°, and 9 µm for 90° build orientations, with minimal differences observed between them. Their findings revealed that the microstructure predominantly comprised elongated columnar grains with finer grains surrounding the boundaries of the melt pool for all build orientations. These columnar grains, elongated along the direction of build, were enveloped by smaller grains. This microstructural arrangement is a result of the rapid melting and subsequent rapid cooling inherent in the L-PBF process. Several studies in the literature also support the notion that build orientation influences the growth of columnar grains, as these grains tend to align with the build direction [52, 114]. This alignment is attributed to the heat flow being oriented along the build direction due to higher thermal gradients, which induces a preferred grain orientation [115].

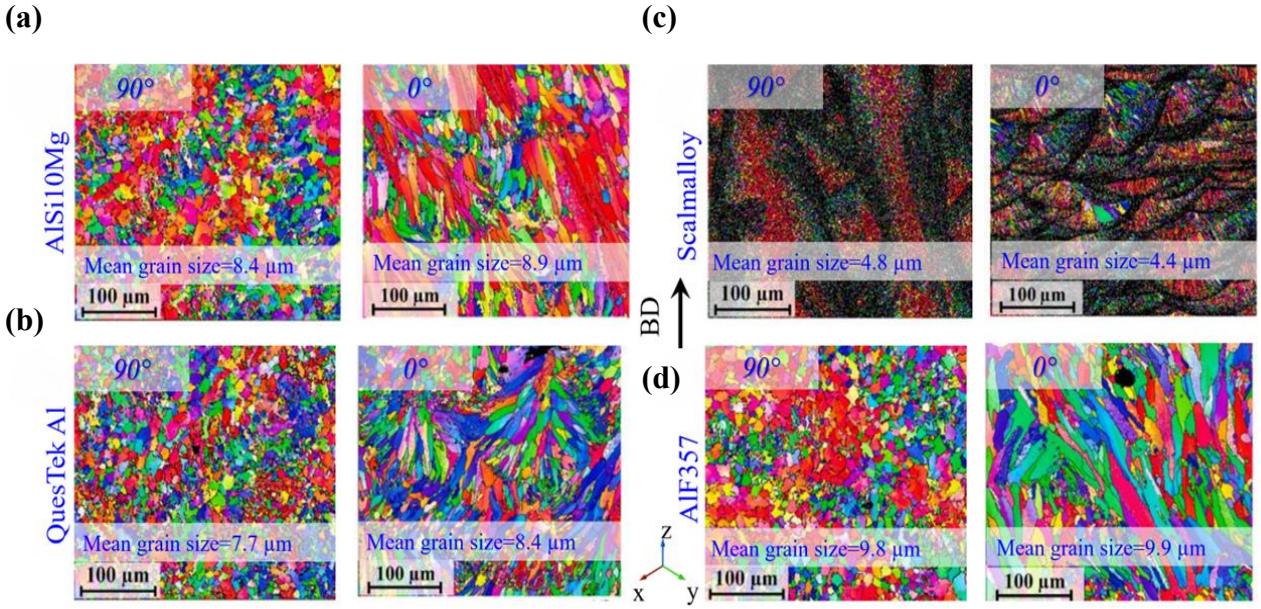

Fig. 25: Inverse Pole Figure maps of different Al alloys including (a) AlSi10Mg, (b) Scalmalloy, (c) QuesTek Al and (d) AlF357 all manufactured by L-PBF with vertical and horizontal build orientations [112].

Ghorbanpour et al. [116] verified the elongation of grains in the direction of build in L-PBF Inconel 71 specimens produced both horizontally and vertically, as illustrated in Fig. 26a. Moreover, the Grain Orientation Spread (GOS) maps obtained (refer to Fig. 26b) revealed higher values for the horizontally built specimens, with a mean GOS of 0.88°, compared to the vertically built specimen, which had a mean GOS of 0.72°. The GOS plots indicate internal grain distortions and residual stress within the material, where higher GOS values indicate greater misorientations and residual stress [117]. Leicht and colleagues [118] explored how different printing angles (90°, 45°, and 30°) affect the microstructure of metal ribs made using L-PBF 316L. Their findings suggest that while ribs printed at inclined angles (45° and 30°) display random texture orientations, the main orientation along the printing direction is still noticeable, though less intense compared to straight ones (90°). Ribs printed at 45° and 30° angles exhibit large, elongated grains along the printing direction. Additionally, small grains are present on the surfaces of inclined ribs, similar to those in vertical ribs. These smaller grains likely form due to varying amounts of unmelted and partially melted powder adhering to both sides of the ribs. Furthermore, these smaller grains don't appear to grow towards the center of the manufactured rib, which is also observed in the straight ribs. Instead, they seem to be slightly stretched along the surface of the part. This change in grain direction suggests differences in temperature gradients. These gradients are influenced by the thermal conductivity of both the powder bed and the part itself. Consequently, heat dissipation varies with changes in build orientation, affecting the direction of grain growth. Additionally, it's worth noting that the rib produced with a 30° build angle was thinner

compared to those with a 45° build angle, highlighting once more the limitations in geometric accuracy when manufacturing parts with inclined features.

Addressing the issue of columnar grain growth along the build direction, there exist divergent findings in the literature. For instance, Wauthle et al., [90] investigated the microstructure of L-PBF Ti6Al4V lattice structures with various build orientations and noted that grains could elongate either in the direction of build or along the strut orientation. Similarly, Murchio et al. [81] examined the microstructure of L-PBF Ti6Al4V dog-bone specimens oriented at 0, 15, 45, and 90 degrees (vertical). They observed no significant disparities in the microstructure among the four groups of specimens. These contrasting results underscore the complexity of the relationship between build orientation and microstructural characteristics in AM processes. Moving forward, further research is needed to discover the underlying mechanisms driving grain growth and its implications for the performance and properties of fabricated components.

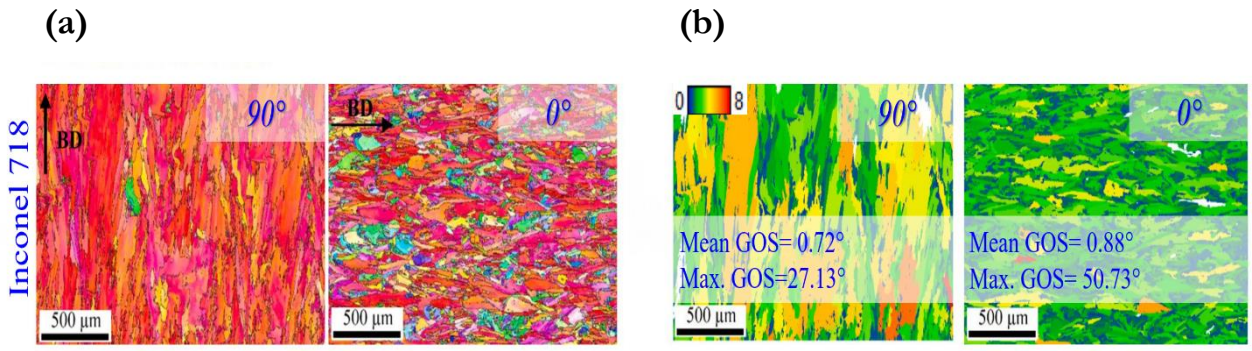

Fig. 26: (a) The stretching of grains in the direction of build observed in L-PBF Inconel 718 specimens manufactured with 90° and 0° (b) the associated GOS maps, which reveal residual stresses and distortions within the grains [116].

2.5.4 Effect of Build Orientation on Hardness

Hardness stands as one of the most extensively examined mechanical attributes in AM, serving as a reliable metric for assessing mechanical performance. Regarding struts, there have been no reported dependencies of microhardness on build orientation [33, 96, 116]. However, an observed correlation exists between height (i.e., distance from the build plate) and microhardness, revealing lower microhardness in the upper layer compared to the lower layers. This phenomenon arises due to the rapid cooling rates nearer to the substrate, leading to a finer microstructure. For instance, the average microhardness (measured in HRC) values for the bottom and top layers of L-PBF Ti6Al4V specimens fabricated in three perpendicular orientations were 33.55-31.65, 32.77-24.01, and 37.67-30.10, respectively [119]. Additionally, Palanisamy et al. [120] noted marginally lower Vickers hardness in 45° Ti6Al4V struts compared to vertical ones in both EB-PBF and L-PBF specimens.

2.5.5 Effect of Build Orientation on Fatigue strength

Comprehending the fatigue behavior of components manufactured through AM is essential for ensuring the reliability of load-bearing parts in applications subjected to cyclic loading, such as aerospace, railway, and automotive industries. It is widely acknowledged that the fatigue strength of AM components, whether bulk or lattice structures, is significantly affected by their build orientation [81, 97, 112, 121, 122, 123, 124, 125, 126, 127, 128, 129, 130, 131]. This influence stems from variations arising during the manufacturing process, including geometric inaccuracies, defects like porosity and staircase effects, microstructural non-uniformity, surface roughness, and residual stresses.

It is crucial to underscore the profound impact of surface defects on the propensity for fatigue crack initiation in as-built specimens. Surfaces exhibiting greater irregularities elevate the likelihood of premature crack initiation due to localized stress concentration, consequently diminishing fatigue resistance [132, 133, 134]. A similar trend is observed regarding porosity, where pores situated at or near the surface can serve as potential stress concentrators, thus becoming favorable sites for crack initiation under cyclic loading. This phenomenon was effectively demonstrated in the study conducted by Chern et al. [131] regarding the fatigue performance of rectangular EB-PBF Ti6Al4V specimens. They noted an anisotropic fatigue behavior during four-point cyclic bending tests on horizontally and vertically built specimens. Vertically built specimens displayed a shorter fatigue life, characterized by lower initiation time and a faster crack propagation rate, attributed to inter-layer melt defects serving as crack initiation sites when subjected to crack opening mode I loading. This observed trend was further supported by another study focusing on L-PBF Ti6Al4V specimens, which examined three different building orientations (0°, 50°, and 90°) in dog-bone specimens [130]. During axial fatigue tests, vertically fabricated specimens (90° orientation) performed better than series fabricated specimens due to a smoother surface profile. On the contrary, the samples made in 0 and 50° directions significantly show roughness of the surface, especially at the down-skin, due to the necessity of using supporting structures. Morettini et al. [129] observed that surface roughness is not the sole factor influencing the fatigue strength of additive AM specimens. They conducted tests on DMLS Ti6Al4V dog-bone specimens subjected to axial fatigue. DMLS, similar to Laser L-PBF, consolidates powders through sintering rather than melting, resulting in lower temperatures and laser power. Their study revealed that vertically built specimens exhibited a fatigue strength 30 MPa lower than their horizontally built counterparts, despite the latter having higher surface roughness. This difference was attributed to the presence of larger compressive residual stresses in the central region of the specimens, generated during the cooling process. These findings contradicted those of Meneghetti et al. [123] regarding DMLS maraging steel specimens, where horizontal specimens displayed the lowest axial fatigue strength even after undergoing an age hardening heat treatment.

The factors influencing how well lattice structures handle fatigue is more complicated because of their intricate design. Research shows that different build orientations can lead to significant surface flaws and holes, which can make them weaker over time [81, 97, 121, 122]. Additionally, the nodes where the struts connect might impact how well the lattice can withstand fatigue [121, 122]. Since lattice structures have small struts, even tiny flaws can have a big impact, making them more likely to break compared to bulk specimens [81]. Persenot et al. [97] conducted a detailed study on thin (2 mm) EB-PBF Ti6Al4V specimens printed at three different angles (90°, 45°, 0°). They found that the specimens printed vertically had the shortest fatigue life. Fig. 27a illustrates radial Micro Computed Tomography (μCT) slices of the specimens printed at various angles. The researchers identified two main types of surface flaws: unmelted powders and irregularities in layer stacking, also known as the staircase effect. Notches were primarily observed in the 90° and 45° specimens, which were perpendicular to the printing direction, as depicted in Fig. 27b. Conversely, they were nearly absent in the horizontal struts. By comparing radial slices of the specimens before and after fatigue failure, and examining the fracture surfaces, researchers discovered that cracks primarily started from the superficial notch-like defects. Interestingly, despite having higher roughness, the 0° specimens exhibited the longest fatigue life. This underscores that surface roughness alone cannot fully determine the fatigue strength of as-built AM specimens.

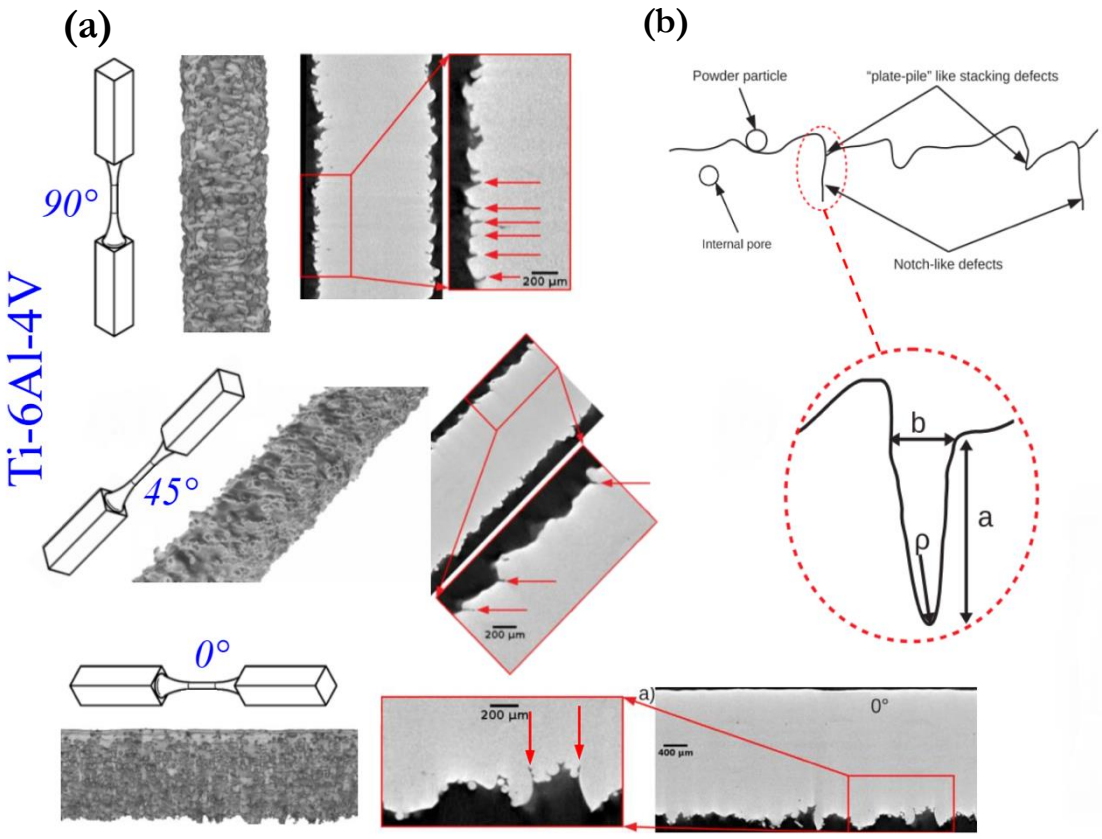

Fig. 27: (a) Influence of build orientation on the surface characteristics of thin EB-PBF Ti6Al4V specimens as they are built, with a close-up view focusing on the defects. (b) Diagram showing various types of defects present on or near the surface of EB-PBF as-built specimens, including the shape of notch-like defects [97].

Using a similar method, Murchio et al.[81] carried out a series of experiments on L-PBF Ti6Al4V struts produced at four different angles. The outcomes emphasized a significant impact of build orientation; however, in contrast to previous research, lower angles of construction resulted in reduced fatigue strength, as depicted by the S-N curves shown in Fig. 28a and b. In this instance, specimens at 0° displayed the weakest fatigue resistance, whereas those at 45° exhibited the strongest. The failure of the struts was attributed to the miniaturization effect, which increased their susceptibility to surface imperfections. Struts at low angles were found to possess greater geometric inaccuracies and surface roughness, making them more vulnerable to crack initiation from surface micro-notches.

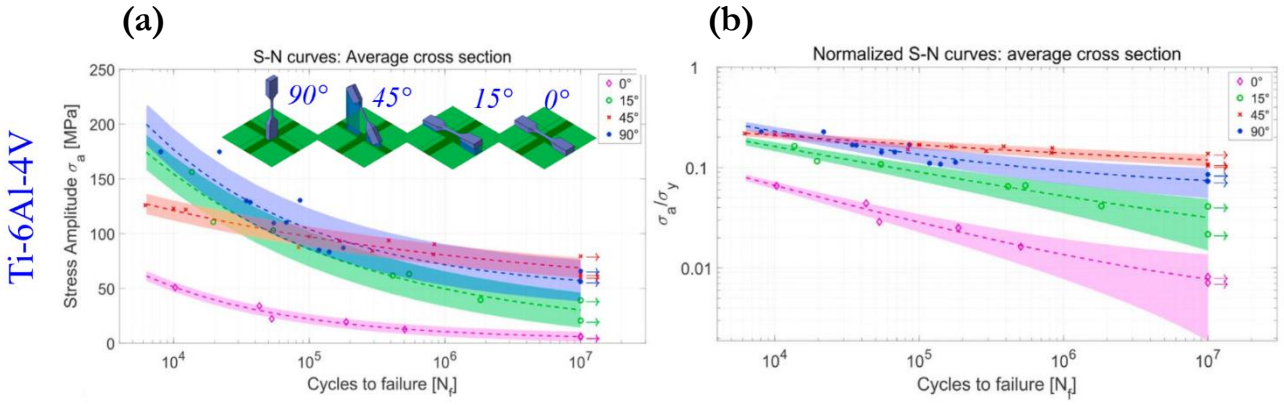

Fig. 28: (a) Semi-logarithmic S-N plots depicting the fatigue performance of strut-shaped L-PBF Ti6Al4V specimens constructed at various angles. (b) Dandlogarithmic S-N plots normalized by the yield strength for each orientation [81].

In another study by the same researchers [121], they investigated the impact of adding nodes along the struts on fatigue resistance. Consistent with their previous findings [81], struts oriented at 45° exhibited the highest fatigue strength. However, horizontal struts were less affected in terms of their fatigue life due to the presence of the node, which reduced the length of unsupported sections. Analysis of fracture surfaces revealed that in vertical and 45° specimens, where geometrical accuracy was better, failure primarily occurred at the node junction, where the fillet radius was smaller, leading to increased stress concentration. Conversely, in 15° and 0° struts, fractures initiated along the gauge length, largely influenced by geometrical inaccuracies and higher surface roughness, particularly in the down-skin region. These findings were similar to those presented by Dallago et al. [122], who investigated the fatigue response of L-PBF Ti6Al4V cubic lattice samples. In vertically constructed struts, the onset of crack formation was observed at the sharper and more irregular node fillet radius situated on the down-skin. However, in horizontally printed load-bearing struts, the critical site was the strut itself, especially at its center, owing to its inherent geometric imperfections. Consequently, this led to a diminished fatigue performance compared to vertically oriented struts, irrespective of the fillet radius. Additionally, it was noted that in specimens where the primary load-bearing struts were vertically printed, cracks initiated near the nodes and then spread to adjacent struts. Conversely, in lattices where the primary load-bearing struts were those printed parallel to the printing plane (horizontally), cracks originated in several struts simultaneously and away from the nodes, resulting in diffuse damage throughout the structure. Solberg et al. [128] extensively explored the impact of build orientation (ranging from 0° to 135°) on fatigue strength. They investigated the uni-axial fatigue behavior of L-PBF maraging steel grade 300 specimens across a broad spectrum of orientations. After reviewing similar studies, they concluded that although the fatigue performance obtained was lower compared to conventional manufacturing methods. Their findings revealed that specimens constructed near the 90° orientation exhibited longer fatigue life compared to those built closer to the 0° orientation (refer to Fig. 29a). Furthermore, as depicted in Fig. 29b, the fracture surfaces of the 0° and 135° specimens indicated that failure originated from the as-built surface, but from different zones: the center for 0° and from the corner for 135°.

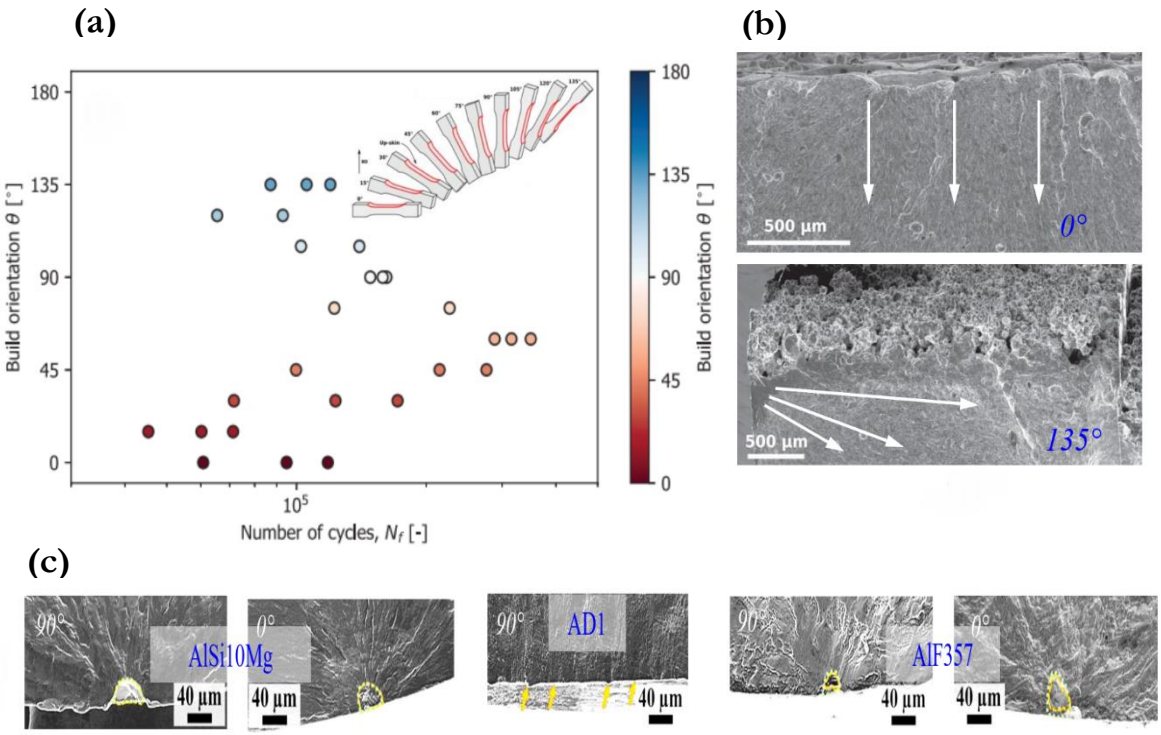

Fig. 29: (a) Uni-axial fatigue life (represented as the number of cycles to failure, Nf, at a 500 MPa load) of L-PBF maraging steel grade 300le-mens based on the building orientation. (b) SEM fracture surfaces of specimens built at 0° and 135°; white arrows indicate the initiation and propagation of fatigue cracks originating from the as-built surface [128]. (c) SEM fracture surfaces of some of the specimens tested [112].

Nezhadfar et al. [112] assessed the impact of build orientation on the fatigue strength of five different Al alloys produced via L-PBF. The authors' findings suggest that volumetric defects significantly influence fatigue crack initiation and, consequently, fatigue performance. Among the specimens tested, Scalmalloy and AD1 exhibited superior performance compared to AlSi10Mg, QuesTek Al, and AlF357, regardless of build orientation, mainly due to their lower defect density. A comparison of fracture surfaces between AlSi10Mg and AD1 specimens (Fig. 29c) illustrates that cracks in the former initiated from volumetric defects near or on the surface, while in the latter, they primarily originated from the surface itself. However, the fatigue behavior of specimens is not solely determined by defect density; the type (such as pores or lack-of-fusion (LoF)) and size of defects also play a crucial role. This distinction was evident in AlF357 and QuesTek Al alloy, which exhibited anisotropic behavior. Vertical AlF357 specimens outperformed horizontal ones because cracks initiated from small pores rather than large LoF defects (refer to Fig. 29c). A separate examination of the L-PBF AlSi10Mg alloy [127] delved into how the initial condition of construction affects its behavior under 3-point bending fatigue. To explore the impact of build orientation and consider the influence of surface characteristics, five distinct sets of specimens were fabricated at varying angles and subsequently tested (refer to Fig. 30a). These specimens were specifically engineered to experience maximum stress at the notched face (refer to Fig. 30b). Analysis of the S-N plots in Fig. 30c revealed that horizontal specimens (series B) exhibited superior fatigue resistance compared to vertical (series C) and diagonal counterparts. Among the inclined specimens, those featuring an up-skin notch (series E) outperformed those with a down-skin notch (series D). Fig. 30d showcases the fracture surfaces of series B and C; in series B, characterized by smoother surfaces and smaller features, cracks initiated from the specimen's corner. In contrast, cracks in series C initiated at the center of the notched face and then propagated between adjacent layers. Additionally, it was noted that residual stresses played a significant role, accounting for the lower fatigue thresholds observed in series C and D compared to the others.

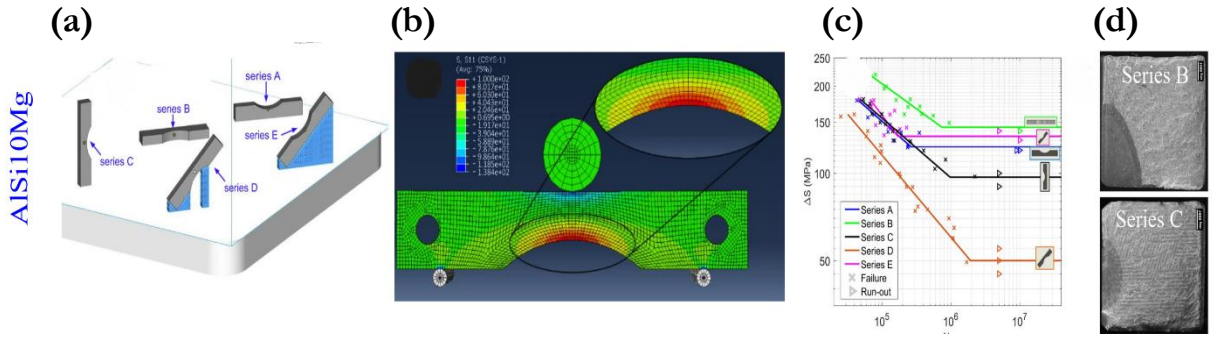

Fig. 30: (a) Various sets of L-PBF AlSi10Mg specimens subjected to 3-point bending fatigue; the blue areas represent the placement of supports utilized for the diagonal series. (b) FE model illustrating stress distribution along the fatigue specimens; highest stresses occur near the notched face. (c) Comparative analysis of S-N plots obtained for each specimen series. (d) SEM images displaying fracture surfaces of series B and C specimens [127].

Ponticelli et al. [126] investigated the fatigue strength of L-PBF 316L specimens under reverse bending loading conditions. They examined the influence of building orientation and volumetric energy density input by producing specimens at three different inclinations using two distinct combinations of process parameters, resulting in two different energy density inputs. The study concluded that building orientation and porosity significantly impacted the performance of L-PBF specimens. Specimens built horizontally exhibited the highest fatigue resistance, whereas vertically built ones showed the lowest. These findings align with those of other studies on this material utilizing uniaxial strain-controlled fatigue tests [124]. Researchers attributed this behavior to the orientation of deposited layers relative to the loading direction; in horizontally built specimens, the layers were preferentially oriented perpendicular to the bending-induced stress, creating a more convoluted path for crack propagation. Moreover, employing higher volumetric energy densities resulted in lower fatigue limits. This was rationalized by the fact that higher energy densities are associated with greater layer thickness, leading

to less efficient consolidation and consequently, a higher density of volumetric defects from which cracks can originate [126]. Shrestha et al. [124] identified three categories of defects found in these specimens: i) voids arising from lack of fusion between consecutive layers, ii) inclusions formed from partially melted powder particles, and iii) unmelted powder particles clustered around a void; among these, the first category posed greater harm when aligned preferentially with the loading direction.

Fracture toughness

Toughness is without a doubt regarded as one of the most vital and necessary material properties to attain the best possible structural performance. The widely accepted method used today to assess fracture toughness in ductile materials—like metals—is predicated on the theory of Elasto-Plastic Fracture Mechanics (EPFM). Finding out how defect size and type, in addition to bulk material parameters, affect toughness is crucial when it comes to AM materials. Within the scientific world of AM, the characterization of PBF parts' fracture toughness has gained significant importance. This is because different kinds of flaws and anisotropy might occur in these kinds of parts. Specifically, research is being done on how building orientation affects defects like porosity, second phases, LoF, and—perhaps most intriguingly—the existence of intrinsic melt pool borders, which may function as crack initiators or have an impact on the formation and spread of cracks.

According to ASTM E1820-18 standard, L-PBF A357 alloy compact tension C(T) specimens were obtained in three distinct orientations. Oliveira de Menezes et al. [135] examined the fracture toughness of these specimens. The three differentially oriented groups of specimens studied are schematically depicted in Fig. 31a, where H, L, and T stand for height, longitude, and thickness directions, respectively. This study demonstrated that the direction of loading and the build orientation had a substantial impact on the material fracture toughness as determined by the JIC integral. When specimens were loaded in the building direction (H) and the notch was positioned along the building plane and orientated in relation to the L direction, the as-built condition of the specimens showed the lowest value of fracture toughness (H-L specimens). The crack in the H-L specimens expanded along the melt pool boundaries, which were neatly aligned with the crack plane, according to an analysis of micrographs taken perpendicular to the crack planes. However, T-L and H-T specimens had a more complex and less focused crack propagation route, which led to a higher fracture toughness (see Fig. 31b). Similarly, in a subsequent study [136], using AlSi7Mg compact tension C(T) specimens produced by L-PBF134, which evaluated the impact of various heat treatments. In this instance, an artificial aging cycle (T6) caused microstructural coarsening, which eliminated the anisotropy, albeit at the expense of lowering the T-L and H-T specimens' total fracture toughness. This behavior was ascribed to a modification in the process of fracture propagation, where porosity and the presence of small, uniformly dispersed Si particles were thought to be the primary reasons for the poor resistance to crack propagation. The fracture toughness of 3-point bending L-PBF AlSi10Mg specimens in three distinct building orientations was examined by Araújo et al. [137]. The values of fracture toughness were highest for horizontal as-built specimens (0°) and lowest for vertically-built specimens (90°).

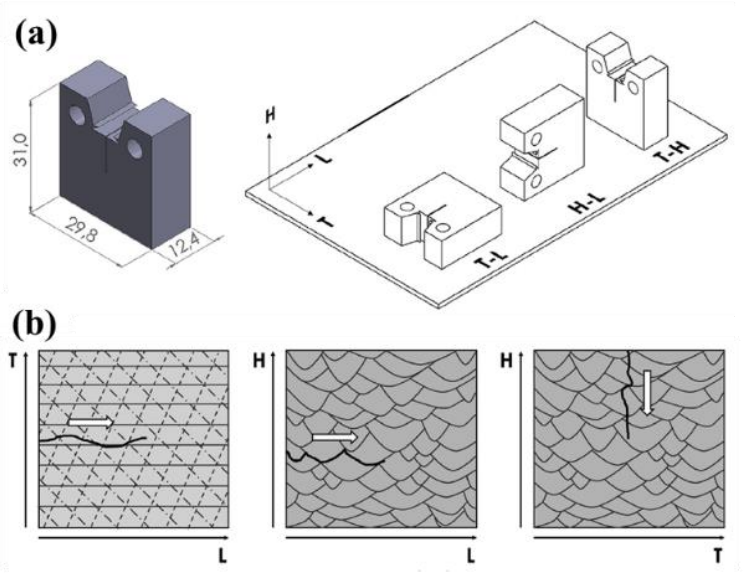

Fig. 31: (a) Diagram of the L-PBF A357 alloy C(T) specimens, showing the building plane (T-L) and building direction (H). (b) A schematic depiction of the three examined directions along the fracture propagation path. The direction of crack propagation is indicated by the arrows [135].

It was also examined how building orientation affected the fracture toughness of specimens made using PBF procedures in different materials, including stainless steels [138], low-alloy steels [139], and Ti6Al4V [136]. These examples offer more proof that loading the material in its as-built state in the building direction results in the lowest fracture toughness. Defects that are aligned at the construction plane are the reason for this. In some circumstances, toughness values may even be 30–40% lower than when the same material is produced in the wrought condition—that is, using a technique other than AM [138]. These investigations also indicated that applying the appropriate thermal treatments can partially eliminate this anisotropic behavior [139, 140].

Wear resistance

Identifying wear mechanisms and wear resistance are of major interest for a wide range of applications. However, comparatively, few studies have been carried out to investigate the effect of build orientation on the wear resistance of AM products [120, 141, 142, 143]. Wear properties are known to be intrinsically dependent substantially on hardness, microstructure, and porosity; in AM materials, these aspects are directly correlated with the fabrication process parameters like the cooling rate experienced by different layers, according to the selected build orientation. As a result, numerous studies have consistently reported findings that align with the main results presented in previous sections. These indicate that the build orientations that promote smoother, more geometrically accurate, and harder surfaces that these characteristics are expected to lead to superior wear resistance. The evidence of this relationship was clearly observed in a study that compared the wear resistance of DMLS Ti6Al4V specimens built in two different orientations [120]. Vertically built specimens showed the highest wear resistance and the highest microhardness. As it was highlighted in previous section, the microstructure found in these specimens played an important role; while the horizontally built specimens exhibited a mixture of α and β phases, in the vertical specimens, harder α’ martensite was also identified. Additionally, these results were also confirmed by Bahshwan et al. [141] who investigated the role of microstructure on wear mechanisms in L-PBF 316L SS disc-shaped specimens built in 3 different orientations. In this research, the vertically oriented disc exhibited the highest abrasive-oxidative wear. Podgornic et al. [142] who studied the influence of the build direction on the wear resistance of L-PBF maraging steel specimens. Among the 3 build orientations of 0°, 45°, and 90°, the best combination of abrasive and adhesive wear resistance was reported for the specimens built horizontally (0°). On the

other hand, the worst wear resistance was found in the vertical specimens (90°) when the sliding took place across the layers. Yang et al. [143] investigated the effect of 3 scanning strategies to promote the rotation of grains and consequently enhance the wear resistance of L-PBF 316L SS specimens. It was demonstrated that the best strategy was to follow a zigzag scanning with a rotation of 90° between subsequent layers. This contributed to the remelting and change in the orientation of the grains, from columnar, epitaxial grains grown along the build direction to grains aligned in the horizontal direction. This configuration showed a higher resistance to slip and, therefore a higher resistance to wear mechanisms. It was suggested that wear resistance can be enhanced by controlling the heat flow during L-PBF to rotate grains away from the "soft" orientation, where the grains have low resistance to slip.

Corrosion resistance

Certain metallic materials used in AM tend to form a passive layer under typical environmental conditions. Titanium alloys, aluminum alloys, and stainless steels, for example, develop surface layers of TiO2, Al2O3, and Cr2O3, respectively. However, numerous studies indicate that the corrosion resistance of AM-produced components is generally lower compared to those made from the same materials using traditional manufacturing methods [144, 145, 146, 147, 148]. Several studies have highlighted that differences in microstructure due to varying build orientations within the same component can impact corrosion resistance [146, 147, 148]. Romero-Resendiz et al. [146] examined the electrochemical behavior of EB-PBF Ti6Al4V samples, finding that the additively manufactured specimens exhibited higher corrosion rates in a 1 M NaCl solution compared to those produced through forging. This was attributed to a preferred grain orientation in the EB-PBF samples, which likely increased surface energy and, in turn, enhanced the corrosion process.

In one another study [149], the corrosion resistance of L-PBF 316L stainless steel specimens in a 0.6 M NaCl solution was investigated. Potentiodynamic curves were compared for specimens built at three orientations (0°, 45°, and 90°) and with the wrought material. Surprisingly, the L-PBF specimens exhibited better resistance to pitting and a wider passivation window than the wrought counterparts. Among the AM samples, those built horizontally showed the highest resistance. Experimental results suggested that a more stable protective oxide layer formed on the AM specimens, although the underlying reason for this trend was not explained. Du et al. [150] studied the impact of build orientation on the corrosion behavior of L-PBF Inconel 718 specimens in a 3.5% wt NaCl solution. The findings showed that corrosion resistance improved as the build angle increased. This was explained by a higher grain boundary density at larger building angles, which contributed to enhanced corrosion resistance.

2.6 Post-treatment

Despite their significant potential, AM technologies face certain limitations that require post-processing techniques to enhance the quality and performance of the as-built components, aiming to meet the standards achieved by traditional manufacturing methods [151].

Printed parts often contain unavoidable defects that can only be partially reduced by fine-tuning process parameters [152]. For instance, the staircase effect, which results in an uneven surface due to the appearance of "steps" caused by excessive layer thickness, cannot be completely eliminated through parameter adjustments. However, post-processing techniques can help minimize this issue [153]. The choice of build direction impacts both the "surface complexity" and the geometric accuracy of a part, depending on its shape. It also affects the amount of support structures required for overhangs, which must be removed after production. Additionally, the scanning strategy used can introduce voids or pores within or between layers, potentially leading to cracks and facilitating their propagation [152]. As a result, post-processing plays a crucial role in mitigating these inherent defects and imperfections.

Post-treatments aimed at addressing the negative effects caused by build orientation are divided into two main categories: bulk treatments, including heat treatments, and surface treatments. Surface treatments are further classified into subtractive, mechanical, coating, and hybrid methods [154]. Additionally, the impact of post-treatments, as influenced by build orientation, is examined in subsections covering microstructure, surface quality, mechanical properties, and fatigue performance. For more detailed information on general post-treatments used in AM materials, regardless of orientation, see [155].

2.6.1 Bulk Post-treatments

Bulk post-treatments include Heat Treatments and HIP. Heat Treatments involve thermal cycles that relieve residual stresses, reduce segregation, alter the microstructure, and adjust mechanical properties such as ductility and strength [154]. HIP combines thermal annealing ($T > 0.7\ Tm$) with high pressure (~100 MPa) in an inert atmosphere, with results varying based on the applied temperature, pressure, and duration. This process is especially effective for closing cracks and pores within AM parts [154].

The effects of stress relieving (heat treatment) at 650°C for 3 hours and HIP at 1000°C, 100 MPa, for 2 hours were studied on L-PBF lattice structure specimens [156]. Stress relieving improved material strength by enhancing homogeneity and maintaining grain orientation. In contrast, HIP, which exceeded the β-transus temperature (980°C), produced a bimodal α/β microstructure, leading to greater strength and fracture strain. Additionally, HIP largely eliminated the columnar and anisotropic structures.

2.6.2 Surface Post-treatments

Subtractive Surface Treatments

These processes involve removing the outer layers of the AM part, where most orientation-related defects, such as porosities, partially melted powders, and spatters, are found. This significantly reduces surface roughness without affecting the internal material, leading to a notable improvement in performance, particularly for load-bearing components subjected to cyclic loading [157, 158].

Machining is one of the most widely used mechanical finishing processes in the AM field. However, its use is limited to simpler geometries and cannot be easily applied to complex shapes due to surface inaccessibility [157]. Serjouei et al. [159] developed a predictive model for S-N fatigue curves, accounting for the effects of build orientation, various heat treatments, mean stress ratios, and the location and size of pores in 316L stainless steel specimens produced by different laser-based AM technologies (e.g., L-PBF, DMLS). Experimental tests generally showed improved fatigue resistance

in machined specimens compared to those in the as-built condition. Wood et al. [160] examined the effects of build orientation and post-treatments, such as machining and shot peening, on the fatigue performance of L-PBF 316L stainless steel specimens built vertically or horizontally. Interestingly, for all build orientations, the machined and shot-peened specimens had similar fatigue resistance, despite differing surface roughness (Ra of 0.7 μm for machined and 4 μm for shot peened), due to the compressive residual stresses generated by shot peening. Compared to the as-built samples, the machined specimens exhibited the highest fatigue strength. However, vertically built specimens showed lower fatigue strength, mainly due to fusion defects, as they were constructed parallel to the loading axis.

Polishing is a widely used post-treatment for AM products and can be carried out through various methods, such as mechanical, chemical, electrochemical, laser polishing, magnetically driven abrasive polishing, hydrodynamic cavitation abrasive finishing, and ultrasonic cavitation abrasive finishing [154]. The goal of all these techniques is to achieve a smooth, mirror-like surface. Several of these treatments are specifically applied for post-processing AM specimens built at different angles.

Cabrini et al. [161] investigated the corrosion resistance of DMLS Al10SiMg specimens built in horizontal and vertical directions, which were then either mechanically polished with emery paper and alumina or shot peened with ceramic microspheres. The study revealed that post-treatments were essential for improving corrosion resistance, as pores and residual unmelted powders on the as-built surface served as corrosion initiation sites. The porosity density varied depending on the build orientation, with horizontally built specimens exhibiting lower average pitting potentials compared to vertical ones, suggesting a reduced likelihood of corrosion pits. During the AM process, laser scanning created an oxide layer that provided minimal protection due to its discontinuity and vulnerability to corrosion along laser tracks. Post-treatments, particularly polishing, were effective in removing this weak layer, with polished specimens showing better pitting resistance than shot-peened ones in both build orientations. After achieving the same surface finish through polishing, horizontally built specimens demonstrated better corrosion resistance than vertically built ones. However, a drawback of polishing for enhancing the mechanical and electrochemical performance of AM materials is its inability to close pores, whereas shot peening can partially seal them. As a result, the effectiveness of the protective oxide layer depends on the quantity and size of the residual or exposed pores.

Chemical etching (CE) and polishing are commonly used post-processing methods for AM materials due to their adaptability to complex geometries. Since they don't require mechanical tools, these techniques are well-suited for addressing surface defects in intricate structures with limited accessibility, such as lattice structures [53, 162]. The process involves submerging the part in an acid solution, which erodes the surface, either with or without the assistance of an electric current. Lhuissier et al. [163] applied CE with varying etching times to EB-PBF Ti6Al4V lattice structures and found it effective in reducing two common defects: partially melted powder particles and irregular stacking patterns. Notably, the etching rate remained consistent for struts oriented in different directions.

Non-subtractive Surface-treatments

Sand blasting is a mechanical surface treatment where sand or ceramic beads are propelled at a specific pressure to impact the surface. Widely used across industries for scale removal and surface cleaning, it can also cause minor surface plastic deformation and alter surface roughness, depending on the size of the beads and the pressure of the compressed air used for bead acceleration [164].

In [165], the effects of sand blasting on Ti6Al4V L-PBF specimens were investigated, revealing that it reduced surface roughness (Ra) from approximately 20 μm to 15 μm by removing partially melted particles that were loosely adhered to the surface. The process also introduced compressive residual stresses in the outermost layer (~6 μm). While the mechanical properties were not significantly

impacted, the reduction in roughness and removal of surface particles could be beneficial for biomedical applications.

Shot peening, a mechanical surface treatment similar in concept to sandblasting, requires more precise control of parameters such as bead type (e.g., steel, ceramic), bead size, bead shape, impact velocity, and the distance between the nozzle and target surface. This technique is widely used across industries to induce compressive residual stresses, promote surface work-hardening, refine surface grains, and primarily improve the cyclic performance of metal components. [166, 167, 168]. Shot peening is commonly used in the post-processing of AM materials to improve surface quality and address the limitations in fatigue performance found in the as-built condition [154, 164, 169]. The two key parameters in shot peening are Almen intensity, which measures the kinetic energy of the impacting beads, and the coverage area treated [170]. Laser shock peening is a non-subtractive surface treatment that induces plastic deformation in the surface layer using pulsed laser exposure. Its high level of control makes it especially effective for AM parts with complex geometries. Like shot peening, laser shock peening results in grain refinement and compressive residual stresses in the surface layer, enhancing fatigue resistance [171]. Additionally, laser shock peened specimens generally have lower surface roughness compared to shot peened ones. The effect of laser shock peening (using a 10 ns pulsed Neodymium Ytterbium Aluminium Garnet (Nd: YAG) laser) was studied on L-PBF 316L stainless steel dog bone specimens with build orientations of 0°, 45°, and 90°. It was found that the 45° specimens showed enhanced ultimate tensile strength and yield strength due to grain refinement and compressive residual stresses. Overall, the treatment improved strength but reduced ductility in the 0° and 45° specimens, while the 90° specimen maintained a good balance between strength and ductility [172].

Coatings

Coating deposition involves applying a film of a different material (such as metal, ceramic, or polymer) to the surface of a part to improve its mechanical or electrochemical properties or to impart specific surface functions. This technique can protect the surface from corrosive environments, reduce surface roughness, conceal defects and pores, and, in some cases, enhance the component's biological response [155]. Coating is an effective solution for addressing issues related to excessive surface roughness or porosity in AM components, as it can fill surface open pores regardless of the build direction [173].

Hybrid Treatments

Hybrid post-treatment solutions combine the advantages of different processes to improve AM materials. Typically, these solutions involve a heat treatment, which is commonly used in AM to achieve microstructural uniformity, address anisotropy, and relieve residual stresses, along with a surface treatment designed to address surface roughness issues.

Jamshidi et al. [174] studied the effects of combining Hot Isostatic Pressing (HIP) with three surface treatments—sand blasting, polishing, and chemical etching (CE)—on L-PBF Ti6Al4V specimens built in vertical and horizontal orientations. HIP effectively removed internal lack-of-fusion (LoF) porosities, increasing the specimen's density, and all surface treatments eliminated partially melted particles. HIP enhanced ductility and reduced porosity in both build directions. Among the treatments, the combination of HIP and CE resulted in the greatest improvement in fatigue performance, with a significant reduction in surface roughness (Sa reduced from 12.2 to 6.6 μm), leading to a fatigue limit approximately eight times higher than the as-built specimens. Other treatments also notably improved the printed parts, with the HIP and polishing combination achieving a fatigue limit six times higher than the as-built condition.

2.6.3 Effects of Post-treatments on Microstructure

This section will compare the effects of different post-treatments, particularly those that influence the microstructure of the bulk material. It will evaluate the outcomes of as-built conditions, heat treatments, and HIP treatments on various materials.

Ren et al. [175] studied L-PBF Ti6Al4V specimens produced at build orientations of 0°, 30°, 45°, 60°, and 90°. Some specimens were left in the as-built state, while others underwent different treatments: heat treatment below the β-transus (BT) (800°C, 2h) in an argon atmosphere, HIP (920°C, 100 MPa, 2h), and heat treatment above the β-transus (AT) (1050°C, 2h). Fig. 32a-h showed clear differences between the treated specimens, though no significant variation was observed based on build direction. SEM analysis of the as-built specimens (Fig. 32a, e) revealed long columnar grains. In the BT-treated samples (Fig. 32b, f), vanadium atoms formed, and a β phase appeared along the grain boundaries. HIP specimens (Fig. 32c, g) exhibited a distinct α phase at the grain boundaries, with an α+β phase within the columnar grains, indicating partial spheroidization of the α phase. In the AT-treated samples (Fig. 32d, h), temperatures above the β-transus led to grain growth, resulting in equiaxed or semi-equiaxed grains.

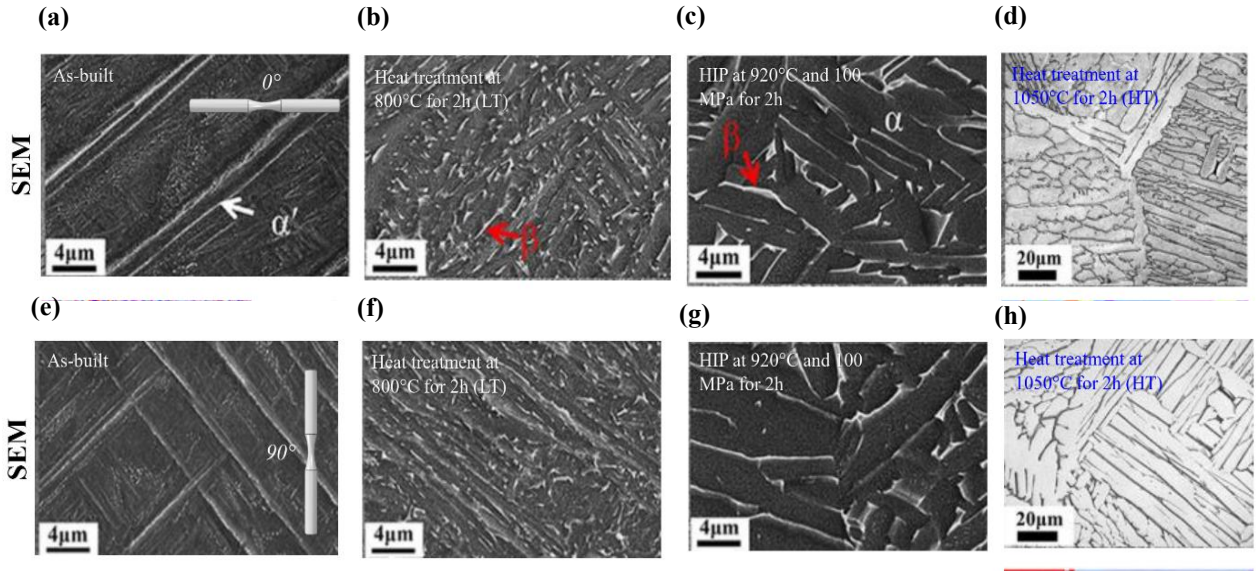

Fig. 32: The microstructure of longitudinal sections from L-PBF Ti6Al4V specimens, oriented at 0° (a-d) and 90° (e-h), is shown in various conditions: as-built (a,e), LT (b,f), HIP (c,g), and HT (d,h) [175].

Ghorbanpour et al. [116] studied the effects of heat treatment and its combination with HIP on L-PBF IN718 specimens, which had both regular and functionally graded structures built in horizontal and vertical directions. Some specimens underwent a heat treatment consisting of homogenization (1065°C for 1 hour) followed by double aging (760°C for 10 hours and 650°C for 8 hours), while others also received an additional HIP treatment (1180°C, 150 MPa, 3 hours). The interface microstructure in the as-built specimens exhibited sharp changes, whereas it became smoother after heat treatment and heat treatment+HIP. Microstructurally, the as-built condition showed a preferential grain orientation. Heat treatment reduced grain size but did not alter their orientation, with residual porosities/defects remaining, especially in vertically built specimens. Heat treatment+HIP further reduced microstructural anisotropy and significantly decreased the number of defects.

Kuo et al. [176] used DMLS to fabricate IN718 specimens in both vertical and horizontal orientations to examine the impact of heat treatments on different orientations. The specimens were either left in the as-built state, subjected to solution treatment (980°C for 1 hour) followed by two-step aging (718°C for 8 hours and 621°C for 10 hours) (STA), or given a direct aging treatment (718°C for 8 hours and

621°C for 10 hours) (DA). δ phases were observed to grow along the build direction in the grains. The laser manufacturing process produced high thermal rates, resulting in a high density of dislocations, which persisted even after the STA treatment. In both STA and DA specimens, γ' and γ'' phases were found throughout the entire microstructure. Sangid et al. [177] examined how heat treatment affected L-PBF Inconel 718 specimens produced in vertical and horizontal orientations. The microstructure of the as-built specimens was highly anisotropic, as illustrated in Fig. 33a and b. All specimens underwent a stress relief treatment (1065°C for 1.5 hours) before being removed from the build plate, and those that only received stress relief were classified as as-built. Another group, labeled heat-treated, underwent additional processes: homogenization (1177°C for 1 hour), solution treatment (982°C for 1 hour), and aging (718°C for 8 hours followed by 621°C for 18 hours). After heat treatment, the microstructural anisotropy was reduced, resulting in a more homogeneous structure in both vertical and horizontal specimens, with dislocations becoming more regular.

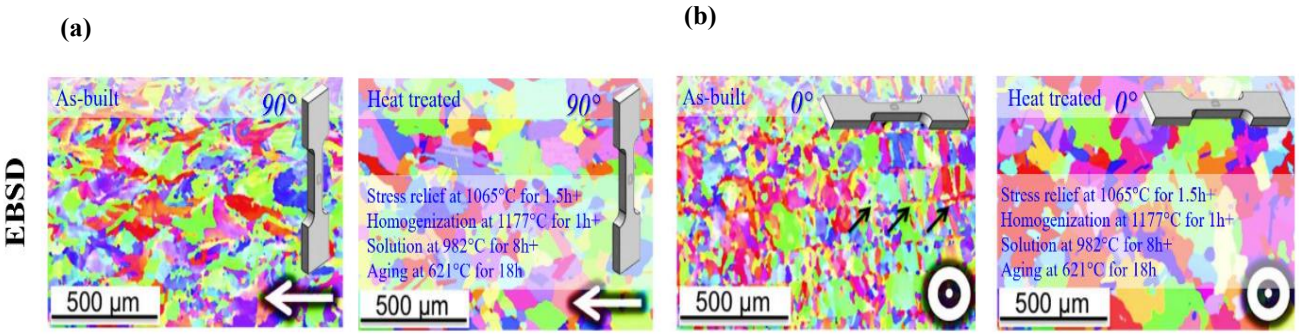

Fig. 33: Inverse pole figures of the microstructure of L-PBF IN718 specimens, both before and after heat treatment, are shown for (a) vertical and (b) horizontal orientations. White arrows in the bottom right corner mark the building direction, while black arrows highlight the fine microstructure resulting from rapid solidification [177].

Delroisse et al. [87] studied the interaction between building orientation and heat treatment on L-PBF AlSi10Mg struts fabricated in vertical and inclined (35.5° from the horizontal plane) orientations. The heat treatments applied included T6, consisting of annealing at 525°C for 5 hours, water quenching, and artificial aging at 165°C for 7 hours. In the as-built inclined struts, two distinct zones were identified (Fig. 34a). Zone A, located in the top part, featured a finer microstructure with small cells of primary Al within the Si eutectic phase. Zone B, at the bottom, had inter-eutectic cells 2.5 to 3 times larger than those in Zone A, attributed to better heat conduction in Zone A, where faster heat flux prevented coarsening. The vertical struts had a more homogeneous microstructure with fewer porosities due to gas entrapment, whereas Zone B exhibited more porosity due to pore growth from extended exposure to high temperatures. After heat treatment, the struts displayed a uniform microstructure, with no visible melt pools, and exhibited Si growth and spheroidization (Fig. 34b).

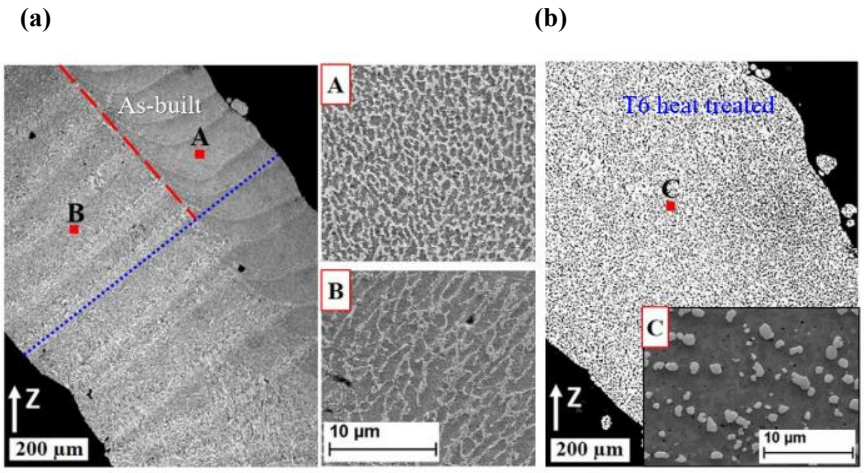

Fig. 34: L-PBF AlSi10Mg struts in the as-built condition, a finer microstructure is present in zone A, whereas a coarsened one is in zone B (a). The strut, after T6 heat treatment, is featured by homogeneous microstructure (b) [87].

2.6.4 Effects of Post-treatments on surface roughness and morphology

A major limitation of AM processes is the poor surface finish quality, which is influenced by the building orientation. This section will explore the connections between building orientation and various post-treatments used to improve surface morphology and roughness, such as shot blasting, shot peening, anodization, etching, and polishing.

Krishna et al. [178] studied the effects of shot blasting on L-PBF 316L stainless steel specimens. Surface roughness was evaluated by analyzing 38 up-skin surfaces of two complex-shaped specimens with inclinations ranging from 0° to 90°. Fig. 35a illustrates the surface topographies in both the as-built and post-processed conditions. The as-built specimens exhibited staircase effects and randomly attached partially melted particles, with particle density increasing as inclination rose. After shot blasting, the attached particles were removed, reducing surface roughness (Sa), although fine features were introduced by the impact of the beads. The surface roughness of post-processed specimens followed a similar trend to the as-built condition, but with reduced amplitude (Fig. 35b). The developed interfacial area ratio (Sdr), representing the additional surface created by texturing relative to a flat plane, increased with build inclination in the as-built state. However, shot blasting significantly reduced Sdr, as shown in Fig. 35c. However, the blasting treatment's overall effect was not influenced by the building orientation.

Maleki et al. [170]. analyzed L-PBF AlSi10Mg notched specimens that underwent shot peening using two different parameter sets: SP1, using cast steel spheres with a 0.43 mm diameter and 10 Almen intensity, and SP2, using ceramic spheres with a 0.1-0.15 mm diameter and 5 Almen intensity, both at 100% coverage. In the as-built condition, the surface morphologies showed irregularities with partially melted and unmelted particles on the up-skin, down-skin, and smooth notch surfaces, with higher density in the down-skin areas. The as-built smooth notch surface had a roughness (Sa) of 60 µm, with increases of 480% and 290% on the down-skin and up-skin areas, respectively. Both SP1 and SP2 treatments significantly altered the surfaces by removing these irregularities (Fig. 36a), with SP2 providing a more effective and homogeneous surface modification. However, shot peening slightly increased roughness on the smooth notch surface due to dimple formation from high-energy impacts. Overall, shot peening improved roughness on inclined surfaces, with the up-skin Sa decreasing by 36% after both SP1 and SP2. The down-skin Sa decreased by 44% after SP1, but remained comparable to the as-built condition after SP2.

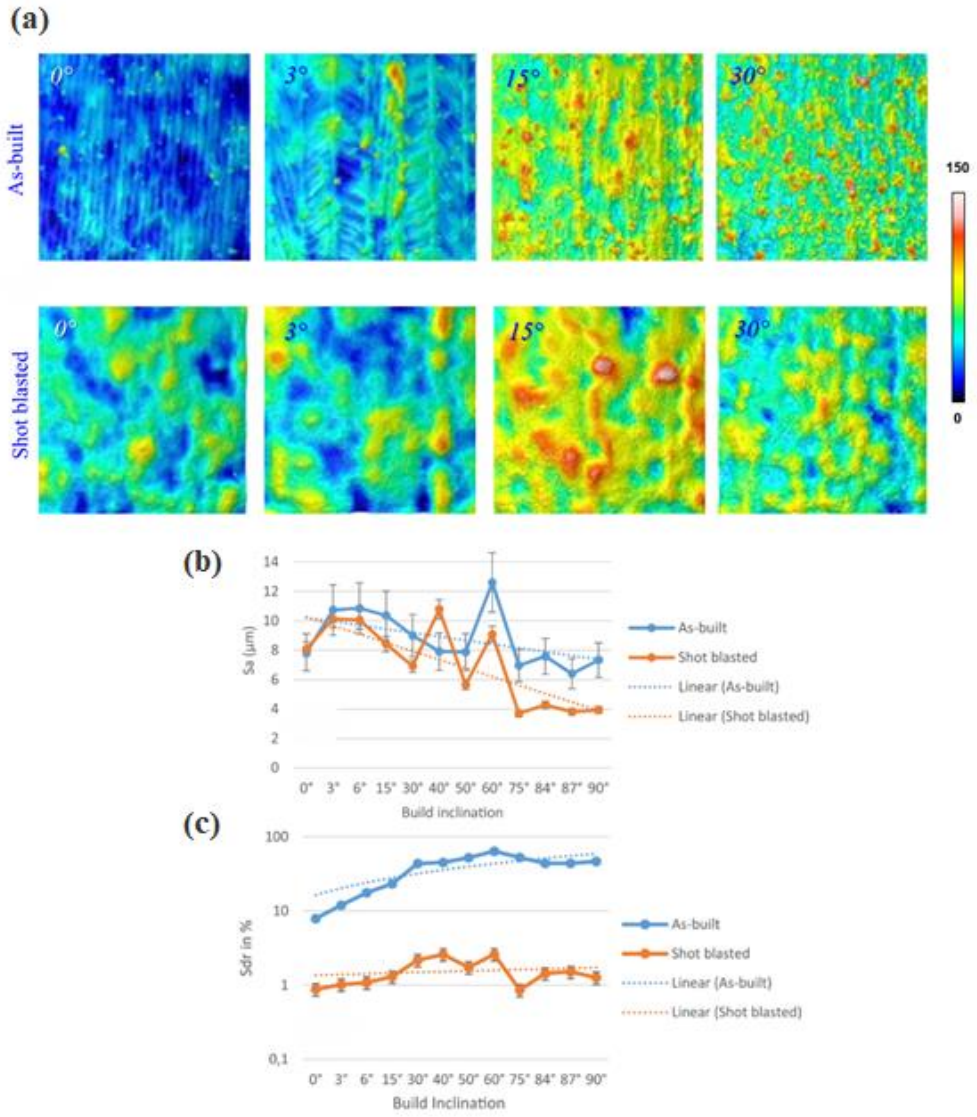

Fig. 35: (a) Surface topography measurements were taken on L-PBF 316L stainless steel specimens in both as-built and shot blasted conditions at inclinations of 0°, 3°, 15°, and 30°, with the measured area being 0.5x0.5 mm²; (b) Sa and (c) Sdr measurements were recorded for both as-built and shot blasted conditions across different building inclinations [178].

Rovetta et al. [179] investigated the effects of anodization and etching on the surface texture of L-PBF AlSi10Mg specimens produced at 0° and 45° orientations. The anodization was carried out at a constant 60 V for 20 minutes, while etching was performed with Kroll reagent for 10 minutes at room temperature. SEM analysis (Fig. 36b) showed a uniform distribution of partially melted particles in the as-built condition for the 0° specimens, whereas the 45° specimens exhibited inhomogeneities due to particle clustering. Anodization did not significantly affect the 0° orientation but caused cracks on particles and increased the number and size of clusters at 45°. In contrast, etching led to the removal of particles and clusters, regardless of build orientation. Roughness results for the 0° and 45° orientations are shown in Fig. 36c and Fig. 36d, respectively. These findings suggest that the choice of post-treatment is more critical than the specimen's orientation

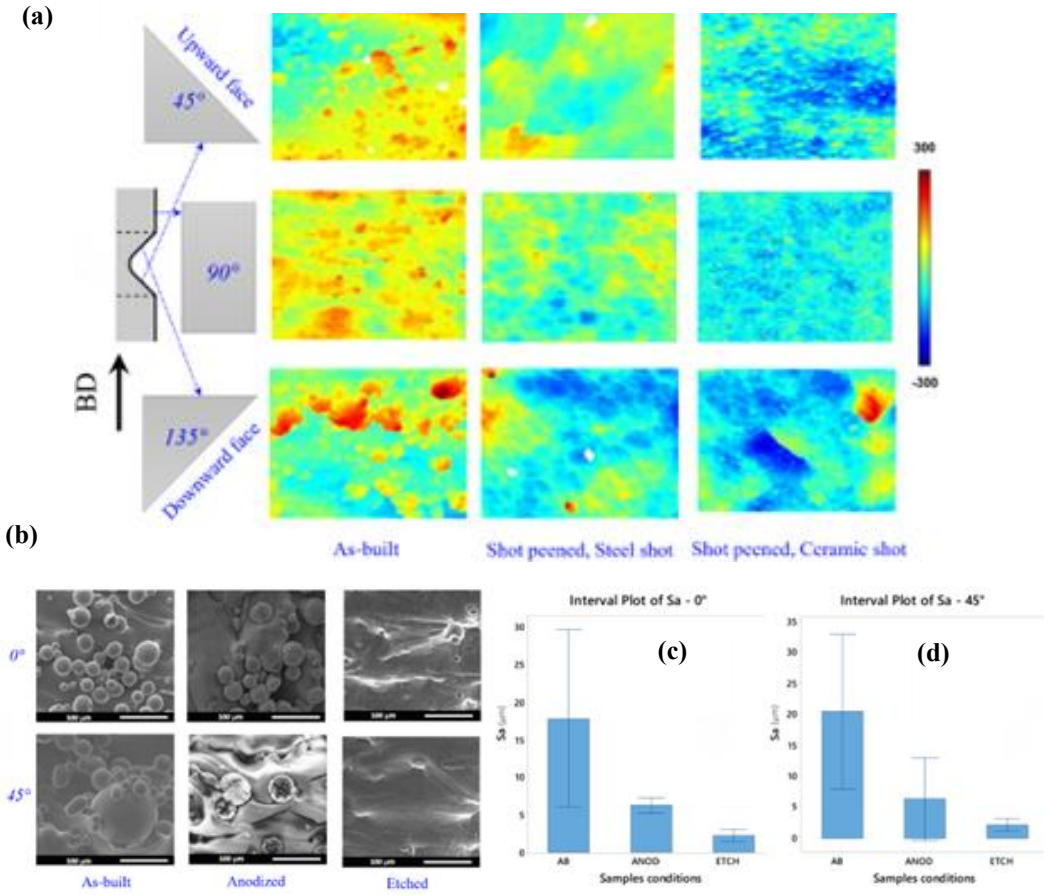

Fig. 36: a) Surface topography of L-PBF AlSi10Mg notched specimens on the up-skin, smooth, and down-skin surfaces of the notch in as-built, and shot peened (SP1 and SP2) conditions [170]. (b) SEM micrographs of L-PBF AlSi10Mg specimen surfaces inclined at 0° and 45°, shown in as-built, anodized, and chemically etched conditions. (c) Comparison of surface roughness for 0° inclined specimens in the as-built, anodized, and chemically etched states. (d) Comparison of surface roughness for 45° inclined specimens in as-built, anodized, and chemically etched states [179].

Magnetic abrasive finishing was employed as a polishing method on L-PBF 316L stainless steel specimens, which were positioned at seven different angles, varying from vertical (90°) to horizontal (0°) [180]. G50 steel grit was used as the abrasive for the finishing process, which was conducted with vibrations at a frequency of 28.8 Hz and an amplitude of 20 mm. In the as-built condition, vertically oriented parts exhibited higher percentages of balling and unmelted particles. After 75 minutes of treatment, most of these defects were removed, though the results varied depending on the build orientation. In specimens with 30°, 45°, and 60° inclinations, a few particles remained in the surface valleys (Fig. 37a). Fig. 37b shows the changes in roughness at different inclinations, measured in 15-minute intervals throughout polishing. Surface roughness (Ra) initially increased with angle up to 60°, then decreased as unmelted particles were reduced. For all orientations, gradual removal of surface imperfections led to a steady reduction in roughness. Although the material removal rate remained constant over time, improvements in surface roughness slowed down and leveled off after 60 minutes of polishing. On average, specimens saw a 56% reduction in Ra, with vertically built specimens showing the greatest decrease, about 76%, due to the ease of particle removal.

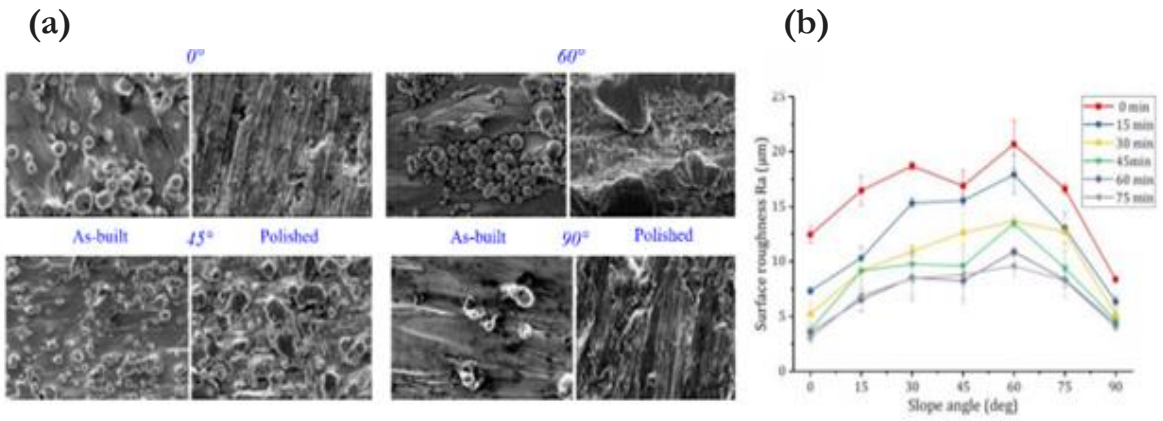

Fig. 37: (a) SEM images of L-PBF 316L stainless steel specimens constructed at different inclinations, shown in both as-built and polished conditions after magnetic abrasive finishing; (b) Ra values measured at different building inclinations to track the effects of magnetic abrasive finishing at 15-minute intervals [180].

2.6.5 Effects of Post-Treatments on Hardness

As previously mentioned, hardness is a key mechanical property in additive manufacturing and serves as a reliable indicator of mechanical performance. Microstructural changes can lead to notable variations in the mechanical properties of a part. Therefore, the following section explores the impact of different post-treatments on material hardness.

Zhang et al. [180] studied L-PBF Cr-Cu-Zr specimens produced in both horizontal and vertical orientations. Ageing treatments were conducted at various temperatures (350°C, 400°C, 450°C, 500°C) and soaking times (ranging from 0 to 600 minutes). The aged specimens showed higher strength compared to the as-built ones, with anisotropic mechanical properties, and the vertical specimens demonstrated superior performance. The optimal ageing conditions for maximizing hardness were determined to be 500°C for 30 minutes (Fig. 38a, b). It was also observed that extending the treatment time reduced hardness. Additionally, the vertically built specimens had greater penetration resistance compared to those built horizontally.

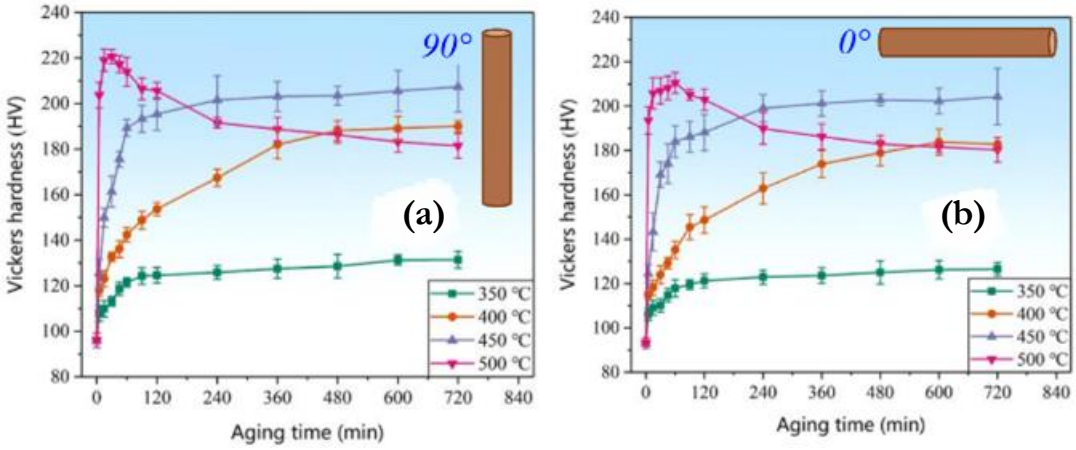

Fig. 38: Vickers hardness measurements (a, b) for L-PBF Cr-Cu-Zr specimens fabricated in the vertical and horizontal directions, respectively [180] .

Ghorbanpour et al. [116] also measured Vickers hardness trends for heat-treated specimens. IN718 L-PBF specimens were produced in both horizontal and vertical orientations. After applying heat treatment (HT) and heat treatment combined with HIP, they concluded that both treatments significantly improved hardness compared to the as-built specimens in both orientations.

2.6.6 Effects of Post-treatments on Fatigue Behaviour

Fatigue behavior is influenced by a combination of factors related to the bulk and surface conditions of the produced part, which can be adjusted using appropriate post-processing methods. This section provides a brief overview of the available data on the impact of post-treatments applied to inclined AM specimens.

The fatigue properties of EBM Ti6Al4V specimens built at 0°, 45°, and 90° orientations were analyzed and compared to those of their machined counterparts [97]. HIP treatment (920°C, 100 MPa, 2 hours) was applied to the 90° specimen. Results showed that machining improved fatigue strength compared to the as-built specimens (see Fig. 39a). The building orientation primarily influenced the microstructure, with horizontal specimens showing better performance. The findings also highlighted that surface condition played a more significant role than internal defects, as the HIP treatment, which removed internal porosities, did not impact fatigue life. Ren et al. [175] conducted fatigue analysis on inclined Ti6Al4V L-PBF specimens after LT, HIP, and heat treatments. Fig. 39b shows the variation in fatigue cycles based on building orientation for the as-built and LT cases, while no significant effect was observed for the HIP and heat-treated specimens. The study concluded that fatigue behavior was primarily influenced by pore size, pore location, and the level of residual stresses. In the near pore-free HIP and heat-treated specimens, crack initiation was associated with plastic slip.

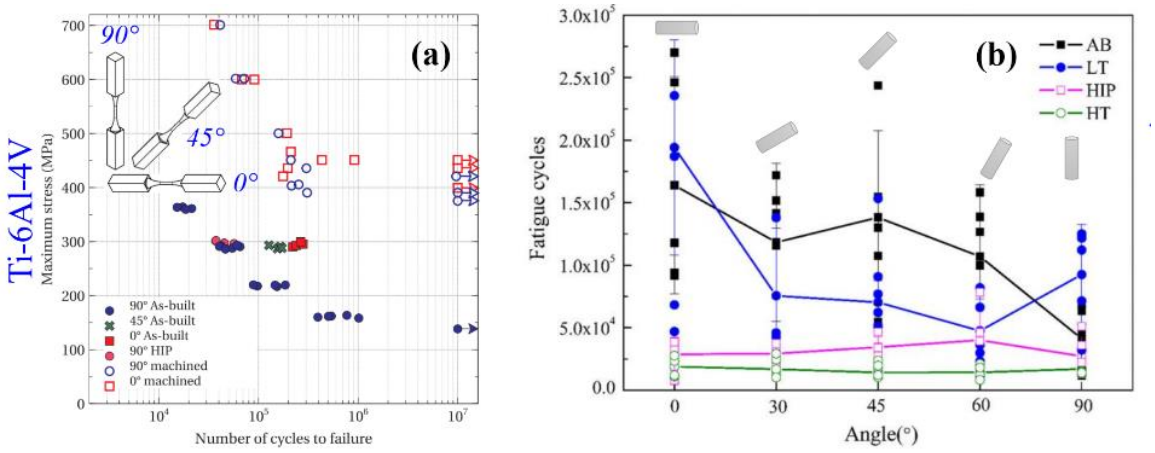

Fig. 39: (a) The number of cycles to failure for EBM Ti6Al4V specimens produced at 0°, 45°, and 90° in the as-built condition, as well as 0° and 90° in the machined and 90° in the HIP-treated conditions [97]. (b) The fatigue life of L-PBF Ti6Al4V specimens oriented at 0°, 30°, 45°, 60°, and 90° in various conditions: as-built, LT, HIP, and HT [175].

Afkhami et al. [181] found that L-PBF 316L specimens exhibited similar fatigue behavior to conventionally manufactured specimens when appropriate post-processing was applied. Horizontally oriented specimens were produced and then machined, while vertically oriented specimens were categorized into as-built, machined, and high-frequency mechanical impact treated (HFMI) (Fig. 40a). Reducing surface roughness improved fatigue strength by eliminating major stress concentration points. For vertical specimens, machining led to an 85% increase in fatigue limit, while HFMI treatment resulted in a 90% increase compared to the as-built specimens. Horizontally oriented specimens showed a 15% improvement in fatigue strength over vertical ones. The impact of build orientation and post-treatment was more pronounced at low-stress amplitudes, where the notch effect was significant. In a separate study, the fatigue behavior of L-PBF maraging steel specimens produced in vertical and horizontal orientations was investigated in as-built, heat-treated (aging at 490°C for 6 hours), machined, and heat-treated + machined conditions [182]. All three post-processes enhanced fatigue life compared to the as-built state, with the vertical specimens showing the greatest improvement. Notably, the impact of build orientation was minimal in parts that underwent both post-processing techniques (see Fig. 40b, c).

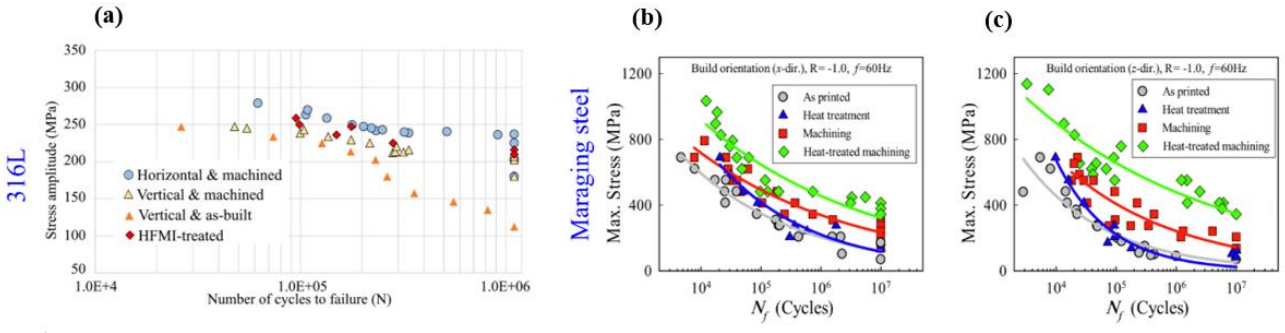

Fig. 40: (a) The number of cycles to failure for L-PBF 316L specimens in horizontal orientation (machined), and in vertical orientation (as-built, machined, and HFMI treated conditions) [181]. The fatigue life of L-PBF maraging steel specimens in as-built, heat-treated, machined, and heat-treated + machined conditions in horizontal (b) and vertical (c) orientations [182].

Poulin et al. [158] examined the influence of build orientation on L-PBF Inconel 625 notched specimens fabricated in four different orientations: horizontal, inclined at 45°, vertical with the notch parallel to the build direction, and vertical with the notch orthogonal to the build direction. Half of the specimens underwent stress-relieving heat treatment (870°C, 1 hour), while the other half received HIP treatment (1120°C, 100 MPa, 4 hours). Staircase effects were prominent on the inclined surfaces, with a high density of partially melted powder particles, especially on the downward-facing areas. Stress relieving did not reduce the anisotropy caused by build orientation, whereas HIP effectively eliminated anisotropy across all specimens and significantly closed pores. Fatigue crack propagation diagrams for the three build directions are presented in Fig. 41a,b. Considering Fig. 41c,d, when they compared crack propagation diagrams for cracks moving parallel to the build plate versus those in the orthogonal direction, L-PBF parts exhibited similar behavior to that of wrought alloy. However, for the HIP-treated series, the results were slightly lower for cracks propagating orthogonally to the build plate compared to those propagating vertically.

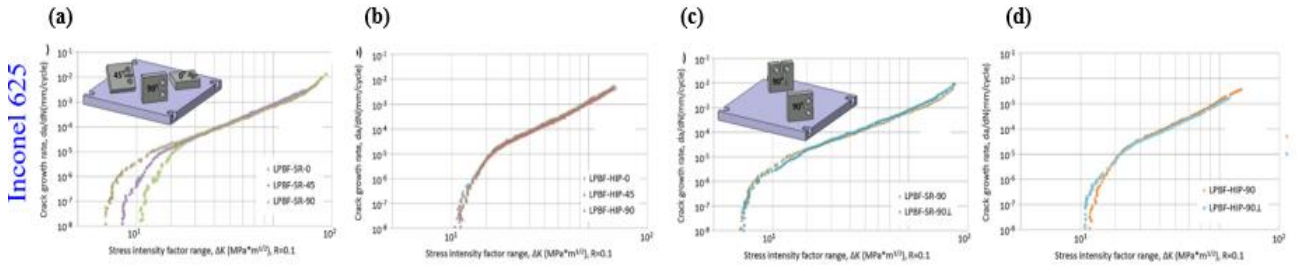

Fig. 41: Fatigue crack propagation diagrams of L-PBF Inconel 625 specimens built in orthogonal and vertical directions under stress-relieved conditions (a, b) and HIP-treated conditions (c, d), showing crack propagation either parallel or orthogonal to the build plate, respectively [158].

2.7 Summary and conclusion of the studies

Metal AM is an emerging technology gaining traction in various sectors, including automotive, aerospace, and biomedical industries. It encompasses a range of techniques, with this review primarily focusing on PBF methods, which involve selective melting of a powder bed to form objects layer by layer. The quality and properties of PBF metal parts are influenced by numerous factors, including powder characteristics, manufacturing technology, process parameters, and post-treatments. Among these, build orientation plays a crucial role in shaping the surface and mechanical properties of the parts. Build orientation is closely tied to the thermal history of the AM part, impacting a range of physical, microstructural, and mechanical attributes. Experimental studies on various metal alloys using different AM techniques have explored the effect of build orientation, where the same part is produced at different orientations and thoroughly analyzed. This review critically examines the significant influence of build orientation on key properties such as surface roughness, porosity, microstructure, fatigue strength, fracture toughness, wear, and corrosion resistance, along with its interaction with various post-processing treatments.

Build orientation has a significant impact on surface roughness in metal AM. In L-PBF, it is generally observed that roughness increases with the inclination angle, with down-skin surfaces typically exhibiting greater roughness and more defects compared to up-skin surfaces. Interestingly, the opposite trend is found in EB-PBF, where roughness decreases as the inclination increases. This dependency of roughness on build orientation creates noticeable surface quality variations in parts with complex geometries, as they often consist of surfaces with different inclinations relative to the build direction. Additionally, the need for supports during manufacturing and their subsequent removal can further degrade surface quality.

The impact of build orientation on porosity shows conflicting results, with the degree of porosity appearing to be highly material-dependent. Some studies find higher porosity in inclined specimens, while others report the highest porosity in vertical specimens. These opposing trends are often attributed to the complex thermal history during the process. Typically, AM parts with inclined surfaces exhibit higher porosity due to factors linked to thermal history variations, such as overheating, underheating, heat buildup, residual stresses, melt pool instability, and insufficient energy density. Variations in thermal history, influenced by geometry and build orientation, can cause areas of the material to become overheated or underheated. Overheating can lead to excessive evaporation of volatile elements, creating volumetric defects, especially on upward-facing surfaces, while underheating may result in incomplete material melting and deposition. For inclined surfaces, heat accumulation is a significant issue, as the heat from the laser or electron beam can affect lower layers. This, combined with rapid cooling or uneven heating, increases thermal stresses. These stresses can cause warping, cracking, or incomplete fusion between layers, leading to higher porosity. The melt pool on inclined surfaces is also less stable due to inconsistent thermal histories, which impact the melt pool’s stability during deposition. Factors like energy reflection, heat dissipation, and temperature fluctuations can result in irregular melt pool shapes, affecting material deposition and increasing porosity. Additionally, insufficient energy density in inclined areas can cause incomplete melting and fusion of powder particles, contributing to pore formation. While overall porosity is often low, the relationship between build orientation, thermal history, and porosity is critical and requires further exploration to optimize AM component quality.

Microstructure, a crucial factor influencing the mechanical properties of metal parts, is heavily reliant on the manufacturing process. In PBF technologies, grains typically elongate along the build direction due to thermal gradient formation. Additionally, grains are coarser in down-skin regions, which remain at higher temperatures for extended periods, while finer grains are found in the up-skin areas. This results in significant anisotropy in the microstructure, which subsequently impacts the part's performance under different service conditions.

Building orientation has been shown to significantly influence fatigue strength, although research findings on this topic are often contradictory. Different surface features affect fatigue performance in various ways, with defects resembling notches being particularly harmful, especially when subjected to specific loading directions. These defects, such as those resulting from the staircase effect, often lead to preferentially aligned lack of fusion defects, which may explain why vertically built specimens generally exhibit the lowest fatigue strength in most studies. Additionally, down-skin surfaces tend to be more detrimental than up-skin surfaces due to their lower geometric accuracy and higher surface roughness, particularly in L-PBF, where support structures are commonly used. Surface irregularities on down-skin areas can act as micro-notches, sometimes overshadowing the influence of geometric notches and causing fractures to occur at these micro-notches rather than at the root of the geometric notch.

Fracture toughness in PBF parts is inherently anisotropic. This is partly due to microstructural variations, with certain orientations promoting crack propagation along weak areas like melt-pool boundaries. As a result, specimens loaded perpendicular to the build plane tend to have the lowest toughness and often display more brittle fracture characteristics.

Few studies have examined the impact of build orientation on properties like wear and corrosion resistance. Most research indicates that microstructure and hardness are key factors influencing these properties in AM metals. Since build orientation affects both, it is likely to also influence wear and corrosion performance. For example, finer grain structures, which increase hardness through the Hall-Petch effect, are expected to improve wear resistance. Some studies suggest that vertically built specimens show lower wear resistance due to the presence of larger columnar grains. Similarly, finer microstructures may enhance the formation of a passive layer for better corrosion resistance. However, there is no consensus on a direct correlation between build orientation and wear or corrosion behavior, with no clear trend established in the literature. Overall, AM materials generally show lower wear and corrosion resistance compared to conventionally manufactured parts.

To address the pronounced inhomogeneity in surface roughness, morphology, residual stress distribution, and microstructural features caused by build orientation in AM parts, the literature emphasizes the importance of post-treatments. Various new or AM-adapted traditional post-processing techniques have been proposed. While many treatments focus on surface improvements, issues like bulk porosity, tensile residual stresses, and microstructural anisotropy can be partially mitigated through appropriate bulk treatments, such as heat treatment. Hybrid post-treatments, combining surface and bulk interventions (e.g., heat treatment followed by surface treatments like severe plastic deformation), have shown great potential for enhancing AM part performance. Although the necessity of post-processing to improve AM parts is well-recognized, a clear roadmap for selecting the optimal post-treatment for specific performance goals is still lacking. Additionally, factors like cost, and the compatibility of post-treatments with the size, geometry, and material properties of the parts, must be considered to achieve optimal outcomes.

Choosing the optimal build orientation (such as minimizing supports or using horizontal struts for better geometric accuracy), along with the right combination of post-treatments, can help narrow the performance gap between traditional and AM processes. This strategy can enhance the competitiveness of AM parts by achieving design complexity with fewer limitations and, when done properly, improving mechanical properties. This thesis highlights the critical role of build orientation in AM design and production, as it significantly influences geometric, surface, microstructural, and mechanical properties. It also guides the selection of appropriate post-treatments. While the literature contains substantial data on this subject, the diversity of specimen types, sizes, materials, and technologies makes it difficult to form universal conclusions about build orientation's actual impact. The variability and conflicting data underline the importance of establishing AM design guidelines that account for build orientation. This will enable more informed decisions during design, optimization,

and production, further driving the successful adoption of AM technologies, especially in fields requiring high geometric and performance precision.

Chapter 3 : Materials and Methods

Within this segment, I will delineate the experimental procedures implemented throughout the campaign. The subsequent sub-section, denoted as System Specification, will then expound upon the presentation of both the goals and the design of experiments.

3.1 System specification

As explained in preceding sections, this work undertook an examination of the attributes of Ti6Al4V specimens, derived through metal AM. The selection of this alloy is primarily because of extensive utilization across various industries, particularly owing to its outstanding mechanical properties, it is used in sectors such as aerospace, automotive, biomedical, etc. Within these domains, there exists a noteworthy emphasis on research directed at enhancing components produced through AM. While contemporary AM techniques enable the production of objects in a single print, a challenge persists in the form of poor surface quality. This deficiency in surface quality precipitates a reduction in mechanical strength, which forces us to resort to post-treatments for quality enhancement. The present thesis is designed to perform a specific post-treatment in order to enhance the characteristics of printed components.

Surely, there's a lot of experimenting we could do, like trying out different combinations of settings and seeing how they affect things. For instance, we could change the shape of the part we're making and see how that affects our analyses. We could also try lots of different ways to treat the part after it's made, both on the surface and inside. Another thing to test is how different printing settings impact the properties of the part when it's first built. We could even use different types of printers, each with its own strengths and weaknesses. But, with so many things to test and mix together, it would take a long time, maybe even years, to do all of it. That's why we decided to focus on some basic tests first. These tests will give us a good starting point for more detailed studies. I'll give you a brief overview of the tests we chose, and then I will get into more details in the following sections.

At first, it was decided to use an L-PBF technology called Print Sharp 250. This machine was picked because it was already in the IAM lab at the Polytechnic of Turin, and I could start using it right away. Next, I had to choose the shape of the specimen that is going to be tested. The decision was to go with a shape called standard fatigue specimens [183] (check out Fig. 42).

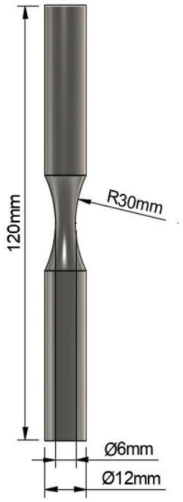

Fig. 42: A diagram showing the design of the fatigue specimen that we're using in our current research.

Using this standard specimen shape has an added benefit – it allows me to study both the tensile and fatigue strength using the right equipment. This enables a more thorough examination of the properties, especially valuable in the industrial context where fatigue and tensile strength are crucial factors for designers. All of my experiments involved specimens printed vertically, not at an angle. I made this choice because I already had a lot of analysis and testing to be performed, and dealing with angled specimens would have added more challenges for fatigue tests. Printing a specimen at an angle would cause a bending effect, making them off-center and causing significant issues in rotary fatigue tests. To avoid these problems and save time, I decided to stick to printing only in **one direction (vertical)**. I then evaluated the characteristics of this print both before and after applying a specific post-treatment

To sum up, final specimens that were tested had that standard shape that I mentioned earlier. I printed them using L-PBF technology, specifically with Ti6Al4V. I am going to compare these vertical specimens to see how post-treatment affects their mechanical properties. For this comparison, I created two sets of specimens. The first set, which I'll call AB, was left as is after printing, without any post-treatment. The second set underwent a surface treatment known as **Tumble Finishing**. With this treatment, I expected the surface roughness to decrease and the fatigue strength to increase.

The initial phase of my work occurred at the IAM. At this laboratory, I handled the printing of all specimens using L-PBF technology, starting from the development of the CAD design and then creating the .STL file for the chosen specimen. Subsequently, a portion of these specimens underwent a process called Tumble Finishing. After wrapping up this initial experimental phase, the specimens were transported to the laboratories at the Polytechnic of Milan for the second part of the project. In this subsequent stage, all specimens were thoroughly examined to assess the impact of post-treatment. The specific tests conducted during this phase are:

- **Microstructure:** This is used to examine if there are any changes in the structure of the material, which could be helpful in shaping the final characteristics of the part.

- **Hardness:** This is one of the key tests widely used in mechanical engineering, and it holds significant practical and industrial importance.
- **Roughness:** Among the most popular mechanical properties, roughness has broad applications in practice. It not only has a substantial impact on fatigue strength but also plays a crucial role in determining surface quality.
- **Residual Stresses:** These stresses can affect fatigue strength, which is why minimizing them is strongly recommended.
- **Fatigue Strength:** As mentioned earlier, this test is pivotal in all research efforts because it provides crucial data used in industry for designing components and assessing their strength.

I am going to explain this procedure in more detail in the next sections. I will get into specifics about the machinery we used, the parameters we set, and any tools or materials involved. Additionally, I'll talk about potential future tests and developments. I'll explore how the research could expand by conducting similar tests but with different starting characteristics. For instance, we might compare parts with different shapes, printed using various AM technologies, with different inclinations, and so on.

3.2 Description of the tools

This chapter is all about the methods and tools used to develop the thesis. As elaborated before, I set up an experiment to test fatigue of Ti6Al4V parts made through L-PBF. This experiment involves various tasks that need different machines and lab techniques. I'll go through them step by step, explaining why it was chosen to do each task.

3.2.1 Specimen production

PBF technology works by building a part layer by layer, melting each cross-section selectively according to a given STL file. The recoater first spreads a layer of powder, and then a laser (our energy source) melts the powder to form the cross-section. To make sure the laser hits the right spot and to guide it onto the powder bed, a system of lenses and mirrors called the optical chain was used (Fig. 43)

After one layer is done, the baseplate goes down, and the feedstock goes up for the next layer. This process repeats until the whole part is finished, and any extra powder is collected for later use. There are some laser-related parameters like power and speed, and other building phase parameters, such as using inert gas to prevent oxidation, deciding on layer thickness for better surface quality, and planning the hatching strategy, which is basically the route the beams take.

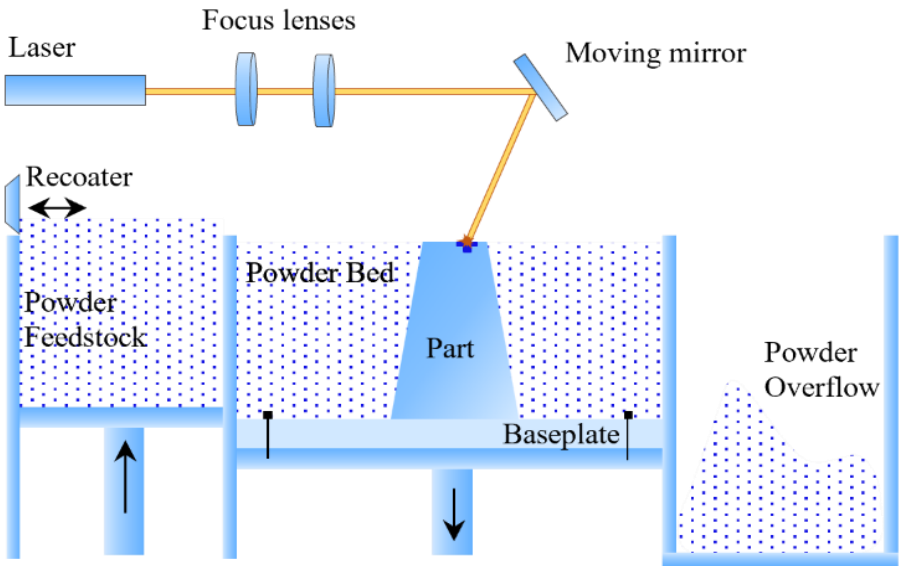

Fig. 43: Diagram illustrating the L-PBF technology.

The machine we used in the experiments is called Print Sharp 250 (Prima Additive), and you can see it in Fig. 44. It's an industrial system that comes with recommended setups for specific metals, but it also lets us adjust the settings as needed. This machine has a single fiber laser in the infrared (IR) with a maximum power of 500 W. The biggest size it can build is 258×258×330 mm, and the speeds can go from 12 to 30 cm^3/h. We can control the thickness of each layer, ranging from 0.02 to 0.1 mm. In my tests with Ti6Al4V specimens.

Fig. 44: The industrial machine utilized is the Print Sharp 250 by Prima Additive in L-PBF.

In our tests with Ti6Al4V specimens, we used the parameters listed in Table 2. Also, all the specimens were made in the same build orientation, which is 90 degrees.

Table 2: Printing parameters

Printing Parameters	
Laser Power [W]	175
Scan Speed [mm/s]	800
Hatch Spacing [mm]	0.105
Layer Thickness [mm]	0.03
Atmosphere [concentration]	Ar (<2%)

3.2.2 Specimen post-processing

The post-treatment method that was selected for this process was Tumble Finishing, a well-established surface finishing technique widely used in various industries to improve surface quality. In this method, the workpieces are placed in a rotating barrel along with abrasive media, which can be of various shapes, sizes, and materials depending on the desired finish. As the barrel rotates, the abrasive media repeatedly comes into contact with the surface of the workpiece, gradually smoothing out rough surfaces, removing burrs, and achieving a more refined finish. This treatment is particularly effective at enhancing surface roughness, which is critical for the overall performance of a part. By improving surface roughness, we can significantly influence the mechanical properties of the part, such as its fatigue strength, wear resistance, and overall durability. A smoother surface reduces the likelihood of stress concentrations, which are often sites where cracks or failures originate, making the treated parts much more reliable in demanding applications.

One of the most interesting aspects of Tumble Finishing is that, despite its ability to refine the surface of the material, it does not interfere with the internal microstructure of the workpiece. In the image below, you can see the machinery used for this process. The equipment is from Silco, a renowned manufacturer of finishing solutions, and it is located in the IAM labs at the Polytechnic of Turin. This advanced machinery ensures precision and consistency in the Tumble Finishing process, providing high-quality surface treatment results.

Fig. 45: The equipment from Silco employed to carry out tumble-finishing on specimens in their as-built state.

To start, the black container was filled with abrasive material. Next, I dipped the specimens into this abrasive material, close the container, and kicked off the process. Once it begun, the container started rotating at the chosen speed, creating friction between the specimens and the abrasive material inside. This friction smoothened the surface of the specimens, as the harder abrasive material impacts their surface, leading to an enhancement in their surface texture. Choosing the right abrasive is crucial for a successful surface treatment. The harder the abrasive is compared to the material of the specimen, the more significant the treatment effect will be. Furthermore, we must pay attention to abrasive materials for Tumble Finishing, the geometry of the abrasive particles becomes a critical factor, directly influencing the overall effectiveness of the treatment. In scenarios involving polymeric specimens, there tends to be a preference for abrasives with softer and more rounded profiles, aligning with the specific characteristics of the material.

In contrast, when confronted with the intrinsic hardness characteristic of Ti6Al4V, a strategic decision was made to employ a ceramic abrasive distinguished by its unique triangular shape. This selection is because of understanding interplay between the material composition of the abrasive, its geometric configuration, and the inherent properties of the Ti6Al4V specimens. Such approach ensures a tailored and impactful post-treatment process, taking advantage of its ability to improve the surface properties of the Ti6Al4V specimens in a way that is both comprehensive and effective. Additionally, the parameters that we set is shown in the Table *3*.

Table 3: Tumble Finishing Parameters

Printing Parameters	
Speed of Rotation [rpm]	2500
Duration of Treatment [minute]	150
Amount of water for Cooling the container*	0.4

*This parameter is entered by using a variable factor between 0 and 1

3.2.3 Microstructural Characterization

Microstructural examination of the vertically printed samples which were undergone of Tumble Finishing, and the as-build one is done. The goal was to compare the effectiveness of the post-treatment on the surface and near-surface zones. Moreover, automatic grinding and manual polishing of 1 μm diamond paste were used so as to have a mirror-like surface. The ultimate polishing was also used with a 0.04 μm colloidal silica suspension. At the end the samples were chemically etched using Kroll's regent, and then an Optical Microscope (OM) was used to observe the changes to the specified zones.

3.2.4 Micro-Hardness Measurement

A FutureTech® FM-810 Microhardness tester with a Vickers diamond indenter was used to conduct micro-hardness tests on the cross-section of the specimens. My goal was to study how the Tumble Finishing treatment might affect the hardness of the specimen. To do this, some tests were performed right on the surface of the specimen, different loads were tried, starting from 50 gf and going up to 500 gf for 15 seconds. This helped us to see if the hardness changed under different pressures.

3.2.5 Surface Roughness Measurements

The surface of the specimens was checked by measuring how rough or uneven it is at a really tiny level. Alicona® Infinite Focus OM was used to create 3D reconstructions of the parts' surfaces. This microscope works by using a contactless focus-variation technology, gathering data at different focus positions, with a super fine vertical resolution of 10 nm. From these 3D reconstructions, I looked at measurements of profile roughness and surface roughness to compare the different conditions. I also took micrographs of the surfaces under various conditions using a SEM and compared them.

To make sure the shape of the specimens didn't affect our measurements, I projected the acquisitions onto a cylinder. Then, I used a plane in the middle of the surface as our reference point for the actual measurements. The purpose is to see if the post-processing makes a positive difference, so I compared the surfaces of specimens built vertically in their original (As-Built) state with those that goes through the Tumble Finishing process.

3.2.6 Residual Stresses Analysis

X-ray diffraction (XRD) was used to check how the internal residual stresses changed when the Tumble-finishing post-process was applied to the vertically built specimens. For this, an AST X-Stress 3000 diffractometer with a Ti-Kα radiation anode was used. The sin2ψ method was employed, with a diffraction angle (2θ) of 137.4° and incident angles ranging from 0° to 90°.

To get a profile across the depth, I removed some material by electro-polishing with a solution of 94% acetic acid and 6% perchloric acid at 30 V, then I reported and compared the residual stresses both axially and radially in each case.

3.2.7 Fatigue Tests

Vertically built specimens were tested in various conditions using an Italsigma® rotating bending fatigue testing machine, as shown in Fig. 46. The tests involved applying stress with varying amplitudes, a run-out limit of 3×106 cycles, a stress ratio (R) of -1, and a rotational speed of approximately 2500 rpm. I followed the ISO 12107:2017 (E) [183] standard for processing fatigue data and calculating fatigue limits.

To examine the broken specimens, fractography analyses were conducted using a SEM. As mentioned earlier, I chose to focus on fatigue, especially rotating bending fatigue, as the primary mechanical property for analysis. This choice was influenced by its ease and speed of application, and the abundance of relevant literature that allows for meaningful comparisons and enhances the significance of our research activities.

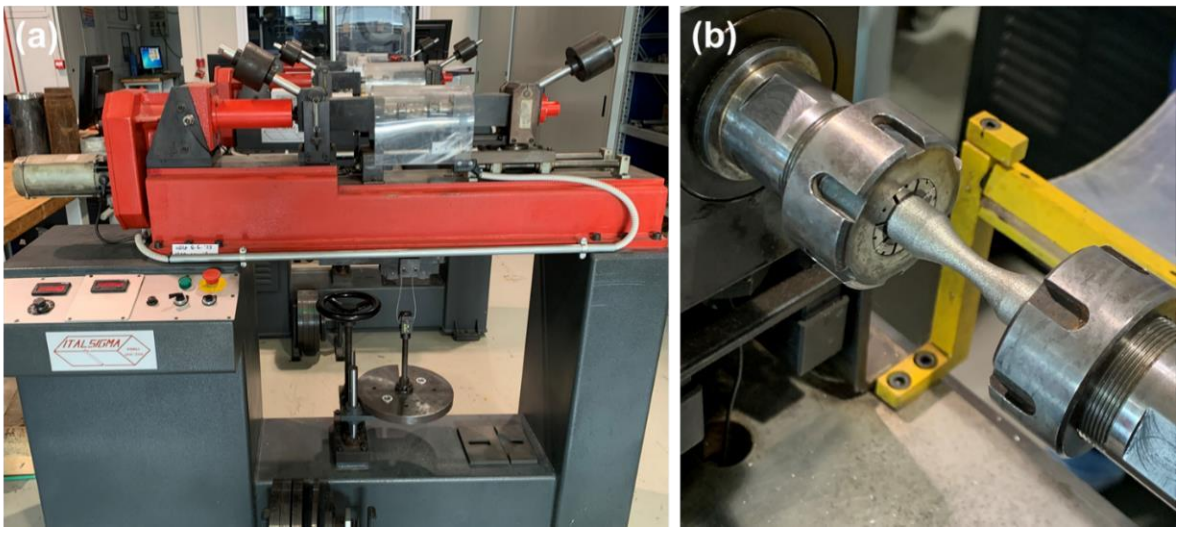

Fig. 46: (a) Rotating bending fatigue testing system by Italsigma. (b) The fatigue specimen is positioned on the machine.

Chapter 4 : Results and Discussion

In this section, I will present and discuss the key findings that emerged from the series of experiments throughout the course of this thesis. My goal is to provide a clear and detailed account of the outcomes, highlighting the most significant observations and insights I gained during the experimental process.

The structure of the following subsections is designed to guide you through the various stages of the research, offering a logical and sequential overview of the work. I have organized the subsections in a manner that reflects the chronological progression of our activities, starting from the initial setup of the experiments to the final conclusions. This arrangement will not only help illustrate the step-by-step approach I adopted in conducting our investigations but will also make it easier for you to follow the methodology and understand how each phase of the research contributed to the ultimate findings. By structuring the section in this way, I aim to provide a comprehensive narrative of the experimental journey, from the early observations to the final results and interpretations

4.1 Powder Morphology

The Ti6Al4V powder had a mostly round particle shape, with an average size of 40 µm. However, smaller particles were also noticeable among the larger ones. Despite this, many particles showed defects typical of the gas atomization process. In Fig. 47b, various types of these defects are pointed out, including hollow powder particles (with open pores in this case), satellites (small powder grains attached to the surface of larger ones), and irregular shapes. When observed under an OM, the particle cross-section confirmed the presence of shape irregularities and internal closed pores (refer to Fig. 47c). Detailed images of the cross-section revealed a standard solidification microstructure (see Fig. 47d).

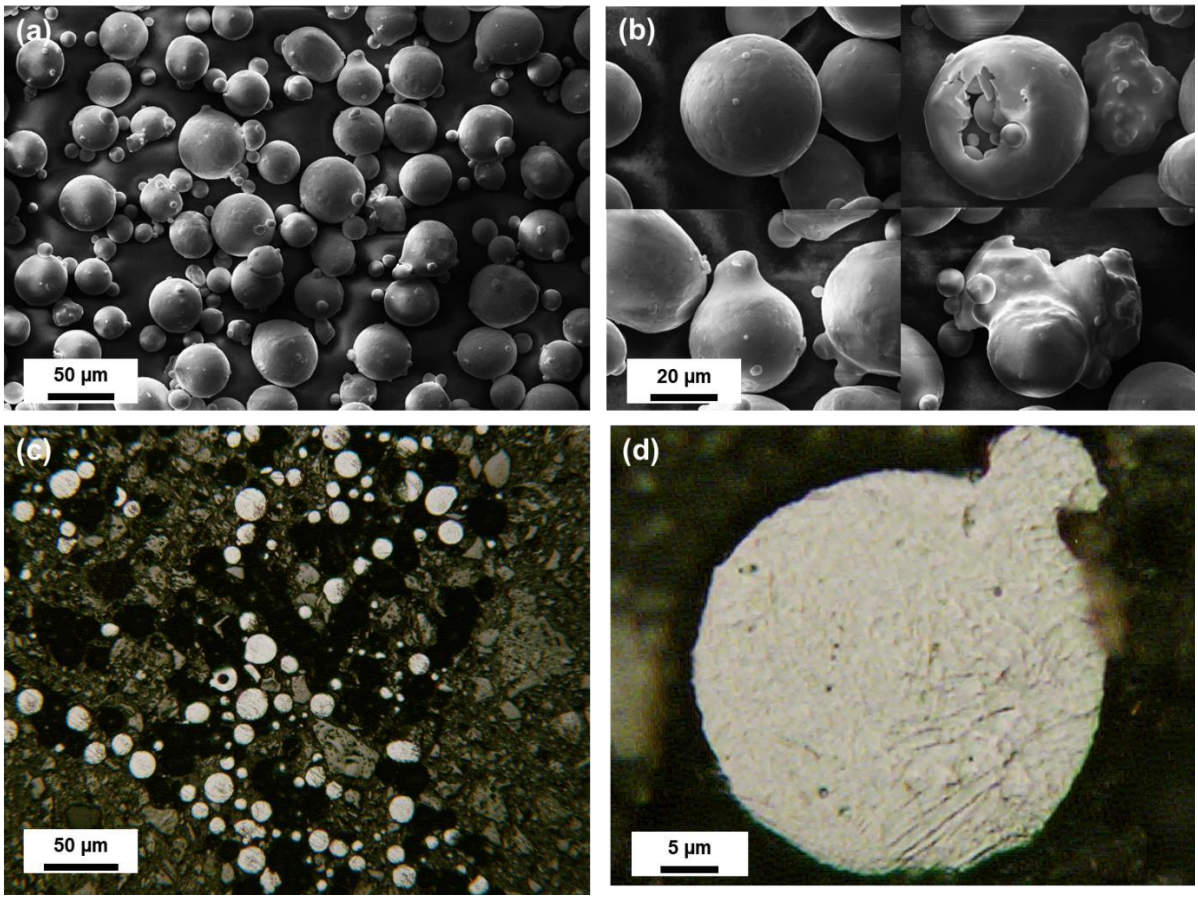

Fig. 47: SEM images of the Ti6Al4V powder are presented: (a) Overview of particle shape and morphology. (b) A comparison highlighting spherical, defect-free particles and common defects observed, including hollow particles, satellites, and irregular shapes. OM images show: (c) An overview of particle cross-section, revealing defects such as shape irregularities and internal porosity. (d) A detailed view of the powder microstructure.

4.2 Microstructural Analysis

Fig. 48 provides a detailed comparison of the cross-sections of vertical specimens in both their AB and Tumble-Finished states, with a specific emphasis on the surface and sub-surface regions. The images clearly illustrate a significant difference in surface quality between the two conditions. In the as-printed specimen, the surface is notably rougher and exhibits less precision, which is largely attributed to the repetitive laser passes during the printing process. This causes a "staircase" effect, where layers are uneven, and results in unmelted powder particles adhering to the surface. These particles, along with the irregularities, contribute to the overall roughness and lack of smoothness in the as-printed state. In contrast, the tumble-finishing process significantly improves the surface quality. By removing a thin outer layer of material, the process smooths the surface, eliminating the

rough profile and resulting in a more refined and polished appearance. Importantly, while the surface is improved, the tumble-finishing treatment does not cause any alterations to the microstructure of the specimen, ensuring that its internal properties remain unaffected by the surface treatment.

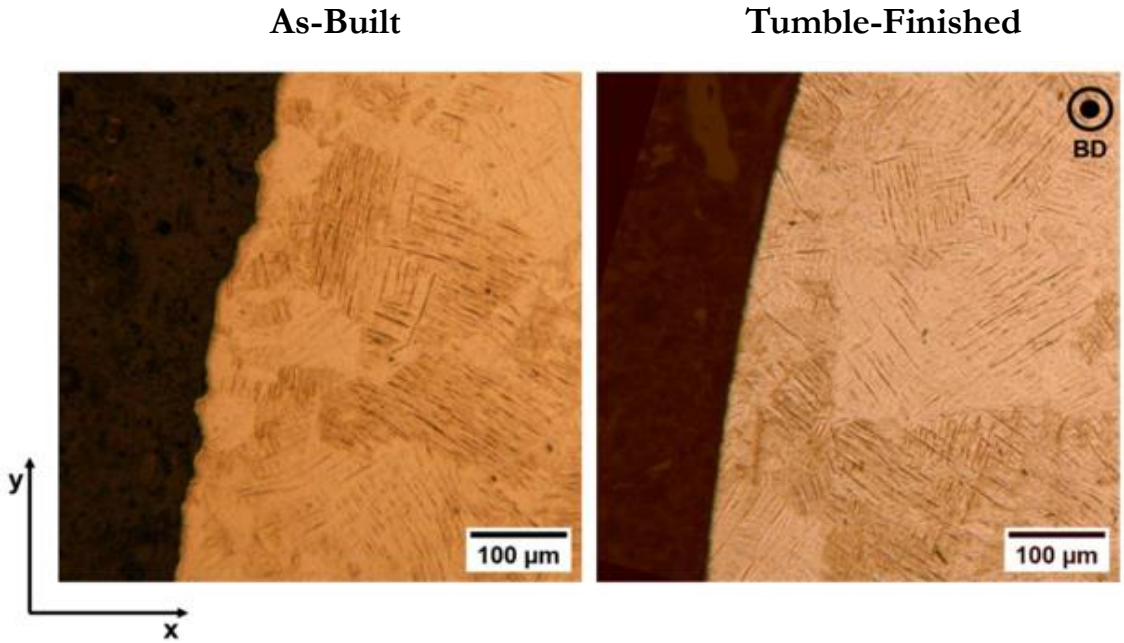

Fig. 48: OM images of cross-sectional views for both AB and Tumbled-Finished specimens, displaying the surface microstructure. The images are magnified 100 times.

4.3 Micro-Hardness

When applying a 50-gram force to measure the microhardness near the surface of the Tumble-Finished specimen, the recorded value was found to be 458 HV, in contrast to the 394 HV measured in the bulk of the material. This noticeable difference in hardness values between the surface and the bulk suggests that the post-treatment process, specifically the tumble-finishing technique, may have contributed to an increase in hardness at the specimen's surface. The slight elevation in hardness at the surface could be attributed to the mechanical action involved in the finishing process, which typically results in surface-level improvements, such as enhanced smoothness and possibly slight work hardening. This increase in hardness at the outermost layer is a common phenomenon observed in surface treatments, where the finishing techniques mechanically affect the material in such a way that its surface properties, including hardness, are improved while maintaining the integrity of the bulk material's properties.

4.4 Surface Roughness

The Alicona system was utilized to accurately measure and quantify both linear and surface roughness for each specimen. A comprehensive set of roughness parameters were evaluated, including Total Roughness (Rt), Roughness Average (Ra), Root Mean Square Height (Rq), Mean Height (Rz), Arithmetic Mean Height (Sa), Maximum Height of Profile (Sp), Root Mean Square Height (Sq), Maximum Depth of Profile (Sv), and Mean Depth (Sz). The roughness data was captured using a magnification of ×10, covering an area of 3.949x1.091 mm². To distinguish between roughness and waviness, a cut-off wavelength of λ=800 µm was applied, with roughness characterized by wavelengths smaller than the cut-off and waviness by larger wavelengths. The linear roughness parameters were determined by averaging five separate measurements, and the variability in the collected data is visually displayed in an interval plot, which helps in identifying the range and consistency of the roughness measurements.

When comparing the As-Built and Tumble-Finished conditions, as shown in Fig. 49a, it becomes evident that the post-treatment process effectively reduced the profile roughness, alongside a decrease in the variability of the measurements. Notably, when examining the Roughness Average (Ra) in both conditions, the Tumble-Finished specimen exhibited a significant reduction of 70.17% in roughness. Specifically, the roughness values changed from RaAB=31.01 µm in the As-Built condition to RaTF=9.25 µm after the Tumble-Finishing process. While a smaller reduction is observed in surface parameters, with a modest 3.71% decrease in the Sa parameter, as shown in Fig. 49b, this trend may be less pronounced due to residual surface grooves left by the surface treatment process, which may compromise the overall surface uniformity.

In terms of the (Sz, the reduction is more substantial, with a 29.57% decrease in this parameter. This significant drop highlights that the As-Built surface is much rougher and bumpier compared to the smoother surface obtained after the Tumble-Finishing post-treatment. This improved surface condition suggests that while some surface imperfections may persist, particularly due to residual grooves, the overall effectiveness of the post-treatment in enhancing surface smoothness and reducing roughness is clearly demonstrated by the data collected.

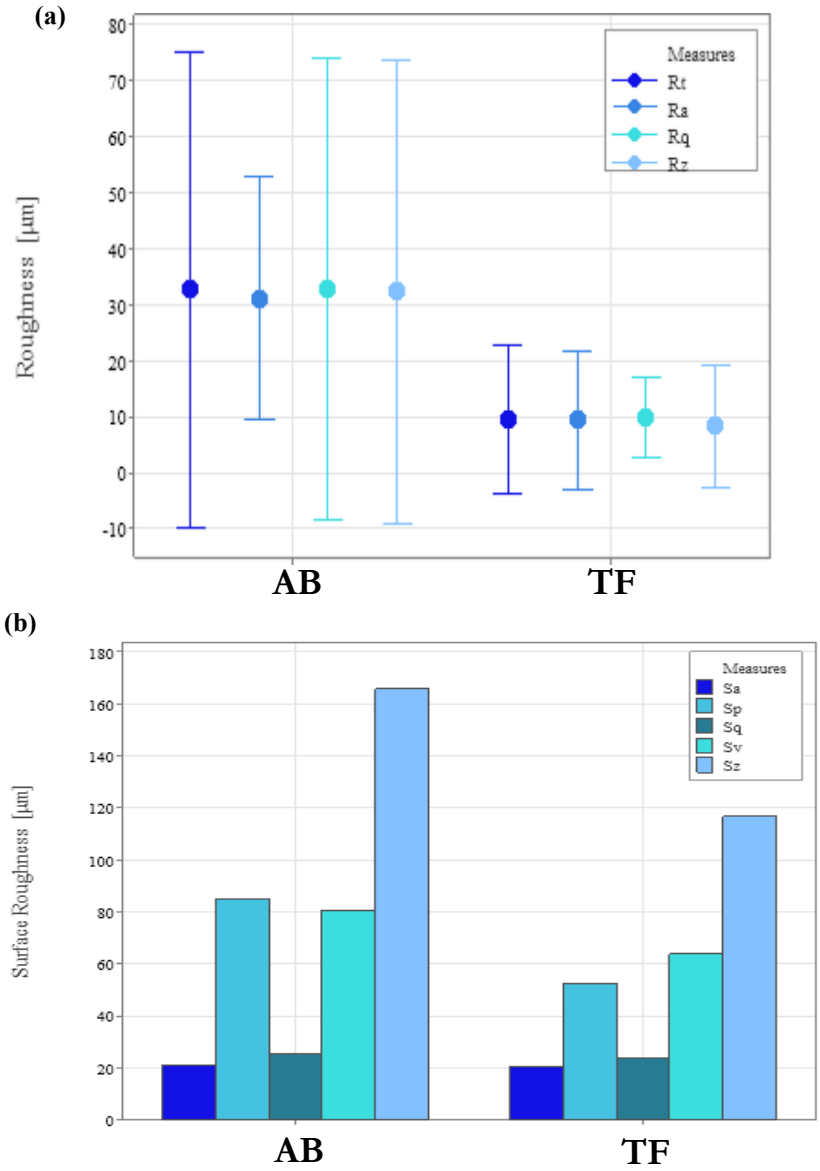

Fig. 49: (a) Linear roughness metrics such as Rt, Ra, Rq, Rz, and (b) Surface roughness metrics including Sa, Sp, Sq, Sv, Sz for both the As Built and Tumble-Finished conditions.

In Fig. 50, detailed side-by-side comparison of the SEM images reveals the surface characteristics of each specimen, specifically where roughness measurements were conducted. This figure also includes 3D texture reconstructions generated using Alicona, providing a comprehensive visual representation of the surface topography for each specimen in both the As-Built and Tumble-Finished conditions. Upon close examination of these images, it becomes evident that the surface of the TF specimen shows a marked improvement, as evidenced by a notable reduction in overall roughness. This reduction is primarily attributed to the effective removal of loose powder particles, which were nearly eliminated as a result of the tumble-finishing process.

However, while the surface treatment significantly enhances the smoothness of the specimen, it does not completely eradicate all surface irregularities. Some imperfections persist, as indicated by the presence of residual grooves that remain visible on the treated surface. These grooves suggest that, although the tumble-finishing process is successful in refining the surface quality and reducing roughness to a considerable extent, it is not able to entirely smooth out the surface to a perfectly uniform finish.

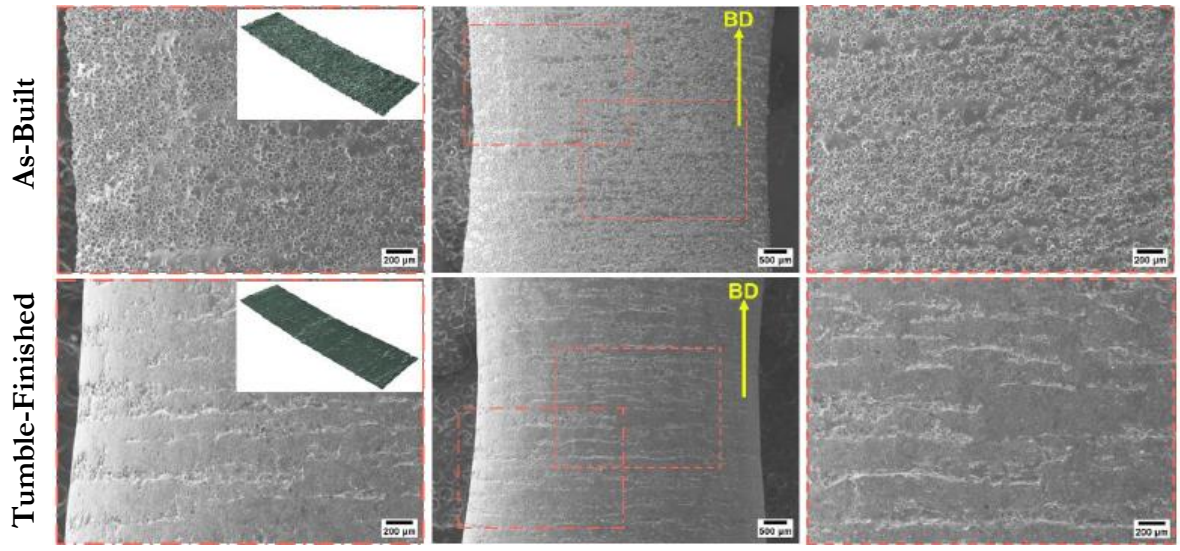

Fig. 50: Displays SEM micrographs capturing the surfaces of various analyzed specimens. Additionally, it features 3D reconstruction textures obtained from Alicona.

4.5 Residual Stresses

Fig. 51 illustrates and compares the profile of residual stresses on specimens printed vertically under different final processing conditions. Both AB and Tumbled-Finished specimens show elevated tensile residual stresses, particularly in the longitudinal direction (along the specimen's longest axis), peaking at around 200 µm depth. These significant tensile stresses, with maximum values reaching 1400 MPa, could significantly impact fatigue strength and should be considered in further analysis. Notably, the Tumbled-Finished post-treatment doesn't alter the residual stress profile as expected. However, it introduces compressive stresses at the surface (400 MPa) and within the top layer of less than 25 µm depth. These compressive residual stresses may contribute to improving the fatigue strength of this set of specimens.

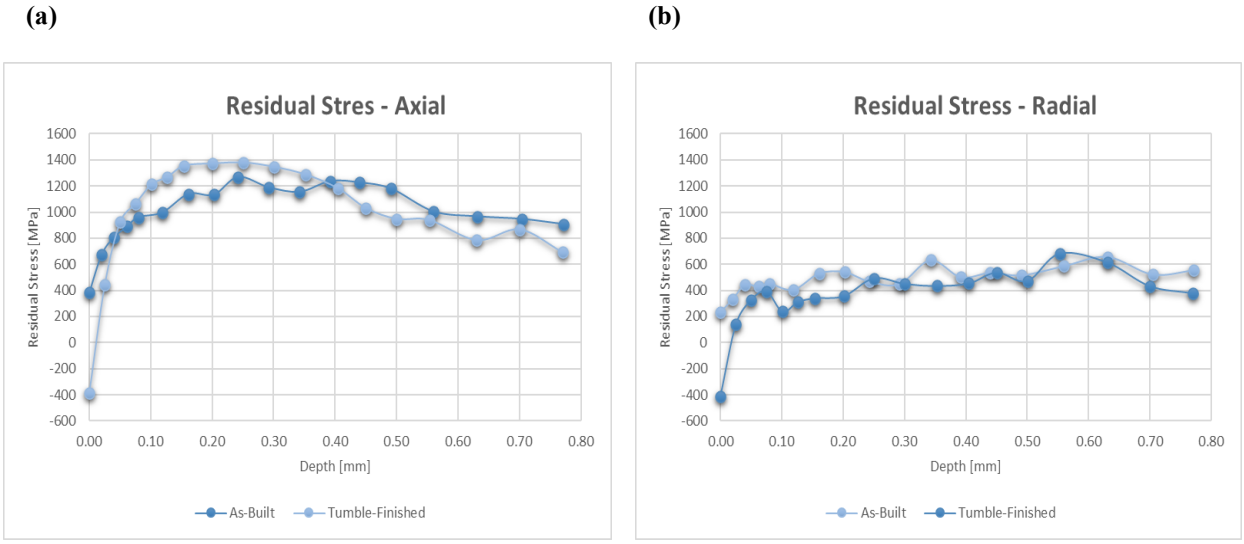

Fig. 51: The residual stress profile, assessed through XRD, in vertical specimens under various finishing conditions: (a) Along the axial direction, (b) Along the radial direction.

4.6 Fatigue Behavior

Fig. 52 summarizes the average fatigue strength limits and their standard deviation for each tested series of specimens, following the procedures outlined in ISO 12107:2017 (E). Notably, the fatigue performance of vertically printed specimens in their as-built state is significantly lower compared to those subjected to post-processing. In fact, the as-built specimens display a notably low fatigue strength when compared to typical values for Ti6Al4V specimens produced through traditional manufacturing processes (around 450 MPa) [184] . This difference could be attributed, first and foremost, to their higher surface roughness, which is linked to a greater concentration of notch-like surface defects that could initiate cracks.

Moreover, the elevated tensile residual stresses, especially those oriented longitudinally, are believed to contribute to crack initiation and propagation by increasing local stresses at the crack tip. Significantly, only with the application of the Tumble-Finishing procedure, the average fatigue limit was more than double increased, jumping from 65 MPa in the as-built condition to 138 MPa in the Tumble-finished condition. This increase can be explained by the reduction in surface roughness, implying fewer and less critical surface defects that could serve as potential notches for the initiation of fatigue cracks. Additionally, the introduction of compressive residual stresses at the surface is thought to enhance the fatigue limit, similar to the way a shot-peening procedure acts to arrest crack propagation. Table 4 offers a comprehensive overview of the various specimens tested under each condition. Only tests considered valid for calculating μ (sample mean) and σ (sample standard deviation) are included in the report.

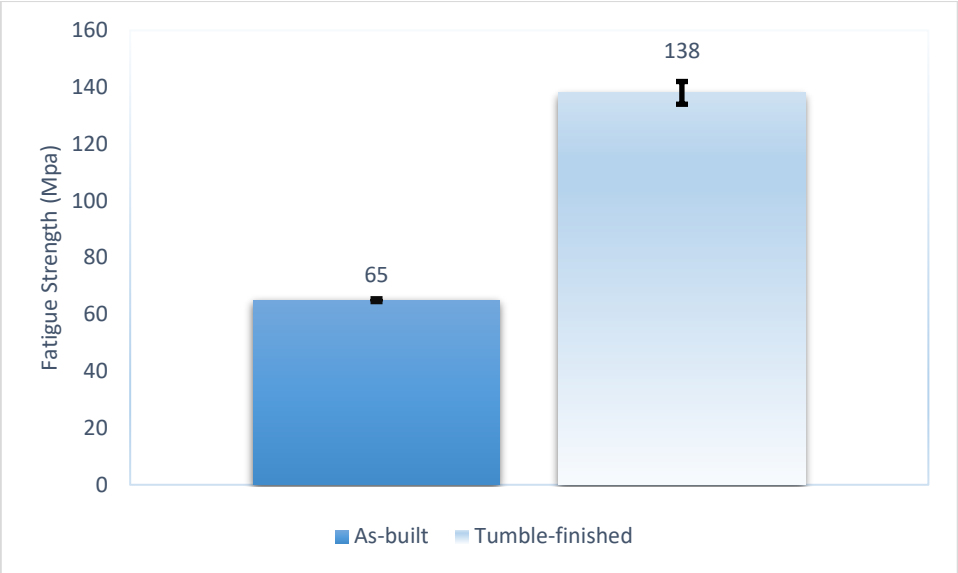

Fig. 52: The fatigue strength was computed for two sets of specimens that were printed in a vertical orientation and underwent a post-processing procedure.

Table 4: Results of the fatigue test (X for failure; O for non-failure)

Stress (MPa)	**Sequence number of specimen**							**μ (MPa)**	**σ (MPa)**
	1	2	3	4	5	6	7		
As-Built									
70		X		X		X		65.0	± 0.5
60	O		O		O				
Tumble-Finished									
150	X				X			138	± 4
140		X		O		X			
130			O				O		

4.7 Fracture Analysis

Fig. 53(a-g) showcase typical fracture surfaces of the as-built specimens, pointing out key details. In Fig. 53(a,d), we can identify two distinct zones: the darker area signifies the region where fatigue cracks propagated, evident from the smooth, beach marked surface. Meanwhile, the brighter zone seems to be a dimpled region where the final fracture occurred.

The yellow arrows indicate the likely direction of crack propagation. Both cases showed non-unique sites for crack initiation, suggesting potential initiation points across the entire external surface of the specimen. Specifically, surface valleys and grooves formed during layer-by-layer production and open porosity could have acted as stress concentrators. These defect types are highlighted in red and detailed in Fig. 53(b,c) for the first specimen and Fig. 53(f,g) for the second one. Fig. 53b depicts a valley on

the specimen's surface, potentially serving as one of the points where fatigue cracks initiated. Surface and sub-surface pores that could contribute to this process are emphasized in Fig. 53(c,f,g).

The fracture surface of the Tumble-Finished specimen in Fig. 53h shows a similar crack propagation mechanism as in the previous cases. However, it is believed that in this instance, the possible points of crack initiation may be better attributed to sub-superficial pores, as shown in Fig. 53(i,j). This is particularly because the Tumble-Finishing treatment significantly reduced surface roughness, consequently reducing the size and criticality of valleys and grooves on the specimen's surface.

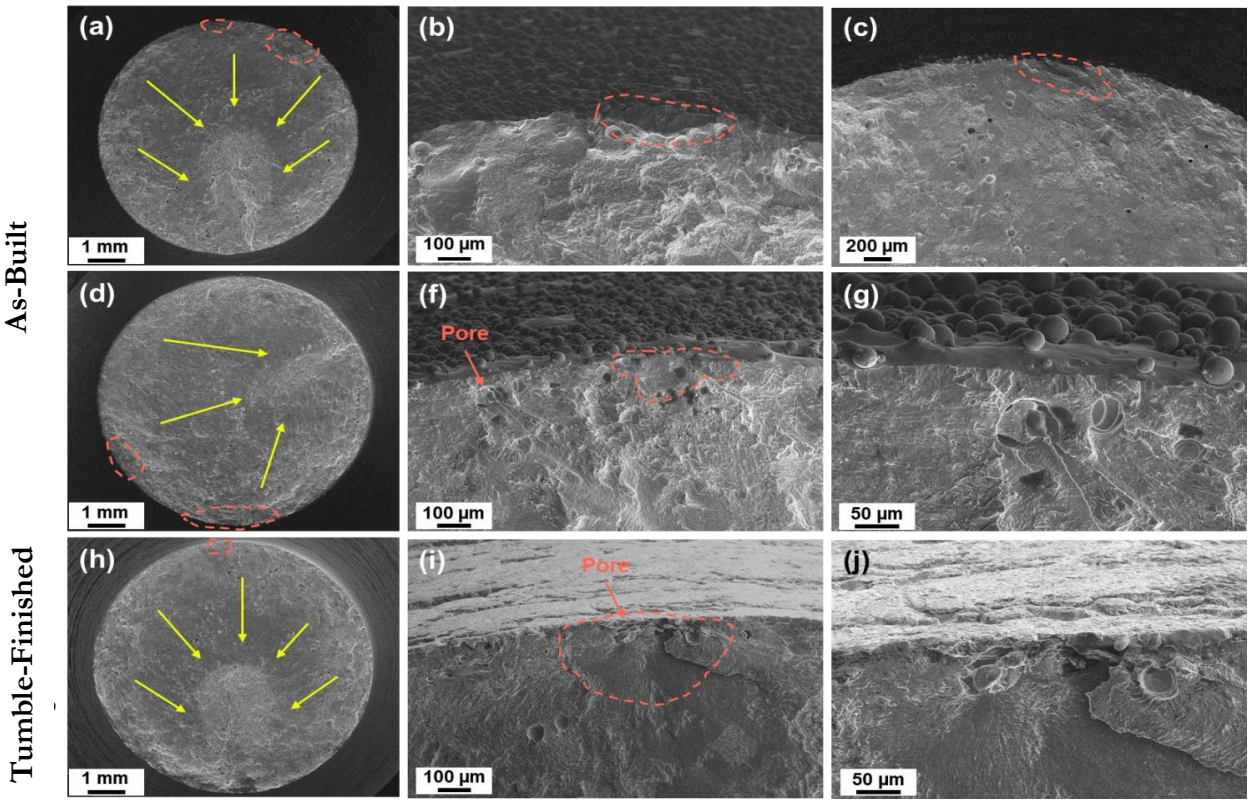

Fig. 53: SEM images were used to examine fatigue fracture surfaces of three distinct specimens. The yellow arrows denote the presumed direction of crack propagation, while red details highlight potential crack initiation points. In (a), the as-built specimen failed after 622,030 cycles at 70 MPa. Surface and sub-surface defects in (b) and (c) respectively are identified as possible crack initiation points. Another as-built specimen in (d) failed after 946,739 cycles at 70 MPa, with pores, surface defects, and sub-surface porosity in (f) and (g) considered as potential crack initiation points. The tumble-finished specimen in (h) failed after 721,140 cycles at 140 MPa, with sub-surface porosity detailed in (i, j) as possible crack initiation points.

Chapter 5 : Conclusions

In this study, an experimental investigation was conducted on additively manufactured specimens, focusing on the impact of post-treatment on fatigue performance. I chose to use one specific metal AM technology, L-PBF, as it is widely used in the industry. Additionally, I selected titanium alloy Ti6Al4V as the material of interest due to its various applications in industries such as aerospace, automotive and biomedical.

Vertical specimens were produced under two conditions: as-built (without any post-treatment) and Tumble-Finished. As detailed in earlier sections, the specimens were thoroughly characterized, with a specific emphasis on determining their fatigue limits.

To sum up and thoroughly interpret the key findings from the main experimental campaign mentioned earlier. Firstly, it's important to highlight the overall success of the experimental efforts, with consistent, meaningful, and scientifically interesting results. My primary discoveries can be summarized as follows:

1. The chosen printing parameters and the raw material used effectively produced nearly fully dense, low-porosity Ti6Al4V rotating bending fatigue specimens.
2. The fatigue performance of the as-built specimens is significantly influenced by their surface condition, the residual stresses generated during fabrication, and their final microstructure. In the case of as-built vertical specimens, the fatigue strength is considerably lower compared to Ti6Al4V specimens produced through traditional manufacturing methods. This is primarily due to their high surface roughness, driven mainly by the presence of surface defects (grooves caused by the staircase effect and open porosity) that could act as potential notches for initiating fatigue cracks. Additionally, the measured high tensile residual stresses contribute to increasing local stresses at the crack tip.
3. The use of the post-processing method notably enhanced the fatigue performance of the initially built vertical specimens. For the Tumble-Finished specimens, the fatigue strength more than

doubled. This improvement can be attributed to a decrease in surface roughness and the introduction of compressive residual stresses at the surface, even though there were no changes in the microstructure.

Chapter 6 : Further research perspectives

As explained earlier, numerous experiments were conducted in this research project to examine the impact of post-treatment on standard specimens. This not only served as a basis for further exploration but also opens the door to various potential directions, depending on the primary focus. Here are some potential avenues for future research:

1. **Different Printing Technology:** Another path is to explore a different printing technology, like EB-PBF, while maintaining standard vertical specimens to enable a fair comparison with the existing data obtained from L-PBF.

2. **Specimen Inclinations:** Exploring the printing of specimens at various inclinations, such as 45° or 60°, could be a third direction. This would involve analyzing microstructure, surface roughness, internal residual stresses, etc.

3. **Additional Post-Treatments:** Further developments could involve analyzing the effects of additional post-treatments, such as shot-peening or heat treatment, and even exploring combinations of treatments to understand the best combinations for improving printed part properties.

4. **Nonstandard Specimens:** Printing nonstandard specimens with different shapes and sizes is another possibility. This allows testing for effects related to part size and evaluating the properties and qualities of various tilts and shapes within the same specimen.

Bibliography

[1] I. Gibson, D. W. Rosen, and B. Stucker, *Additive Manufacturing Technologies*. Boston, MA: Springer US, 2010. doi: 10.1007/978-1-4419-1120-9.

[2] M. Armstrong, H. Mehrabi, and N. Naveed, 'An overview of modern metal additive manufacturing technology', *J Manuf Process*, vol. 84, pp. 1001–1029, Dec. 2022, doi: 10.1016/J.JMAPRO.2022.10.060.

[3] V. Madhavadas *et al.*, 'A review on metal additive manufacturing for intricately shaped aerospace components', *CIRP J Manuf Sci Technol*, vol. 39, pp. 18–36, Nov. 2022, doi: 10.1016/J.CIRPJ.2022.07.005.

[4] 'ASTM International - ASTM F3187-16 - Standard Guide for Directed Energy Deposition of Metals | GlobalSpec'. Accessed: May 05, 2024. [Online]. Available: https://standards.globalspec.com/std/3862763/astm-f3187-16

[5] A. Bacciaglia, A. Ceruti, and A. Liverani, 'Additive Manufacturing Challenges and Future Developments in the Next Ten Years', *Lecture Notes in Mechanical Engineering*, pp. 891–902, 2020, doi: 10.1007/978-3-030-31154-4_76.

[6] A. S. Johnson, S. Shao, N. Shamsaei, S. M. Thompson, and L. Bian, 'Microstructure, Fatigue Behavior, and Failure Mechanisms of Direct Laser-Deposited Inconel 718', *JOM*, vol. 69, no. 3, pp. 597–603, Mar. 2017, doi: 10.1007/S11837-016-2225-2/METRICS.

[7] M. Attaran, 'The rise of 3-D printing: The advantages of additive manufacturing over traditional manufacturing', *Bus Horiz*, vol. 60, no. 5, pp. 677–688, Sep. 2017, doi: 10.1016/J.BUSHOR.2017.05.011.

[8] D. I. Wimpenny, P. M. Pandey, and L. Jyothish Kumar, 'Advances in 3D Printing & additive manufacturing technologies', *Advances in 3D Printing and Additive Manufacturing Technologies*, pp. 1–186, Jan. 2016, doi: 10.1007/978-981-10-0812-2/COVER.

[9] X. Yu *et al.*, 'Influence of post-heat-treatment on the microstructure and fracture toughness properties of Inconel 718 fabricated with laser directed energy deposition additive manufacturing', *Materials Science and Engineering: A*, vol. 798, p. 140092, Nov. 2020, doi: 10.1016/J.MSEA.2020.140092.

[10] S. L. Sing, C. F. Tey, J. H. K. Tan, S. Huang, and W. Y. Yeong, '3D printing of metals in rapid prototyping of biomaterials: Techniques in additive manufacturing', *Rapid Prototyping of Biomaterials: Techniques in Additive Manufacturing*, pp. 17–40, Jan. 2020, doi: 10.1016/B978-0-08-102663-2.00002-2.

[11] J. C. Najmon, S. Raeisi, and A. Tovar, 'Review of additive manufacturing technologies and applications in the aerospace industry', *Additive Manufacturing for the Aerospace Industry*, pp. 7–31, Jan. 2019, doi: 10.1016/B978-0-12-814062-8.00002-9.

[12] B. Wu *et al.*, 'A review of the wire arc additive manufacturing of metals: properties, defects and quality improvement', *J Manuf Process*, vol. 35, pp. 127–139, Oct. 2018, doi: 10.1016/J.JMAPRO.2018.08.001.

[13] I. Gibson, D. Rosen, and B. Stucker, 'Directed Energy Deposition Processes', *Additive Manufacturing Technologies*, pp. 245–268, 2015, doi: 10.1007/978-1-4939-2113-3_10.

[14] M. Zenou and L. Grainger, 'Additive manufacturing of metallic materials', *Additive Manufacturing: Materials, Processes, Quantifications and Applications*, pp. 53–103, Jan. 2018, doi: 10.1016/B978-0-12-812155-9.00003-7.

[15] R. M. Mahamood and E. T. Akinlabi, 'Effect of Powder Flow Rate on Surface Finish in Laser Additive Manufacturing Process', *IOP Conf Ser Mater Sci Eng*, vol. 391, no. 1, p. 012005, Jul. 2018, doi: 10.1088/1757-899X/391/1/012005.

[16] I. Bahnini, M. Rivette, A. Rechia, A. Siadat, and A. Elmesbahi, 'Additive manufacturing technology: the status, applications, and prospects', *International Journal of Advanced Manufacturing Technology*, vol. 97, no. 1–4, pp. 147–161, Jul. 2018, doi: 10.1007/S00170-018-1932-Y/METRICS.

[17] W. J. Sames, F. A. List, S. Pannala, R. R. Dehoff, and S. S. Babu, 'The metallurgy and processing science of metal additive manufacturing', *International Materials Reviews*, vol. 61, no. 5, pp. 315–360, 2016, doi: 10.1080/09506608.2015.1116649.

[18] *ADDITIVE MANUFACTURING : innovations, advances, and applications*. CRC PRESS, 2020. Accessed: Jul. 15, 2024. [Online]. Available: https://www.routledge.com/Additive-Manufacturing-Innovations-Advances-and-Applications/Srivatsan-Sudarshan/p/book/9780367737788

[19] 'GE Dramatically Expanding Their Recent 3D Metal Acquisitions « Fabbaloo'. Accessed: Jul. 15, 2024. [Online]. Available: https://www.fabbaloo.com/2017/03/ge-dramatically-expanding-their-recent-3d-metal-acquisitions

[20] B. Vayre, F. Vignat, and F. Villeneuve, 'Identification on Some Design Key Parameters for Additive Manufacturing: Application on Electron Beam Melting', *Procedia CIRP*, vol. 7, pp. 264–269, Jan. 2013, doi: 10.1016/J.PROCIR.2013.05.045.

[21] M. A. Lodes, R. Guschlbauer, and C. Körner, 'Process development for the manufacturing of 99.94% pure copper via selective electron beam melting', *Mater Lett*, vol. 143, pp. 298–301, Mar. 2015, doi: 10.1016/J.MATLET.2014.12.105.

[22] C. Körner, 'Additive manufacturing of metallic components by selective electron beam melting — a review', *International Materials Reviews*, vol. 61, no. 5, pp. 361–377, 2016, doi: 10.1080/09506608.2016.1176289.

[23] A. A. Antonysamy, J. Meyer, and P. B. Prangnell, 'Effect of build geometry on the β-grain structure and texture in additive manufacture of Ti6Al4V by selective electron beam melting', *Mater Charact*, vol. 84, pp. 153–168, Oct. 2013, doi: 10.1016/J.MATCHAR.2013.07.012.

[24] A. Klassen, A. Bauereiß, and C. Körner, 'Modelling of electron beam absorption in complex geometries', *J Phys D Appl Phys*, vol. 47, no. 6, p. 065307, Jan. 2014, doi: 10.1088/0022-3727/47/6/065307.

[25] I. Gibson, D. W. Rosen, and B. Stucker, 'Additive manufacturing technologies: Rapid prototyping to direct digital manufacturing', *Additive Manufacturing Technologies: Rapid Prototyping to Direct Digital Manufacturing*, pp. 1–459, 2010, doi: 10.1007/978-1-4419-1120-9/COVER.

[26] L. Yang *et al.*, 'Additive Manufacturing of Metals: The Technology, Materials, Design and Production', 2017, doi: 10.1007/978-3-319-55128-9.

[27] E. Marin, M. Pressacco, S. Fusi, A. Lanzutti, S. Turchet, and L. Fedrizzi, 'Characterization of grade 2 commercially pure Trabecular Titanium structures', *Materials Science and Engineering: C*, vol. 33, no. 5, pp. 2648–2656, Jul. 2013, doi: 10.1016/J.MSEC.2013.02.034.

[28] J. E. Biemond, G. Hannink, N. Verdonschot, and P. Buma, 'Bone ingrowth potential of electron beam and selective laser melting produced trabecular-like implant surfaces with and without a biomimetic coating', *J Mater Sci Mater Med*, vol. 24, no. 3, pp. 745–753, Mar. 2013, doi: 10.1007/S10856-012-4836-7.

[29] S. Ponader *et al.*, 'Effects of topographical surface modifications of electron beam melted Ti-6Al-4V titanium on human fetal osteoblasts.', *J Biomed Mater Res A*, vol. 84, no. 4, pp. 1111–1119, Mar. 2008, doi: 10.1002/JBM.A.31540.

[30] L. E. Murr, S. M. Gaytan, E. Martinez, F. Medina, and R. B. Wicker, 'Next generation orthopaedic implants by additive manufacturing using electron beam melting', *Int J Biomater*, vol. 2012, 2012, doi: 10.1155/2012/245727.

[31] A. Mazzoli, M. Germani, and R. Raffaeli, 'Direct fabrication through electron beam melting technology of custom cranial implants designed in a PHANToM-based haptic environment', *Mater Des*, vol. 30, no. 8, pp. 3186–3192, Sep. 2009, doi: 10.1016/J.MATDES.2008.11.013.

[32] J. Wang and H. Tang, 'Review on metals additively manufactured by SEBM', *Materials Technology*, vol. 31, no. 2, pp. 86–89, 2016, doi: 10.1179/1753555715Y.0000000081.

[33] R. R. Dehoff *et al.*, 'Case Study: Additive Manufacturing of Aerospace Brackets', *Advanced Materials and Processes*, vol. 171, no. 3, Jan. 2013.

[34] L. E. Murr *et al.*, 'Characterization of titanium aluminide alloy components fabricated by additive manufacturing using electron beam melting', *Acta Mater*, vol. 58, no. 5, pp. 1887–1894, Mar. 2010, doi: 10.1016/J.ACTAMAT.2009.11.032.

[35] H. P. Tang, G. Y. Yang, W. P. Jia, W. W. He, S. L. Lu, and M. Qian, 'Additive manufacturing of a high niobium-containing titanium aluminide alloy by selective electron beam melting', *Materials Science and Engineering: A*, vol. 636, pp. 103–107, Jun. 2015, doi: 10.1016/J.MSEA.2015.03.079.

[36] J. Schwerdtfeger and C. Körner, 'Selective electron beam melting of Ti–48Al–2Nb–2Cr: Microstructure and aluminium loss', *Intermetallics (Barking)*, vol. 49, pp. 29–35, Jun. 2014, doi: 10.1016/J.INTERMET.2014.01.004.

[37] G. Baudana *et al.*, 'Electron beam melting of Ti-48Al-2Nb-0.7Cr-0.3Si: Feasibility investigation', *Intermetallics (Barking)*, vol. 73, pp. 43–49, Jun. 2016, doi: 10.1016/J.INTERMET.2016.03.001.

[38] S. Biamino *et al.*, 'Electron beam melting of Ti–48Al–2Cr–2Nb alloy: Microstructure and mechanical properties investigation', *Intermetallics (Barking)*, vol. 19, no. 6, pp. 776–781, Jun. 2011, doi: 10.1016/J.INTERMET.2010.11.017.

[39] F. Trevisan, ' Study and characterization of different metal alloys processed through Laser Powder Bed Fusion', Politecnico di Torino, Turin, 2018.

[40] F. Trevisan *et al.*, 'On the Selective Laser Melting (SLM) of the AlSi10Mg Alloy: Process, Microstructure, and Mechanical Properties', *Materials*, vol. 10, no. 1, p. 76, Jan. 2017, doi: 10.3390/ma10010076.

[41] 'F3049 Standard Guide for Characterizing Properties of Metal Powders Used for Additive Manufacturing Processes'. Accessed: Jul. 21, 2024. [Online]. Available: https://www.astm.org/f3049-14r21.html

[42] S. Di Falco, 'Optimisation of process parameters for Directed Energy Deposition (DED) of IN718 nickel-based superalloy', Oct. 2019.

[43] S. BIAMINO, 'Optimization of process parameters for DED of IN718 superalloys via Single scan track and single-layer analysis - Webthesis'. Accessed: Jul. 26, 2024. [Online]. Available: https://webthesis.biblio.polito.it/18290/

[44] LANGNAU LESLIE, 'In auto racing, 3D printing wins the race for part production'. Accessed: Jul. 26, 2024. [Online]. Available: https://www.makepartsfast.com/in-auto-racing-3d-printing-wins-the-race-for-part-production/

[45] W. W. Wits, S. J. Weitkamp, and J. Van Es, 'Metal Additive Manufacturing of a High-pressure Micro-pump', *Procedia CIRP*, vol. 7, pp. 252–257, Jan. 2013, doi: 10.1016/J.PROCIR.2013.05.043.

[46] '3ders.org - AIRBUS A320 saves weight with 3D printed bionic partition, made from high strength scalmalloy metal alloy | 3D Printer News & 3D Printing News'. Accessed: Jul. 26, 2024. [Online]. Available: https://www.3ders.org/articles/20151202-airbus-a320-3d-printed-bionic-partition-made-from-high-strength-scalmalloy-metal-alloy.html

[47] 'Printing the future: Airbus expands its applications of the revolutionary additive layer manufacturing process'. Accessed: Jul. 26, 2024. [Online]. Available: https://www.aerocontact.com/en/aerospace-aviation-news/44590-printing-the-future-airbus-expands-its-applications-of-the-revolutionary-additive-layer-manufacturing-process

[48] 'Opportunities and Challenges for Additive Manufacturing in Space Applications | Request PDF'. Accessed: Jul. 26, 2024. [Online]. Available: https://www.researchgate.net/publication/309040764_Opportunities_and_Challenges_for_Additive_Manufacturing_in_Space_Applications

[49] L. Jyothish Kumar and C. G. Krishnadas Nair, 'Current Trends of Additive Manufacturing in the Aerospace Industry', *Advances in 3D Printing and Additive Manufacturing Technologies*, pp. 39–54, Jan. 2017, doi: 10.1007/978-981-10-0812-2_4.

[50] R. Huang *et al.*, 'Energy and emissions saving potential of additive manufacturing: the case of lightweight aircraft components', *J Clean Prod*, vol. 135, pp. 1559–1570, Nov. 2016, doi: 10.1016/J.JCLEPRO.2015.04.109.

[51] '(2) Opportunities and Challenges for Additive Manufacturing in Space Applications | Request PDF'. Accessed: Jul. 29, 2024. [Online]. Available: https://www.researchgate.net/publication/309040764_Opportunities_and_Challenges_for_Additive_Manufacturing_in_Space_Applications

[52] V. Weißmann, R. Bader, H. Hansmann, and N. Laufer, 'Influence of the structural orientation on the mechanical properties of selective laser melted Ti6Al4V open-porous scaffolds', *Mater Des*, vol. 95, pp. 188–197, Apr. 2016, doi: 10.1016/J.MATDES.2016.01.095.

[53] G. Pyka *et al.*, 'Surface Modification of Ti6Al4V Open Porous Structures Produced by Additive Manufacturing', *Adv Eng Mater*, vol. 14, no. 6, pp. 363–370, Jun. 2012, doi: 10.1002/ADEM.201100344.

[54] R. Hasan, R. Mines, and P. Fox, 'Characterization of selectively laser melted Ti-6Al-4 V micro-lattice struts', *Procedia Eng*, vol. 10, pp. 536–541, Jan. 2011, doi: 10.1016/J.PROENG.2011.04.090.

[55] J. Wieding *et al.*, 'Biomechanical behavior of bone scaffolds made of additive manufactured tricalciumphosphate and titanium alloy under different loading conditions', *J Appl Biomater Funct Mater*, vol. 11, no. 3, pp. 159–166, 2013, doi: 10.5301/JABFM.2013.10832.

[56] C. Mangano, M. Raspanti, T. Traini, A. Piattelli, and R. Sammons, 'Stereo imaging and cytocompatibility of a model dental implant surface formed by direct laser fabrication', *J Biomed Mater Res A*, vol. 88, no. 3, pp. 823–831, Mar. 2009, doi: 10.1002/JBM.A.32033.

[57] T. Traini, C. Mangano, R. L. Sammons, F. Mangano, A. Macchi, and A. Piattelli, 'Direct laser metal sintering as a new approach to fabrication of an isoelastic functionally graded material for manufacture of porous titanium dental implants', *Dental Materials*, vol. 24, no. 11, pp. 1525–1533, Nov. 2008, doi: 10.1016/J.DENTAL.2008.03.029.

[58] D. K. Pattanayak *et al.*, 'Fabrication of Bioactive Porous Ti Metal with Structure Similar to Human Cancellous Bone by Selective Laser Melting', *Bioceram Dev Appl*, vol. 1, pp. 1–3, 2010, doi: 10.4303/BDA/D101206.

[59] C. Emmelmann, P. Scheinemann, M. Munsch, and V. Seyda, 'Laser Additive Manufacturing of Modified Implant Surfaces with Osseointegrative Characteristics', *Phys Procedia*, vol. 12, no. PART 1, pp. 375–384, Jan. 2011, doi: 10.1016/J.PHPRO.2011.03.048.

[60] Y. Yan, G. L. Nash, and P. Nash, 'Effect of density and pore morphology on fatigue properties of sintered Ti–6Al–4V', *Int J Fatigue*, vol. 55, pp. 81–91, Oct. 2013, doi: 10.1016/J.IJFATIGUE.2013.05.015.

[61] A. Fukuda *et al.*, 'Osteoinduction of porous Ti implants with a channel structure fabricated by selective laser melting', *Acta Biomater*, vol. 7, no. 5, pp. 2327–2336, 2011, doi: 10.1016/J.ACTBIO.2011.01.037.

[62] X. Wang *et al.*, 'Topological design and additive manufacturing of porous metals for bone scaffolds and orthopaedic implants: A review', *Biomaterials*, vol. 83, pp. 127–141, Mar. 2016, doi: 10.1016/J.BIOMATERIALS.2016.01.012.

[63] J. Sun, Y. Yang, and D. Wang, 'Parametric optimization of selective laser melting for forming Ti6Al4V samples by Taguchi method', *Opt Laser Technol*, vol. 49, pp. 118–124, Jul. 2013, doi: 10.1016/J.OPTLASTEC.2012.12.002.

[64] L. C. Zhang and H. Attar, 'Selective Laser Melting of Titanium Alloys and Titanium Matrix Composites for Biomedical Applications: A Review', *Adv Eng Mater*, vol. 18, no. 4, pp. 463–475, Apr. 2016, doi: 10.1002/ADEM.201500419.

[65] C. M. Haslauer, J. C. Springer, O. L. A. Harrysson, E. G. Loboa, N. A. Monteiro-Riviere, and D. J. Marcellin-Little, 'In vitro biocompatibility of titanium alloy discs made using direct metal fabrication', *Med Eng Phys*, vol. 32, no. 6, pp. 645–652, Jul. 2010, doi: 10.1016/J.MEDENGPHY.2010.04.003.

[66] S. Ponader *et al.*, 'In vivo performance of selective electron beam-melted Ti-6Al-4V structures', *J Biomed Mater Res A*, vol. 92A, no. 1, pp. 56–62, Jan. 2010, doi: 10.1002/JBM.A.32337.

[67] K. C. Nune, R. D. K. Misra, S. M. Gaytan, and L. E. Murr, 'Interplay between cellular activity and three-dimensional scaffold-cell constructs with different foam structure processed by electron beam melting', *J Biomed Mater Res A*, vol. 103, no. 5, pp. 1677–1692, May 2015, doi: 10.1002/JBM.A.35307.

[68] J. Wieding, A. Jonitz, and R. Bader, 'The Effect of Structural Design on Mechanical Properties and Cellular Response of Additive Manufactured Titanium Scaffolds', *Materials*, vol. 5, no. 8, p. 1336, 2012, doi: 10.3390/MA5081336.

[69] 'Wohlers Report 2015 - Wohlers Associates'. Accessed: Jul. 29, 2024. [Online]. Available: https://wohlersassociates.com/product/wohlers-report-2015/

[70] F. Trevisan *et al.*, 'Additive manufacturing of titanium alloys in the biomedical field: processes, properties and applications', *J Appl Biomater Funct Mater*, vol. 16, no. 2, pp. 57–67, Apr. 2018, doi: 10.5301/JABFM.5000371/ASSET/IMAGES/LARGE/10.5301_JABFM.5000371-FIG3.JPEG.

[71] A. Bandyopadhyay, T. Gualtieri, and S. Bose, 'Global Engineering and Additive Manufacturing', *Addit Manuf*, pp. 1–18, Sep. 2015, doi: 10.1201/B18893-2.

[72] M. Cronskär, M. Bäckström, and L. E. Rännar, 'Production of customized hip stem prostheses - A comparison between conventional machining and electron beam melting (EBM)', *Rapid Prototyp J*, vol. 19, no. 5, pp. 365–372, 2013, doi: 10.1108/RPJ-07-2011-0067.

[73] A. J. Pinkerton, '[INVITED] Lasers in additive manufacturing', *Opt Laser Technol*, vol. 78, pp. 25–32, Apr. 2016, doi: 10.1016/J.OPTLASTEC.2015.09.025.

[74] 'Wohlers 2017 Report on 3D Printing Industry Points to Softened Growth - Digital Engineering 24/7'. Accessed: Aug. 12, 2024. [Online]. Available: https://www.digitalengineering247.com/article/wohlers-2017-report-on-3d-printing-industry-points-to-softened-growth/

[75] X. Z. Zhang, H. P. Tang, M. Leary, T. Song, L. Jia, and M. Qian, 'Toward Manufacturing Quality Ti-6Al-4V Lattice Struts by Selective Electron Beam Melting (SEBM) for Lattice Design', *JOM*, vol. 70, no. 9, pp. 1870–1876, Sep. 2018, doi: 10.1007/S11837-018-3030-X/METRICS.

[76] P. Das, R. Chandran, R. Samant, and S. Anand, 'Optimum Part Build Orientation in Additive Manufacturing for Minimizing Part Errors and Support Structures', *Procedia Manuf*, vol. 1, pp. 343–354, Jan. 2015, doi: 10.1016/J.PROMFG.2015.09.041.

[77] Y. Wu and L. Yang, 'Modeling and analysis of material anisotropy-topology effects of 3D cellular structures fabricated by powder bed fusion additive manufacturing', *Int J Mech Sci*, vol. 197, p. 106325, May 2021, doi: 10.1016/J.IJMECSCI.2021.106325.

[78] V. Weißmann, P. Drescher, R. Bader, H. Seitz, H. Hansmann, and N. Laufer, 'Comparison of Single Ti6Al4V Struts Made Using Selective Laser Melting and Electron Beam Melting Subject to Part Orientation', *Metals 2017, Vol. 7, Page 91*, vol. 7, no. 3, p. 91, Mar. 2017, doi: 10.3390/MET7030091.

[79] H. D. Nguyen *et al.*, 'A critical review on additive manufacturing of Ti-6Al-4V alloy: microstructure and mechanical properties', *Journal of Materials Research and Technology*, vol. 18, pp. 4641–4661, May 2022, doi: 10.1016/J.JMRT.2022.04.055.

[80] E. W. Hovig, A. S. Azar, F. Grytten, K. Sørby, and E. Andreassen, 'Determination of anisotropic mechanical properties for materials processed by laser powder bed fusion', *Advances in Materials Science and Engineering*, vol. 2018, 2018, doi: 10.1155/2018/7650303.

[81] S. Murchio *et al.*, 'Additively manufactured Ti–6Al–4V thin struts via laser powder bed fusion: Effect of building orientation on geometrical accuracy and mechanical properties', *J Mech Behav Biomed Mater*, vol. 119, p. 104495, Jul. 2021, doi: 10.1016/J.JMBBM.2021.104495.

[82] B. Zhang, X. Han, C. Chen, W. Zhang, H. Liao, and B. Chen, 'Effect of the strut size and tilt angle on the geometric characteristics of selective laser melting AlSi10Mg', *Rapid Prototyp J*, vol. 27, no. 5, pp. 879–889, 2021, doi: 10.1108/RPJ-08-2020-0187/FULL/PDF.

[83] M. Leary *et al.*, 'Selective laser melting (SLM) of AlSi12Mg lattice structures', *Mater Des*, vol. 98, pp. 344–357, May 2016, doi: 10.1016/J.MATDES.2016.02.127.

[84] S. Murchio *et al.*, 'Additively manufactured Ti–6Al–4V thin struts via laser powder bed fusion: Effect of building orientation on geometrical accuracy and mechanical properties', *J Mech Behav Biomed Mater*, vol. 119, p. 104495, Jul. 2021, doi: 10.1016/J.JMBBM.2021.104495.

[85] M. Suard *et al.*, 'Mechanical equivalent diameter of single struts for the stiffness prediction of lattice structures produced by Electron Beam Melting', *Addit Manuf*, vol. 8, pp. 124–131, Oct. 2015, doi: 10.1016/J.ADDMA.2015.10.002.

[86] G. MacUlotti, G. Piscopo, G. Marchiandi, E. Atzeni, A. Salmi, and L. Iuliano, 'Build orientation effect on Ti6Al4V thin-wall topography by electron beam powder bed fusion', *Procedia CIRP*, vol. 108, no. C, pp. 222–227, Jan. 2022, doi: 10.1016/J.PROCIR.2022.03.039.

[87] P. Delroisse, P. J. Jacques, E. Maire, O. Rigo, and A. Simar, 'Effect of strut orientation on the microstructure heterogeneities in AlSi10Mg lattices processed by selective laser melting', *Scr Mater*, vol. 141, pp. 32–35, Dec. 2017, doi: 10.1016/J.SCRIPTAMAT.2017.07.020.

[88] T. Fritsch, L. Farahbod-Sternahl, I. Serrano-Muñoz, F. Léonard, C. Haberland, and G. Bruno, '3D Computed Tomography Quantifies the Dependence of Bulk Porosity, Surface Roughness, and Re-Entrant Features on Build Angle in Additively Manufactured IN625 Lattice Struts', *Adv Eng Mater*, vol. 24, no. 6, p. 2100689, Jun. 2022, doi: 10.1002/ADEM.202100689.

[89] J. Bültmann, S. Merkt, C. Hammer, C. Hinke, and U. Prahl, 'Scalability of the mechanical properties of selective laser melting produced micro-struts', *J Laser Appl*, vol. 27, no. S2, p. 29206, Feb. 2015, doi: 10.2351/1.4906392/313994.

[90] B. Vrancken, 'Effects of build orientation and heat treatment on the microstructure and mechanical properties of selective laser melted Ti6Al4V lattice structures', *Addit Manuf*, Jan. 2014, Accessed: Feb. 20, 2024. [Online]. Available: https://www.academia.edu/27747218/Effects_of_build_orientation_and_heat_treatment_on_th

e_microstructure_and_mechanical_properties_of_selective_laser_melted_Ti6Al4V_lattice_structures

[91] N. T. Aboulkhair, N. M. Everitt, I. Ashcroft, and C. Tuck, 'Reducing porosity in AlSi10Mg parts processed by selective laser melting', *Addit Manuf*, vol. 1–4, pp. 77–86, Oct. 2014, doi: 10.1016/J.ADDMA.2014.08.001.

[92] S. Ball, M. Ghayoor, S. Pasebani, and A. Tabei, 'Statistical Analysis of Porosity and Process Parameter Relationships in Metal Additive Manufacturing', *Procedia Manuf*, vol. 53, pp. 343–347, Jan. 2021, doi: 10.1016/J.PROMFG.2021.06.037.

[93] A. du Plessis, 'Effects of process parameters on porosity in laser powder bed fusion revealed by X-ray tomography', *Addit Manuf*, vol. 30, p. 100871, Dec. 2019, doi: 10.1016/J.ADDMA.2019.100871.

[94] M. Suard, L. Barrière, P. Lhuissier, S. Perusin, B. Filloux, and R. Dendievel, 'Influence of manufacturing orientations on the morphology of alloy 718 single struts manufactured by selective laser melting', *Material Design & Processing Communications*, vol. 3, no. 1, p. e140, Feb. 2021, doi: 10.1002/MDP2.140.

[95] X. Z. Zhang *et al.*, 'Additive manufacturing of intricate lattice materials: Ensuring robust strut additive continuity to realize the design potential', *Addit Manuf*, vol. 58, p. 103022, Oct. 2022, doi: 10.1016/J.ADDMA.2022.103022.

[96] A. Sombatmai, V. Uthaisangsuk, S. Wongwises, and P. Promoppatum, 'Multiscale investigation of the influence of geometrical imperfections, porosity, and size-dependent features on mechanical behavior of additively manufactured Ti-6Al-4V lattice struts', *Mater Des*, vol. 209, p. 109985, Nov. 2021, doi: 10.1016/J.MATDES.2021.109985.

[97] T. Persenot, A. Burr, G. Martin, J. Y. Buffiere, R. Dendievel, and E. Maire, 'Effect of build orientation on the fatigue properties of as-built Electron Beam Melted Ti-6Al-4V alloy', *Int J Fatigue*, vol. 118, pp. 65–76, Jan. 2019, doi: 10.1016/J.IJFATIGUE.2018.08.006.

[98] M. Awd, F. Stern, A. Kampmann, D. Kotzem, J. Tenkamp, and F. Walther, 'Microstructural Characterization of the Anisotropy and Cyclic Deformation Behavior of Selective Laser Melted AlSi10Mg Structures', *Metals 2018, Vol. 8, Page 825*, vol. 8, no. 10, p. 825, Oct. 2018, doi: 10.3390/MET8100825.

[99] U. Hossain, S. Ghouse, K. Nai, and J. R. T. Jeffers, 'Mechanical and morphological properties of additively manufactured SS316L and Ti6Al4V micro-struts as a function of build angle', *Addit Manuf*, vol. 46, p. 102050, Oct. 2021, doi: 10.1016/J.ADDMA.2021.102050.

[100] J. Du *et al.*, 'Improving the microstructure and mechanical properties of laser powder bed fusion-fabricated tantalum by high laser energy density', *Mater Lett*, vol. 333, p. 133547, Feb. 2023, doi: 10.1016/J.MATLET.2022.133547.

[101] 'Laser Powder Bed Fusion of Ti-rich TiNi lattice structures: Process optimisation, geometrical integrity, and phase transformations | Request PDF'. Accessed: Feb. 27, 2024. [Online]. Available: https://www.researchgate.net/publication/332528543_Laser_Powder_Bed_Fusion_of_Ti-rich_TiNi_lattice_structures_Process_optimisation_geometrical_integrity_and_phase_transformations

[102] S. Ehsan Saghaian *et al.*, 'Effect of hatch spacing and laser power on microstructure, texture, and thermomechanical properties of laser powder bed fusion (L-PBF) additively manufactured NiTi', *OptLT*, vol. 149, p. 107680, May 2022, doi: 10.1016/J.OPTLASTEC.2021.107680.

[103] J. Vishwakarma, K. Chattopadhyay, and N. C. Santhi Srinivas, 'Effect of build orientation on microstructure and tensile behaviour of selectively laser melted M300 maraging steel', *Materials Science and Engineering: A*, vol. 798, p. 140130, Nov. 2020, doi: 10.1016/J.MSEA.2020.140130.

[104] L. Thijs, F. Verhaeghe, T. Craeghs, J. Van Humbeeck, and J. P. Kruth, 'A study of the microstructural evolution during selective laser melting of Ti–6Al–4V', *Acta Mater*, vol. 58, no. 9, pp. 3303–3312, May 2010, doi: 10.1016/J.ACTAMAT.2010.02.004.

[105] Q. Zhou *et al.*, 'Selective electron beam melting of NiTi: Microstructure, phase transformation and mechanical properties', *Materials Science and Engineering: A*, vol. 744, pp. 290–298, Jan. 2019, doi: 10.1016/J.MSEA.2018.12.023.

[106] A. Kreitcberg, V. Brailovski, and S. Turenne, 'Effect of heat treatment and hot isostatic pressing on the microstructure and mechanical properties of Inconel 625 alloy processed by laser powder bed fusion', *Materials Science and Engineering: A*, vol. 689, pp. 1–10, Mar. 2017, doi: 10.1016/J.MSEA.2017.02.038.

[107] Y. Kok *et al.*, 'Anisotropy and heterogeneity of microstructure and mechanical properties in metal additive manufacturing: A critical review', *Mater Des*, vol. 139, pp. 565–586, Feb. 2018, doi: 10.1016/J.MATDES.2017.11.021.

[108] L. Thijs, M. L. Montero Sistiaga, R. Wauthle, Q. Xie, J. P. Kruth, and J. Van Humbeeck, 'Strong morphological and crystallographic texture and resulting yield strength anisotropy in selective laser melted tantalum', *Acta Mater*, vol. 61, no. 12, pp. 4657–4668, Jul. 2013, doi: 10.1016/J.ACTAMAT.2013.04.036.

[109] M. Mukherjee, 'Effect of build geometry and orientation on microstructure and properties of additively manufactured 316L stainless steel by laser metal deposition', *Materialia (Oxf)*, vol. 7, p. 100359, Sep. 2019, doi: 10.1016/J.MTLA.2019.100359.

[110] S. Zhang, B. Lane, J. Whiting, and K. Chou, 'An Investigation into Metallic Powder Thermal Conductivity in Laser Powder Bed Fusion Additive Manufacturing', 2018, doi: 10.26153/TSW/17169.

[111] Z. Dong, Y. Liu, W. Li, and J. Liang, 'Orientation dependency for microstructure, geometric accuracy and mechanical properties of selective laser melting AlSi10Mg lattices', *J Alloys Compd*, vol. 791, pp. 490–500, Jun. 2019, doi: 10.1016/J.JALLCOM.2019.03.344.

[112] P. D. Nezhadfar, S. Thompson, A. Saharan, N. Phan, and N. Shamsaei, 'Structural integrity of additively manufactured aluminum alloys: Effects of build orientation on microstructure, porosity, and fatigue behavior', *Addit Manuf*, vol. 47, p. 102292, Nov. 2021, doi: 10.1016/J.ADDMA.2021.102292.

[113] J. P. Isaac, S. Lee, S. Thompson, A. Saharan, N. Shamsaei, and H. V. Tippur, 'Role of build orientation on quasi-static and dynamic fracture responses of additively manufactured AlF357 and AlSi10Mg alloys', *Addit Manuf*, vol. 59, p. 103080, Nov. 2022, doi: 10.1016/J.ADDMA.2022.103080.

[114] D. S. Watring, J. T. Benzing, N. Hrabe, and A. D. Spear, 'Effects of laser-energy density and build orientation on the structure–property relationships in as-built Inconel 718 manufactured by laser powder bed fusion', *Addit Manuf*, vol. 36, p. 101425, Dec. 2020, doi: 10.1016/J.ADDMA.2020.101425.

[115] Y. Guo *et al.*, 'The role of pore structures on the fatigue properties of additively manufactured porous tantalum scaffolds produced by electron beam powder bed fusion', *Journal of Materials Research and Technology*, vol. 19, pp. 3461–3473, Jul. 2022, doi: 10.1016/J.JMRT.2022.06.096.

[116] S. Ghorbanpour *et al.*, 'Additive manufacturing of functionally graded inconel 718: Effect of heat treatment and building orientation on microstructure and fatigue behaviour', *J Mater Process Technol*, vol. 306, p. 117573, Aug. 2022, doi: 10.1016/J.JMATPROTEC.2022.117573.

[117] Y. Zhao, K. Li, M. Gargani, and W. Xiong, 'A comparative analysis of Inconel 718 made by additive manufacturing and suction casting: Microstructure evolution in homogenization', *Addit Manuf*, vol. 36, p. 101404, Dec. 2020, doi: 10.1016/J.ADDMA.2020.101404.

[118] A. Leicht, U. Klement, and E. Hryha, 'Effect of build geometry on the microstructural development of 316L parts produced by additive manufacturing', *Mater Charact*, vol. 143, pp. 137–143, Sep. 2018, doi: 10.1016/J.MATCHAR.2018.04.040.

[119] P. Hartunian and M. Eshraghi, 'Effect of Build Orientation on the Microstructure and Mechanical Properties of Selective Laser-Melted Ti-6Al-4V Alloy', *Journal of Manufacturing and Materials Processing*, vol. 2, no. 4, p. 69, Oct. 2018, doi: 10.3390/jmmp2040069.

[120] C. Palanisamy, S. Bhero, B. Abiodun Obadele, and P. Apata Olubambi, 'Effect of build direction on the microhardness and dry sliding wear behaviour of laser additive manufactured Ti-6Al-4V', *Mater Today Proc*, vol. 5, no. 1, pp. 397–402, Jan. 2018, doi: 10.1016/J.MATPR.2017.11.097.

[121] S. Murchio *et al.*, 'On the effect of the node and building orientation on the fatigue behavior of L-PBF Ti6Al4V lattice structure sub-unital elements', *Material Design & Processing Communications*, vol. 3, no. 6, p. e258, Dec. 2021, doi: 10.1002/MDP2.258.

[122] M. Dallago, S. Raghavendra, V. Luchin, G. Zappini, D. Pasini, and M. Benedetti, 'The role of node fillet, unit-cell size and strut orientation on the fatigue strength of Ti-6Al-4V lattice materials additively manufactured via laser powder bed fusion', *Int J Fatigue*, vol. 142, p. 105946, Jan. 2021, doi: 10.1016/J.IJFATIGUE.2020.105946.

[123] G. Meneghetti, D. Rigon, D. Cozzi, W. Waldhauser, and M. Dabalà, 'Influence of build orientation on static and axial fatigue properties of maraging steel specimens produced by additive manufacturing', *Procedia Structural Integrity*, vol. 7, pp. 149–157, Jan. 2017, doi: 10.1016/J.PROSTR.2017.11.072.

[124] R. Shrestha, J. Simsiriwong, N. Shamsaei, S. M. Thompson, and L. Bian, 'Effect of Build Orientation on the Fatigue Behavior of Stainless Steel 316L Manufactured via a Laser-Powder Bed Fusion Process', 2016, *University of Texas at Austin*. Accessed: Mar. 03, 2024. [Online]. Available: https://hdl.handle.net/2152/89615

[125] E. Maleki, S. Bagherifard, F. Sabouri, and M. Guagliano, 'Effects of hybrid post-treatments on fatigue behaviour of notched LPBF AlSi10Mg: experimental and deep learning approaches', *Procedia Structural Integrity*, vol. 34, pp. 141–153, Jan. 2021, doi: 10.1016/J.PROSTR.2021.12.021.

[126] G. S. Ponticelli, R. Panciroli, S. Venettacci, F. Tagliaferri, and S. Guarino, 'Experimental investigation on the fatigue behavior of laser powder bed fused 316L stainless steel', *CIRP J Manuf Sci Technol*, vol. 38, pp. 787–800, Aug. 2022, doi: 10.1016/J.CIRPJ.2022.07.007.

[127] S. Beretta, M. Gargourimotlagh, S. Foletti, A. du Plessis, and M. Riccio, 'Fatigue strength assessment of "as built" AlSi10Mg manufactured by SLM with different build orientations', *Int J Fatigue*, vol. 139, p. 105737, Oct. 2020, doi: 10.1016/J.IJFATIGUE.2020.105737.

[128] K. Solberg, E. W. Hovig, K. Sørby, and F. Berto, 'Directional fatigue behaviour of maraging steel grade 300 produced by laser powder bed fusion', *Int J Fatigue*, vol. 149, p. 106229, Aug. 2021, doi: 10.1016/J.IJFATIGUE.2021.106229.

[129] G. Morettini, N. Razavi, and G. Zucca, 'Effects of build orientation on fatigue behavior of Ti-6Al-4V as-built specimens produced by direct metal laser sintering', *Procedia Structural Integrity*, vol. 24, pp. 349–359, Jan. 2019, doi: 10.1016/J.PROSTR.2020.02.032.

[130] A. Cutolo, C. Elangeswaran, G. K. Muralidharan, and B. Van Hooreweder, 'On the role of building orientation and surface post-processes on the fatigue life of Ti-6Al-4V coupons manufactured by laser powder bed fusion', *Materials Science and Engineering: A*, vol. 840, p. 142747, Apr. 2022, doi: 10.1016/J.MSEA.2022.142747.

[131] A. H. Chern *et al.*, 'Build orientation, surface roughness, and scan path influence on the microstructure, mechanical properties, and flexural fatigue behavior of Ti–6Al–4V fabricated by electron beam melting', *Materials Science and Engineering: A*, vol. 772, p. 138740, Jan. 2020, doi: 10.1016/J.MSEA.2019.138740.

[132] E. Maleki, O. Unal, M. Guagliano, and S. Bagherifard, 'Analysing the Fatigue Behaviour and Residual Stress Relaxation of Gradient Nano-Structured 316L Steel Subjected to the Shot Peening via Deep Learning Approach', *Metals and Materials International*, vol. 28, no. 1, pp. 112–131, Jan. 2022, doi: 10.1007/S12540-021-00995-8/TABLES/6.

[133] E. Maleki, O. Unal, M. Guagliano, and S. Bagherifard, 'The effects of shot peening, laser shock peening and ultrasonic nanocrystal surface modification on the fatigue strength of Inconel 718', *Materials Science and Engineering: A*, vol. 810, p. 141029, Apr. 2021, doi: 10.1016/J.MSEA.2021.141029.

[134] E. Maleki, S. Bagherifard, A. Heydari Astaraee, S. Sgarbazzini, M. Bandini, and M. Guagliano, 'Application of gradient severe shot peening as a novel mechanical surface treatment on fatigue behavior of additively manufactured AlSi10Mg', *Materials Science and Engineering: A*, vol. 881, p. 145397, Aug. 2023, doi: 10.1016/J.MSEA.2023.145397.

[135] J. T. Oliveira de Menezes, E. M. Castrodeza, and R. Casati, 'Effect of build orientation on fracture and tensile behavior of A357 Al alloy processed by Selective Laser Melting', *Materials Science and Engineering: A*, vol. 766, p. 138392, Oct. 2019, doi: 10.1016/J.MSEA.2019.138392.

[136] J. T. O. de Menezes, E. M. Castrodeza, L. Patriarca, and R. Casati, 'Effect of heat treatments and loading orientation on the tensile properties and fracture toughness of AlSi7Mg alloy produced by Laser Powder Bed Fusion', *Int J Fract*, vol. 235, no. 1, pp. 145–157, May 2022, doi: 10.1007/S10704-022-00631-5/FIGURES/16.

[137] L. C. Araújo *et al.*, 'Effects of build orientation and heat treatments on the tensile and fracture toughness properties of additively manufactured AlSi10Mg', *Int J Mech Sci*, vol. 213, p. 106868, Jan. 2022, doi: 10.1016/J.IJMECSCI.2021.106868.

[138] H. Ramadas, A. K. Nath, S. Sarkar, P. Ganesh, R. Kaul, and J. D. Majumdar, 'Fatigue crack growth rate and fracture toughness evaluation of 15-5 precipitation hardening stainless steel fabricated by laser powder bed fusion process', *Materials Science and Engineering: A*, vol. 861, p. 144356, Dec. 2022, doi: 10.1016/J.MSEA.2022.144356.

[139] M. Abdelwahed, S. Bengtsson, M. Boniardi, A. Casaroli, R. Casati, and M. Vedani, 'An investigation on the plane-strain fracture toughness of a water atomized 4130 low-alloy steel processed by laser powder bed fusion', *Materials Science and Engineering: A*, vol. 855, p. 143941, Oct. 2022, doi: 10.1016/J.MSEA.2022.143941.

[140] J. Dzugan *et al.*, 'The effects of post-processing on the local fracture toughness properties of electron beam powder bed fusion Ti-6Al-4V alloy', *Eng Fract Mech*, vol. 273, p. 108697, Oct. 2022, doi: 10.1016/J.ENGFRACMECH.2022.108697.

[141] M. Bahshwan, C. W. Myant, T. Reddyhoff, and M. S. Pham, 'The role of microstructure on wear mechanisms and anisotropy of additively manufactured 316L stainless steel in dry sliding', *Mater Des*, vol. 196, p. 109076, Nov. 2020, doi: 10.1016/J.MATDES.2020.109076.

[142] B. Podgornik, M. Šinko, and M. Godec, 'Dependence of the wear resistance of additive-manufactured maraging steel on the build direction and heat treatment', *Addit Manuf*, vol. 46, p. 102123, Oct. 2021, doi: 10.1016/J.ADDMA.2021.102123.

[143] Y. Yang, X. Li, M. M. Khonsari, Y. Zhu, and H. Yang, 'On enhancing surface wear resistance via rotating grains during selective laser melting', *Addit Manuf*, vol. 36, p. 101583, Dec. 2020, doi: 10.1016/J.ADDMA.2020.101583.

[144] E. Maleki, O. Unal, S. Shao, and N. Shamsaei, 'Effects of Laser Shock Peening on Corrosion Resistance of Additive Manufactured AlSi10Mg', *Coatings 2023, Vol. 13, Page 874*, vol. 13, no. 5, p. 874, May 2023, doi: 10.3390/COATINGS13050874.

[145] B. Wu, Z. Pan, S. Li, D. Cuiuri, D. Ding, and H. Li, 'The anisotropic corrosion behaviour of wire arc additive manufactured Ti-6Al-4V alloy in 3.5% NaCl solution', *Corros Sci*, vol. 137, pp. 176–183, Jun. 2018, doi: 10.1016/J.CORSCI.2018.03.047.

[146] L. Romero-Resendiz *et al.*, 'Microstructural, mechanical, electrochemical, and biological studies of an electron beam melted Ti-6Al-4V alloy', *Mater Today Commun*, vol. 31, p. 103337, Jun. 2022, doi: 10.1016/J.MTCOMM.2022.103337.

[147] X. Zhou *et al.*, 'Mechanical properties, corrosion behavior and cytotoxicity of Ti-6Al-4V alloy fabricated by laser metal deposition', *Mater Charact*, vol. 179, p. 111302, Sep. 2021, doi: 10.1016/J.MATCHAR.2021.111302.

[148] X. Zhou *et al.*, 'Microstructural evolution and corrosion behavior of Ti–6Al–4V alloy fabricated by laser metal deposition for dental applications', *Journal of Materials Research and Technology*, vol. 14, pp. 1459–1472, Sep. 2021, doi: 10.1016/J.JMRT.2021.07.006.

[149] G. Sander, A. P. Babu, X. Gao, D. Jiang, and N. Birbilis, 'On the effect of build orientation and residual stress on the corrosion of 316L stainless steel prepared by selective laser melting', *Corros Sci*, vol. 179, p. 109149, Feb. 2021, doi: 10.1016/J.CORSCI.2020.109149.

[150] D. Du *et al.*, 'Influence of build orientation on microstructure, mechanical and corrosion behavior of Inconel 718 processed by selective laser melting', *Materials Science and Engineering: A*, vol. 760, pp. 469–480, Jul. 2019, doi: 10.1016/J.MSEA.2019.05.013.

[151] X. Peng, L. Kong, J. Y. H. Fuh, and H. Wang, 'A Review of Post-Processing Technologies in Additive Manufacturing', *Journal of Manufacturing and Materials Processing 2021, Vol. 5, Page 38*, vol. 5, no. 2, p. 38, Apr. 2021, doi: 10.3390/JMMP5020038.

[152] M. Taufik and P. K. Jain, 'Role of build orientation in layered manufacturing: A review', *International Journal of Manufacturing Technology and Management*, vol. 27, no. 1–3, pp. 47–73, 2013, doi: 10.1504/IJMTM.2013.058637.

[153] N. N. Kumbhar and A. V. Mulay, 'Post Processing Methods used to Improve Surface Finish of Products which are Manufactured by Additive Manufacturing Technologies: A Review', *Journal of The Institution of Engineers (India): Series C*, vol. 99, no. 4, pp. 481–487, Aug. 2018, doi: 10.1007/S40032-016-0340-Z/FIGURES/3.

[154] C. Ye, C. Zhang, J. Zhao, and Y. Dong, 'Effects of Post-processing on the Surface Finish, Porosity, Residual Stresses, and Fatigue Performance of Additive Manufactured Metals: A Review', *Journal of Materials Engineering and Performance 2021 30:9*, vol. 30, no. 9, pp. 6407–6425, Jul. 2021, doi: 10.1007/S11665-021-06021-7.

[155] E. Maleki, S. Bagherifard, M. Bandini, and M. Guagliano, 'Surface post-treatments for metal additive manufacturing: Progress, challenges, and opportunities', *Addit Manuf*, vol. 37, p. 101619, Jan. 2021, doi: 10.1016/J.ADDMA.2020.101619.

[156] S. Gangireddy, E. J. Faierson, and R. S. Mishra, 'Influences of Post-processing, Location, Orientation, and Induced Porosity on the Dynamic Compression Behavior of Ti–6Al–4V Alloy Built Through Additive Manufacturing', *Journal of Dynamic Behavior of Materials*, vol. 4, no. 4, pp. 441–451, Dec. 2018, doi: 10.1007/S40870-018-0157-3/METRICS.

[157] R. Ponche, O. Kerbrat, P. Mognol, and J. Y. Hascoet, 'A novel methodology of design for Additive Manufacturing applied to Additive Laser Manufacturing process', *Robot Comput Integr Manuf*, vol. 30, no. 4, pp. 389–398, Aug. 2014, doi: 10.1016/j.rcim.2013.12.001.

[158] J. R. Poulin, V. Brailovski, and P. Terriault, 'Long fatigue crack propagation behavior of Inconel 625 processed by laser powder bed fusion: Influence of build orientation and post-processing conditions', *Int J Fatigue*, vol. 116, pp. 634–647, Nov. 2018, doi: 10.1016/J.IJFATIGUE.2018.07.008.

[159] A. Serjouei and S. Afazov, 'Predictive Model to Design for High Cycle Fatigue of Stainless Steels Produced by Metal Additive Manufacturing', *SSRN Electronic Journal*, May 2022, doi: 10.2139/SSRN.4103898.

[160] P. Wood, T. Libura, Z. L. Kowalewski, G. Williams, and A. Serjouei, 'Influences of Horizontal and Vertical Build Orientations and Post-Fabrication Processes on the Fatigue Behavior of Stainless Steel 316L Produced by Selective Laser Melting', *Materials 2019, Vol. 12, Page 4203*, vol. 12, no. 24, p. 4203, Dec. 2019, doi: 10.3390/MA12244203.

[161] A. Alghamdi, D. Downing, M. McMillan, M. Brandt, M. Qian, and M. Leary, 'Experimental and numerical assessment of surface roughness for Ti6Al4V lattice elements in selective laser melting', *International Journal of Advanced Manufacturing Technology*, vol. 105, no. 1–4, pp. 1275–1293, Nov. 2019, doi: 10.1007/S00170-019-04092-4/METRICS.

[162] N. Vanderesse, P. Bocher, N. Nuño, A. Yánez, and L. A. Hof, 'On the characterization of roughness and geometrical irregularities of additively manufactured single titanium-alloy struts', *Addit Manuf*, vol. 54, p. 102731, Jun. 2022, doi: 10.1016/J.ADDMA.2022.102731.

[163] P. Lhuissier, C. de Formanoir, G. Martin, R. Dendievel, and S. Godet, 'Geometrical control of lattice structures produced by EBM through chemical etching: Investigations at the scale of individual struts', *Mater Des*, vol. 110, pp. 485–493, Nov. 2016, doi: 10.1016/J.MATDES.2016.08.029.

[164] S. Bagherifard, N. Beretta, S. Monti, M. Riccio, M. Bandini, and M. Guagliano, 'On the fatigue strength enhancement of additive manufactured AlSi10Mg parts by mechanical and thermal post-processing', *Mater Des*, vol. 145, pp. 28–41, May 2018, doi: 10.1016/J.MATDES.2018.02.055.

[165] E. Cerri, E. Ghio, and G. Bolelli, 'Effect of surface roughness and industrial heat treatments on the microstructure and mechanical properties of Ti6Al4V alloy manufactured by laser powder bed fusion in different built orientations', *Materials Science and Engineering: A*, vol. 851, p. 143635, Aug. 2022, doi: 10.1016/J.MSEA.2022.143635.

[166] S. Bagherifard, 'Enhancing the Structural Performance of Lightweight Metals by Shot Peening', *Adv Eng Mater*, vol. 21, no. 7, p. 1801140, Jul. 2019, doi: 10.1002/ADEM.201801140.

[167] E. Maleki, N. Maleki, A. Fattahi, O. Unal, M. Guagliano, and S. Bagherifard, 'Mechanical characterization and interfacial enzymatic activity of AISI 316L stainless steel after surface nanocrystallization', *Surf Coat Technol*, vol. 405, p. 126729, Jan. 2021, doi: 10.1016/J.SURFCOAT.2020.126729.

[168] E. Maleki, O. Unal, K. Reza Kashyzadeh, S. Bagherifard, and M. Guagliano, 'A systematic study on the effects of shot peening on a mild carbon steel: Microstructure, mechanical properties, and axial fatigue strength of smooth and notched specimens', *Applied Surface Science Advances*, vol. 4, p. 100071, Jun. 2021, doi: 10.1016/J.APSADV.2021.100071.

[169] S. Bagherifard, S. Slawik, I. Fernández-Pariente, C. Pauly, F. Mücklich, and M. Guagliano, 'Nanoscale surface modification of AISI 316L stainless steel by severe shot peening', *Mater Des*, vol. 102, pp. 68–77, Jul. 2016, doi: 10.1016/J.MATDES.2016.03.162.

[170] E. Maleki *et al.*, 'Fatigue behaviour of notched laser powder bed fusion AlSi10Mg after thermal and mechanical surface post-processing', *Materials Science and Engineering: A*, vol. 829, p. 142145, Jan. 2022, doi: 10.1016/J.MSEA.2021.142145.

[171] R. Bikdeloo, G. H. Farrahi, A. Mehmanparast, and S. M. Mahdavi, 'Multiple laser shock peening effects on residual stress distribution and fatigue crack growth behaviour of 316L stainless steel', *Theoretical and Applied Fracture Mechanics*, vol. 105, p. 102429, Feb. 2020, doi: 10.1016/J.TAFMEC.2019.102429.

[172] W. W. Deng, H. F. Lu, Y. H. Xing, K. Y. Luo, and J. Z. Lu, 'Effect of laser shock peening on tensile properties and microstructure of selective laser melted 316L stainless steel with different build

directions', *Materials Science and Engineering: A*, vol. 850, p. 143567, Aug. 2022, doi: 10.1016/J.MSEA.2022.143567.

[173] W. Tillmann, N. F. Lopes Dias, D. Stangier, C. Schaak, and S. Höges, 'Coatability of diamond-like carbon on 316L stainless steel printed by binder jetting', *Addit Manuf*, vol. 44, p. 102064, Aug. 2021, doi: 10.1016/J.ADDMA.2021.102064.

[174] P. Jamshidi *et al.*, 'Selective Laser Melting of Ti-6Al-4V: The Impact of Post-processing on the Tensile, Fatigue and Biological Properties for Medical Implant Applications', *Materials 2020, Vol. 13, Page 2813*, vol. 13, no. 12, p. 2813, Jun. 2020, doi: 10.3390/MA13122813.

[175] S. Ren, Y. Chen, T. Liu, and X. Qu, 'Effect of Build Orientation on Mechanical Properties and Microstructure of Ti-6Al-4V Manufactured by Selective Laser Melting', *Metall Mater Trans A Phys Metall Mater Sci*, vol. 50, no. 9, pp. 4388–4409, Sep. 2019, doi: 10.1007/S11661-019-05322-W/METRICS.

[176] Y. L. Kuo, S. Horikawa, and K. Kakehi, 'The effect of interdendritic δ phase on the mechanical properties of Alloy 718 built up by additive manufacturing', *Mater Des*, vol. 116, pp. 411–418, Feb. 2017, doi: 10.1016/J.MATDES.2016.12.026.

[177] M. D. Sangid *et al.*, 'Role of heat treatment and build orientation in the microstructure sensitive deformation characteristics of IN718 produced via SLM additive manufacturing', *Addit Manuf*, vol. 22, pp. 479–496, Aug. 2018, doi: 10.1016/J.ADDMA.2018.04.032.

[178] A. V. Krishna, O. Flys, V. V. Reddy, J. Berglund, and B. G. Rosen, 'Areal surface topography representation of as-built and post-processed samples produced by powder bed fusion using laser beam melting', *Surf Topogr*, vol. 8, no. 2, p. 024012, Jun. 2020, doi: 10.1088/2051-672X/AB9B73.

[179] R. Rovetta, P. Ginestra, R. M. Ferraro, K. Zohar-Hauber, S. Giliani, and E. Ceretti, 'Building Orientation and Post Processing of Ti6Al4V Produced by Laser Powder Bed Fusion Process', *Journal of Manufacturing and Materials Processing 2023, Vol. 7, Page 43*, vol. 7, no. 1, p. 43, Feb. 2023, doi: 10.3390/JMMP7010043.

[180] J. Zhang, A. Chaudhari, and H. Wang, 'Surface quality and material removal in magnetic abrasive finishing of selective laser melted 316L stainless steel', *J Manuf Process*, vol. 45, pp. 710–719, Sep. 2019, doi: 10.1016/J.JMAPRO.2019.07.044.

[181] S. Afkhami, M. Dabiri, H. Piili, and T. Björk, 'Effects of manufacturing parameters and mechanical post-processing on stainless steel 316L processed by laser powder bed fusion', *Materials Science and Engineering: A*, vol. 802, p. 140660, Jan. 2021, doi: 10.1016/J.MSEA.2020.140660.

[182] J. Doh, N. Raju, N. Raghavan, D. W. Rosen, and S. Kim, 'Bayesian inference-based decision of fatigue life model for metal additive manufacturing considering effects of build orientation and post-processing', *Int J Fatigue*, vol. 155, p. 106535, Feb. 2022, doi: 10.1016/J.IJFATIGUE.2021.106535.

[183] 'ISO 1143:2021 - Metallic materials — Rotating bar bending fatigue testing'. Accessed: Sep. 14, 2024. [Online]. Available: https://www.iso.org/standard/79575.html

[184] M. Janeček *et al.*, 'The very high cycle fatigue behaviour of Ti-6Al-4V alloy', *Acta Phys Pol A*, vol. 128, no. 4, pp. 497–502, Oct. 2015, doi: 10.12693/APHYSPOLA.128.497.

[185] I. Ünsal, M. Hirtler, A. Sviridov, and M. Bambach, 'Material Properties of Features Produced from EN AW 6016 by Wire-Arc Additive Manufacturing', *Procedia Manuf*, vol. 47, pp. 1129–1133, Jan. 2020, doi: 10.1016/J.PROMFG.2020.04.131.

[186] W. J. Oh, J. Y. Son, G. Y. Baek, and D. S. Shim, 'Excess deposition for suppressing interfacial defects induced on parts repaired using direct energy deposition', *International Journal of Advanced Manufacturing Technology*, vol. 106, no. 3–4, pp. 1303–1316, Feb. 2020, doi: 10.1007/S00170-019-04650-W/METRICS.

[187] '3D Printed Hip Prosthesis Approved by China Food and Drug Administration – 3D PRINTING STORE'. Accessed: Jul. 16, 2024. [Online]. Available: https://www.stampa3dstore.com/protesi-anca-stampata-in-3d-approvata-dalla-cina-food-and-drug-administration/

[188] '3D Printing Metal Interview with Arcam CEO Magnus René - 3D Printing Industry'. Accessed: Aug. 05, 2024. [Online]. Available: https://3dprintingindustry.com/news/3d-printing-metal-interview-magnus-rene-arcam-group-ceo-83724/

[189] 'Industrial applications of Renishaw metal additive manufacturing technology'. Accessed: Aug. 05, 2024. [Online]. Available: https://www.renishaw.com/en/industrial-applications-of-renishaw-metal-additive-manufacturing-technology--15256

[190] 'Medicine - Prostir 3d'. Accessed: Aug. 05, 2024. [Online]. Available: https://prostir3d.com/en/medicine